APPLICATION OF METALLOCENES FOR THE SYNTHESIS OF MULTIWALLED CARBON NANOTUBES

by

Nonjabulo Philile Dominica Ngidi

Submitted in fulfilment of the academic requirement for the degree of Master of Science in the School of Chemistry and Physics University of KwaZulu-Natal, Durban, Westville campus

February 2016

ABSTRACT

Multiwalled carbon nanotubes (MWCNTs) are carbon materials which have one-dimensional structure. They possess unique properties such as semi-conductor and high tensile strength that allow them to be widely used in many applications. MWCNTs and other shaped carbon nanomaterials (SCNMs) were synthesized by chemical vapour deposition (CVD) method. Three factors that affect the morphology, thermal, chemical, mechanical and electrical properties of SCNMs were investigated. The parameters are: carbon source, catalyst (metallocenes), and growth temperature. Two different carbon sources were studied for the synthesis of MWCNTs *i.e.*, toluene and acetonitrile (also used as a nitrogen source). The metallocenes: nickelocene, cobaltocene and ruthenocene were used as catalysts (2.5 wt.%) while ferrocene was employed as control. These metallocenes were investigated because they have similar structure as ferrocene, a well-known catalyst for the synthesis of SCNMs. The synthesis was carried out at five different growth temperatures, 800, 850, 900, 950 and 1000 °C.

As-synthesized MWCNTs and other SCNMs were further purified, in order to remove amorphous carbon and this was performed by testing different methods of purification. The effective method for purification of MWCNTs was method 2 which involved refluxing for 24 hours. It was chosen to be the best method because it produced purer MWCNTs as compared to other methods which caused damage to the MWCNTs. The SCNMs obtained were characterized using various techniques namely, transmission electron microscopy, scanning electron microscopy, electron dispersive X-ray spectroscopy, Raman spectroscopy, thermogravimetric analysis, elemental analysis, Branuaer-Emmet-Teller surface area and porosity analysis.

It was observed that growth temperature has an impact on the yield and SCNMs distribution. At higher growth temperatures of 900, 950 and 1000 °C, carbon spheres were mainly formed while lower growth temperature (800 °C) favoured the formation of amorphous carbon. The best growth temperatures, in terms of high yield of MWCNTs, thermal stability and

crystallinity, was observed to be 850 °C. Apart from growth temperature, the morphology of the SCNMs was also found to be carbon source dependent. Acetonitrile as a carbon source, was found to form nitrogen-doped MWCNTs with bamboo compartments while toluene produced pristine-MWCNTs. In all cases other SCNMs were obtained.

The length of the bamboo compartments in the nitrogen-doped MWCNTs decreased at lower growth temperatures. Smaller bamboo compartment lengths correlate with lower thermal stability and crystallinity. This suggests a larger incorporation of nitrogen in the MWCNT framework. The highest nitrogen-doping level was obtained at a growth temperature of 850 °C in all catalysts used. MWCNTs formed from toluene were more thermally stable as compared to those synthesized from acetonitrile. The catalyst had a great influence in determining the morphology of the N-MWCNTs. Ferrocene and nickelocene produced well-aligned N-MWCNTs while cobaltocene and ruthenocene yielded ‘spaghetti-like’ structures. This study has shown that the synthesis of MWCNTs is highly dependent on the catalyst, carbon source and growth temperature of reaction used.

PREFACE

The experimental work described in this thesis was carried out in the School of Chemistry and Physics, University of KwaZulu-Natal, Durban, from February 2014 to February 2016, under the supervision of Prof Vincent O. Nyamori and co-supervised by Dr Bernard O. Owaga.

These studies represent original work by the author and have not otherwise been submitted in any form for any degree or diploma to any tertiary institution. Where use has been made of the work of others it is duly acknowledged in the text.

Signed: _____

DECLARATION 1 – PLAGIARISM

I, **Nonjabulo Philile Dominica Ngidi** declare that;

1. The research reported in thesis, except where otherwise indicated, is my original research.
2. This thesis has not been submitted for any degree or examination at any other University.
3. This thesis does not contain other person's data, pictures, graphs or other information, unless specifically acknowledged as being sourced from the persons.
4. This thesis does not contain other person's writing, unless specifically acknowledged as being sourced from other researchers. Where other written sources have been quoted, then:
   a. Their words have been re-written but, the general information attributed to them has been referenced.
   b. Where their exact words have been used, then their writing has been placed in italics and inside quotation marks, and referenced.
5 This thesis does not contain text, graphics or tables copied and pasted from the internet, unless specifically acknowledged, and the source being detailed in the thesis and in the references sections.

Signed: _____

DECLARATION 2 – PRESENTATIONS AND PUBLICATION

Presentations

1. Nonjabulo P. D. Ngidi, Vincent O. Nyamori and Bernard O. Owaga. Application of metallocenes for the synthesis of multiwalled carbon nanotubes. UKZN, College of Agriculture, Engineering and Science Postgraduate Research Day. Pietermaritzburg, South Africa, 22nd September 2015.

2. Nonjabulo P. D. Ngidi, Vincent O. Nyamori and Bernard O. Owaga. Application of metallocenes for the synthesis of nitrogen-doped multiwalled carbon nanotube. 42nd National Convention of the South African Chemical Institute. Durban, South Africa, 30th November – 4th December 2015.

Publication

A manuscript is being prepared for submission under the title "Effect of carbon source, metallocene and temperature on carbon nanotubes".

Signed: _____

ACKNOWLEGDEMENTS

It gives me great pleasure in expressing my gratitude to all those people who have supported me and had their contributions in making this study possible. First and foremost, I would like to acknowledge and thank the Almighty God, for blessing, protecting and guiding me throughout this period.

I would like to offer my sincerest gratitude to my supervisors, Prof V.O. Nyamori and Dr B.O. Owaga, who have supported me throughout my project with their patience and knowledge, whilst allowing me the room to work independently. I attribute the level of my Masters degree to their encouragement and without them this project would not have been completed in time.

I also wish to thank the other academic staff, technical staff in the School of Chemistry and Physics and as well as the members of the Microscopy Units for their valuable contribution and assistance with the instruments.

Special gratitude goes to Mr Siphesihle Zulu for introducing me to my best friend ever, thin layer chromatography. After all, it is the fastest, cheapest and easiest way to obtain meaningful information about what is going on in your reaction. My deepest gratitude also goes to Dr Moses Ollengo, Dr Godfrey Keru, Mr Eric Njogu and Mr Bheki Gumbi for their critical comment and proofreading of my thesis. Many thanks go to my fellow labmates in Nanochemistry research group: Ntokozo, Samantha, Josiana, Tonde, Kudzai, Ayomide and close friends who constantly motivated me even when times were hard and I appreciate you all. Through all the ups and downs, for the many hours that we spent together, I would not replace any of you I have worked with in the laboratory.

I can't imagine my current position without the love and support from my family. I thank my parents, Mr Nqaba and Mrs Hlengiwe Ngidi for striving hard to provide a good education for me and my siblings. I always fall short of words to adequately describe their support. Thank you for giving me strength to reach for the stars and chase my dreams. My sisters: Nolwazi

and Minenhle, brothers: Philani and Mvelo, cousins: Kholiwe and Sphamandla, grandfather: Mr Vusimuzi Ngidi, aunties and uncles deserve my wholehearted thanks as well. I would like to remember and thank my late paternal grandmother, Mrs Nokwethuka Ngidi (may her soul rest in peace). She might not be physically around but her prayers are.

This work would not have been possible without the financial contribution of National Research Foundation (NRF) of South Africa.

Last but not least, although there may be many who remain unacknowledged in this humble note of gratitude there is none who remain unappreciated.

DEDICATION

My dissertation work is dedicated to my parents who introduced me to the joy of reading from birth, enabling such a study to take place today.

TABLE OF CONTENTS

LIST OF FIGURES

LIST OF TABLES

LIST OF SCHEMES

LIST OF ABBREVIATION, FORMULAE AND SYMBOLS

Abbreviation and symbol	Full meaning
Å	Angstroms
AC	Amorphous carbon
Ar	Argon
Ave.	Average
B-MWCNTs	Boron-doped multiwalled carbon nanotubes
BET	Branuaer-Emmet-Teller
°C	Degree Celsius
°C min^{-1}	Degree Celsius per minute
CHNS	Carbon, hydrogen, nitrogen and sulfur
CNFs	Carbon nanofibers
CNTs	Carbon nanotubes
CNSs	Carbon nanospheres
CO	Carbon monoxide
CO_2	Carbon dioxide
Co	Cobalt
$CoCp^+$	Cobaltocenium ion
Cp	Cyclopentadienyl
CVD	Chemical vapour deposition
DNA	Deoxyribonucleic acid
DWCNTs	Double-walled carbon nanotubes
e^-	Electron
EDX	Electron dispersive X-ray spectroscopy
G	Gram

GPa	Gigapascal
H_2	Hydrogen gas
HNO_3	Nitric acid
HRTEM	High resolution transmission electron
Hr	Hour
ID	Inner diameter
I_D	Disorder band
I_D/I_G	Ratio of D-band intensity to G-band intensity in Raman spectroscopy
I_G	Graphitic band
K	Kelvin
kW cm^{-2}	Kilowatt per square centimetre
Mbar	Megabar
Mg	Milligram
Min	Minute
mL	Millilitre
mL min^{-1}	Millilitre per minute
Mol	Moles
m.p.	Melting point
m/z	Mass-to-charge ratio
MWCNTs	Multi-walled carbon nanotubes
NaOH	Sodium hydroxide
N-CNTs	Nitrogen-doped carbon nanotubes
N-MWCNTs	Nitrogen-doped multiwalled carbon nanotubes
Ni	Nickel

Nm	Nanometre
NPs	Nanoparticles
OD	Outer diameter
SCNMs	Shaped carbon nanomaterials
SEM	Scanning electron microscopy
SWCNTs	Single-walled carbon nanotubes
TEM	Transmission electron microscopy
TLC	Thin layer chromatography
TGA	Thermogravimetric analysis
T_{max}	Reaction temperature
Ts	Tubes
v/v	Volume-by-volume concentration
$Wm^{-1}K^{-1}$	Watt per meter per Kelvin
w.t %	Mass by mass percentage

CHAPTER 1: INTRODUCTION

This chapter presents background information on nanotechnology, problem statement, motivation, aim and objectives, research questions, approach and outline of the thesis.

1.1 Background

Nanotechnology represent a wide range of different technologies which are conducted on a nanometre scale.[1] It involves the design, production, characterization, system and application by maintaining the size and shape on the nanometre scale. It is not only based in making components but also make instruments work better. Nanotechnology enables substitution of small structures assigned with low cost, precision and simplicity which results in economic growth. Dr Richard Feynman presented the first concept of nanotechnology in 1959.[2] In his presentation, he talked about the ways of manipulating matter at the nanoscale and its future. However, the term nanotechnology was first used in 1974 by Norio Taniguchi.[3]

A nanometre (nm) is one thousand millionth of a meter.[4] A perfect way to describe the nanometre scale is by outlining a range of length scales from millimetre down to the nanometre scale. For instance, the scale of a head of a pin is between 1 and 2 mm while dust mites are about 200 μm[5] and that of human hair is known to be half the size of the dust mite.[6] Human red blood cells have a diameter of 8μm.[7] Double helix of DNA is not greater than 20 nm wide and lastly, the atoms are less than 1 nm in size.[8] In nanotechnology we therefore refer to particle with a measurement in the ranges between 1 – 100 nm at least in one dimension.

The recognition of new materials on the nanoscale started with the discovery of buckminsterfullerene. However, in 1991, the focus on nanoscale material developed into intense research because of the discovery of carbon nanotubes (CNTs) by Sumio Iijima[9] and since then, several novel nanoscale materials have been reported. Nanomaterials are well known to enhance chemical,[10] biological,[11] physical,[12,13] magnetic,[14] thermal,[15,16] optical[17] and electrical[18] properties relative to their bulk counterparts.[19] For instance, gold is a heavy metal in its bulk form and inert,[20] however, gold nanoparticles show unique chemical properties, *e.g.* catalytic activity or different physical properties, *e.g.* different colours at nanometre scale size.

Reduction of bulk size can be achieved in different ways.[20-22] However, the two most common methods are 'bottom-up' and 'top-down' approaches.[23] In the bottom-up approach, the arrangement of smaller components is more complex. For examples atoms can be assembled into molecules and molecules into nanostructure.[24-26] This arrangement is achieved by covalent or non-covalent bonding.[27] Top-up approach often uses microfabrication and nanofabrication methods whereby externally controlled tools are employed in the breaking down of the single crystal (bulk material) into an aqueous form or powder for production of nanomaterials.[28-30]

The most talked-about nanotechnologies materials are nanoparticles,[31] quantum dot[32] and shaped carbon nanomaterials (SCNMs).[33] Nanoparticles are small objects that act as a whole unit during their transport and physicochemical properties.[31] Quantum dot are nano-sized crystals. Their size ranges from 2 – 20 nm and have a diameter of 10 nm.[32] The main synthesis of quantum dots involves the use of metals or semiconducting materials. SCNMs are materials that are made of carbon such as carbon nanospheres, carbon nanofibers and CNTs. The main research topic in the study of SCNMs is based on CNTs. CNTs are made of long cylinders of layers of graphene. They are classified into three categories: single-walled carbon nanotubes (SWCNTs) (single cylinder), double walled carbon nanotubes (DWCNTs) (double cylinder walls) and multiwalled carbon nanotubes (MWCNTs) (consisting of more than two cylinders walls).[33] CNTs are extremely strong mechanically[34] and very good conductors of electric current.[35] They are stronger, stiffer and harder than diamond and good thermal conductors. The advantages of using CNTs are that they are smaller, and can be used to produce smaller and faster components.

The industries that benefit from nanotechnology are those that produce energy, electronic products,[36] manufacturing sectors[37] and medical world.[38] In the medical sector, nanotechnology is used in the synthesis of smart drugs; that are target specific, limited side effects[39-41] and faster action. Areas of focus are normal bone repair,[42] tissue regeneration[43] and immunity.[38] Manufacturing sectors uses materials such as nanoparticles and aerogels to produce their products because these materials are stronger, lighter and more durable.[37] Nanotechnology in energy sectors, involve the development of energy storage,[44] energy

absorbing and energy producing devices.[45-47] These energy devices include fuel cells,[48] solar cells[49] and batteries.[50,51]

1.2 Motivation

In the context of South Africa (SA), very little has been done regarding the commercialization of CNTs. To date, only one manufacturing company is registered with the SA government to produce CNTs and other shaped carbon nanomaterials (SCNMs) in a large scale. There are many technical projects which are in progress including development of cheaper solar cells, atomic modelling, and synthesis of nanoparticles and electrocatalyst. The global market for CNTs has grown during the past few years and expected to register a healthy growth on account of growth in the key and end-user industries (such as batteries, capacitors, medical and energy composite).

A number of working groups report the use of iron pentacarbonyl ($Fe(CO)_5$)[52] and ferrocene($FeCp_2$),[53,54] together with their derivatives, as catalysts and precursors for the synthesis of MWCNTs. The effects of changing synthesis parameters such as the growth temperature, gas flow rate, catalyst injection rate and catalyst concentration have been studied extensively using $FeCp_2$ compounds as catalytic precursor. Other metallocenes are also very promising candidates as catalysts for the synthesis of MWCNTs. However, very little research has been done on their application in the synthesis of MWCNTs.

Metals frequently used to synthesize MWCNTs are normally transition metals, specifically iron (Fe), nickel (Ni) and cobalt (Co). This is because of the solubility of carbon on the metallocene. However, the primary reason of applying transition metals in MWCNTs formation is that they possess partially filled "d" shells which enables them to interact with hydrocarbons.[55] The hydrocarbons adsorb on the metal particles and are catalytically decomposed. This results in carbon dissolving into the particle forming a liquid eutectic. Upon supersaturation, carbon precipitates in a tubular, crystalline form.[55] Hence, the transition metal nanoparticles serve as a seed of MWCNTs in order to strongly influence the quality and structure.

Variety of methods are used to synthesize MWCNTs such as laser ablation, arc discharge and chemical vapour deposition (CVD). The CVD method was chosen in this study because of its low cost, its ease of scale-up and produce of high yields. The novelty in this work is the choice of the carbon source, the growth temperature program employed and the comparison of the various metallocenes used. Several working groups have reported methods of synthesizing CNTs using ferrocene. However, novel synthetic strategies need to be explored to make SCNMs with well-defined properties, morphologies and size.

1.3 Aims and objectives

The purpose of this study is to determine optimal conditions for the synthesis of MWCNTs with respect to growth temperatures, carbon sources, catalysts and the effective removal of residual metal catalyst.

1.3.1. The specific objectives were as follows:

- To study the effect of using a different variety of metallocenes on the type of MWCNTs and other SCNMs formed.
- To evaluate the effect of varying the reaction temperature (800, 850, 900, 950 and 1000 °C) on the distribution, crystallinity, yield, surface area and thermal stability of the MWCNTs.
- To examine the effect of varying the carbon source (toluene *vs.* acetonitrile).
- To investigate the effectiveness of three different purification methods for the removal of the residual metal catalyst.

1.3.2. Research questions

- Apart from ferrocene and its derivatives, which are well known catalysts for MWCNTs, is it possible to use other metallocenes such as nickelocene, cobaltocene or ruthenocene for the synthesis of MWCNTs?
- Can MWCNTs be produced with well-defined properties?
- Can metallocenes be used as catalyst for the synthesis of nitrogen–doped MWCNTs (N-MWCNTs)?

- What are the effects of varying the reaction condition (growth temperature) namely: 800, 850, 900, 950 and 1000 °C on MWCNTs/N-MWCNTs?
- Which is a better method for purification of MWCNTs?
- What are the effects of purifying the MWCNTs (synthesized from metallocenes)?

1.4 Research approach

The focus of this study was on nanomaterials preparation, characterization and modifications. Commercial metallocenes were used as a catalyst for the synthesis of SCNMs. Two different carbon sources were used; toluene and acetonitrile. The SCNMs were prepared through the CVD method. The heating programme in the CVD method chosen for the synthesis was 800, 850, 900, 950 or 1000 °C. After their synthesis, the MWCNTs were acid-treated. This was done to remove residual metal catalyst and to add oxygen-containing functional groups onto the tube.

After synthesis and purification of the MWCNTs they were characterized by a number of techniques, namely, transmission electron microscope (TEM) was used to determine the dimensions of MWCNTs while the high resolution transmission electron microscopy was used for close overview of the structure of the MWCNTs. Scanning electron microscopy (SEM) was used to investigate the surface morphology of the MWCNTs. SEM was coupled with electron dispersive X-ray (EDX) which was used to determine the elemental composition of the MWCNTs. The composition and thermal stability was further investigated using thermogravimetric analysis (TGA). Textural studies such as surface area and pore volume were also investigated by use of Brunauer-Emmett-Teller (BET) analysis.

1.5 Outline of this dissertation

This dissertation has been prepared in the format outlined below:

- **Chapter 1**

This chapter provides overall introduction that gives background information on this research. The introduction also contains the research objectives, motivation and the dissertation outline.

- **Chapter 2**

This chapter provides an overview on the current advances and knowledge of SCNMs, especially MWCNTs. Introduction and literature on the preparation methods of MWCNTs and modification strategies (including surface functionalization and doping) are also presented in this part of the dissertation.

- **Chapter 3**

This chapter describes the materials and experimental procedures employed, whereby details of the synthesis conditions, strategies and characterization techniques are given.

- **Chapter 4**

The focus of this chapter was on the use of metallocenes to fine tune the diameters and morphology of MWCNTs. The effect of toluene as carbon source and the effect of varying the growth temperature were evaluated. An investigation on the physicochemical properties of the MWCNTs is presented.

- **Chapter 5**

This chapter describes the synthesis (and properties) of nitrogen-doped MWCNTs and other SCNMs produced using metallocene. It investigated and provides a summary of effects that physical parameters such as temperature and concentration of nitrogen source among other variables, have on the type of SCNMs formed, size and yields, as well as the nitrogen content incorporated into the tubes that are produced by metallocenes.

- **Chapter 6**

This chapter gives conclusion based on the experimental findings. It summarizes all the work carried out in this research and also provides recommendations for future work.

1.6 References

1. M. Anisa, S. D. Abdallah and A. S. Peter, *Nanotechnology*, 2003, 14, 9.
2. R. P. Feynman, *Engineering and Science*, 1960, 23, 22-36.
3. N. Taniguchi, *Japan Society of Precision Engineering*, 1974, 1, 18-23.
4. G. Stix, *Scientific American*, 2001, 285, 26-31.
5. J. E. M. H. van Bronswijk, B. Drs and R. N. Sinha, *Journal of Allergy and Clinical Immunology*, 1971, 47, 31-52.
6. B. Bhushan, *Progress in Materials Science*, 2008, 53, 585-710.
7. I. I. Slowing, C.-W. Wu, J. L. Vivero-Escoto and V. S. Y. Lin, *Small*, 2009, 5, 57-62.
8. C. R. Treadway, M. G. Hill and J. K. Barton, *Chemical Physics*, 2002, 281, 409-428.
9. S. Iijima, *Nature* 1991, 354, 56-58.
10. C. Burda, X. Chen, R. Narayanan and M. A. El-Sayed, *Chemical Reviews*, 2005, 105, 1025-1102.
11. R. Bhattacharya and P. Mukherjee, *Advanced Drug Delivery Reviews*, 2008, 60, 1289-1306.
12. J. T. Lue, *Encyclopedia of Nanoscience and Nanotechnology*, 2007, 10, 10-46.
13. R. Andrievski and A. Glezer, *Scripta Materialia*, 2001, 44, 1621-1624.
14. M. J. Iqbal and M. R. Siddiquah, *Journal of Alloys and Compounds*, 2008, 453, 513-518.
15. G. Zhang and B. Li, *Nanoscale*, 2010, 2, 1058-1068.
16. X. Wang, X. Xu and S. U. S. Choi, *Journal of Thermophysics and Heat Transfer*, 1999, 13, 474-480.
17. J. Z. Zhang, *Optical Properties and Spectroscopy of Nanomaterials*, World Scientific, Singapore, 2009, vol. XVI, pp. 359-383.
18. G. Y. Yurkov, A. Fionov, Y. A. Koksharov, V. Koleso and S. Gubin, *Inorganic Materials*, 2007, 43, 834-844.
19. G. A. Ozin, *Advanced Materials*, 1992, 4, 612-649.

20. S. Eustis and M. A. El-Sayed, *Chemical Society Reviews*, 2006, 35, 209-217.

21. E. E. Connor, J. Mwamuka, A. Gole, C. J. Murphy and M. D. Wyatt, *Small*, 2005, 1, 325-327.

22. W. Rechberger, A. Hohenau, A. Leitner, J. Krenn, B. Lamprecht and F. Aussenegg, *Optics Communications*, 2003, 220, 137-141.

23. D. Mijatovic, J. Eijkel and A. Van Den Berg, *Lab on a Chip*, 2005, 5, 492-500.

24. M. Shimomura and T. Sawadaishi, *Current Opinion in Colloid & Interface Science*, 2001, 6, 11-16.

25. G. M. Whitesides, J. P. Mathias and C. T. Seto, *Molecular Self-assembly and Nanochemistry*, 1991, 254, 1312-1319.

26. C. Park, J. Yoon and E. L. Thomas, *Polymer*, 2003, 44, 6725-6760.

27. G. M. Whitesides, E. E. Simanek, J. P. Mathias, C. T. Seto, D. Chin, M. Mammen and D. M. Gordon, *Accounts of Chemical Research*, 1995, 28, 37-44.

28. P. Inkyu, L. Zhiyong, P. P. Albert and R. S. Williams, *Nanotechnology*, 2010, 21, 501-539.

29. D. A. Canelas, K. P. Herlihy and J. M. DeSimone, *Nanomedicine and Nanobiotechnology*, 2009, 1, 391-404.

30. O. H. Elibol, D. Morisette, D. Akin, J. P. Denton and R. Bashir, *Applied Physics Letters*, 2003, 83, 4613-4615.

31. M. T. Swihart, *Current Opinion in Colloid & Interface Science*, 2003, 8, 127-133.

32. S. K. Mishra, R. K. Srivastava, S. G. Prakash, R. S. Yadav and A. C. Panday, *Electronic Materials Letters*, 2011, 7, 31-38.

33. R. H. Baughman, A. A. Zakhidov and W. A. de Heer, *Science*, 2002, 297, 787-792.

34. B. I. Yakobson and P. Avouris, *Carbon Nanotubes*, Springer, Berlin, 2001, vol. 80, pp. 287-327.

35. T. Ebbesen and P. Ajayan, *Nature*, 1992, 358, 220-222.

36. M. T. Bohr, *Nanotechnology*, 2002, 1, 56-62.

37. J. Weiss, P. Takhistov and D. J. McClements, *Journal of Food Science*, 2006, 71, 107-116.

38. D. Khang, J. Carpenter, Y. W. Chun, R. Pareta and T. J. Webster, *Biomedical Microdevices*, 2010, 12, 575-587.

39. O. C. Farokhzad and R. Langer, *Journal of American Chemical Society*, 2009, 3, 16-20.

40. T. Tanaka, P. Decuzzi, M. Cristofanilli, J. Sakamoto, E. Tasciotti, F. Robertson and M. Ferrari, *Biomedical Microdevices*, 2009, 11, 49-63.

41. M. D. Wang, D. M. Shin, J. W. Simons and S. Nie, *Expert Review of Anticancer Therapy*, 2007, 7, 833-837.

42. E. J. Harvey, J. E. Henderson and S. T. Vengallatore, *Journal of Orthopaedic Trauma*, 2010, 24, 25-30.

43. L. Zhang and T. J. Webster, *Nano Today*, 2009, 4, 66-80.

44. P. Banerjee, I. Perez, L. Henn-Lecordier, S. B. Lee and G. W. Rubloff, *Nature Nanotechnology*, 2009, 4, 292-296.

45. E. Serrano, G. Rus and J. Garcia-Martinez, *Renewable and Sustainable Energy Reviews*, 2009, 13, 2373-2384.

46. K. Sobolev and M. F. Gutiérrez, *American Ceramic Society Bulletin*, 2005, 84, 14.

47. Z. L. Wang and W. Wu, *Angewandte Chemie International Edition*, 2012, 51, 11700-11721.

48. L. Carrette, K. Friedrich and U. Stimming, *Fuel Cells*, 2001, 1, 5-39.

49. M. A. Green, *Solar Cells*, 1982, 7, 337-340.

50. M. Armand and J.-M. Tarascon, *Nature*, 2008, 451, 652-657.

51. P. G. Bruce, B. Scrosati and J. M. Tarascon, *Angewandte Chemie International Edition*, 2008, 47, 2930-2946.

52. A. Moisala, A. G. Nasibulin, D. P. Brown, H. Jiang, L. Khriachtchev and E. I. Kauppinen, *Chemical Engineering Science*, 2006, 61, 4393-4402.

53. B. C. Satishkumar, A. Govindaraj and C. N. R. Rao, *Chemical Physics Letters*, 1999, 307, 158-162.

54. V. O. Nyamori and N. J. Coville, *Organometallics*, 2007, 26, 4083-4085.

55. U. Weissker, S. Hampel, A. Leonhardt and B. Buechner, *Materials*, 2010, 3, 4387-4427.

CHAPTER 2: LITERATURE REVIEW

In this chapter, an overview of the background of metallocenes, metallocene derivatives and shaped carbon nanomaterials (SCNMs) are discussed. The discussion involves basic definition of the structures, properties, syntheses, growth mechanism, purification and application of SCNMs.

2.1 Metallocenes

Metallocenes are organometallic compounds made up of a metal center which is bound to one or two cyclopentadienyl anion rings (Cp-ring).[1] They were discovered in mid-1950s by Dunitz *et al*.[2] Metallocenes, normally contain metal center from transition metals and rare-earth metals on the periodic table. They are classified into two classes; *i.e*. sandwich and half-sandwich metallocenes.[3] Sandwich metallocenes contains metals facially bonded to two cyclopentadienyl rings.[4] They appear in two isoenergetic conformation being staggered (D_{5d} symmetry) and eclipsed (D_{5h} symmetry).

The first sandwich metallocene discovered was ferrocene (Figure 2.1 a); by Kealy *et al*.[5] Ferrocene is an orange coloured solid with an electron count of 18 valence electrons, which satisfies the 18 electron rule, hence, it has remarkable stability.[6] It electron count can be expressed in two ways; one possibility is iron(II) coordinated by two 6–electron cyclopentadienide ($C_5H_5^-$) ions and second possibility is iron(0) complex with two 5-electron C_5H_5 ligands. Its vacancy d-orbitals make it possible for the metal to form a bond with the cyclopentadienyl anions yielding derivatives.

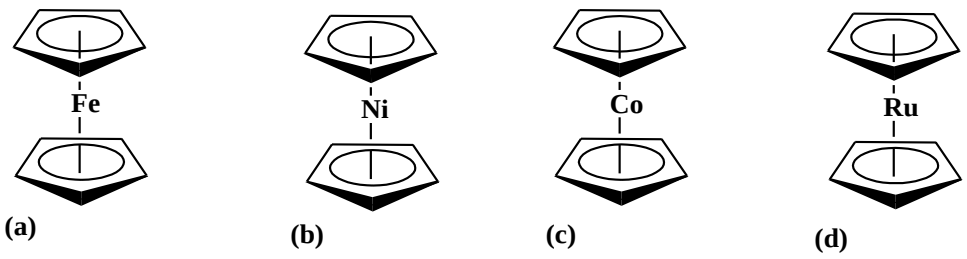

Figure 2.1: Structures of metallocenes: (a) ferrocene, (b) nickelocene, (c) cobaltocene and (d) ruthenocene

The discovery of ferrocene generated wide interest in the synthesis, characterization and applications of metallocenes of other transition metals such as nickelocene, cobaltocene, ruthenocene (Figure 2.1 b-d). These metallocenes have similar structure as ferrocene but they do not obey the eighteen electron count rule.[7] The extra electrons confer important physicochemical characteristics to the metallocenes. For instance, those metallocenes with 19 and 20 valence electron counts have electron occupancy in the slightly antibonding orbitals (largely D_{yz} and D_{xz} in character); as a consequence, the metal-ligand distance increases, and correspondingly their enthalpy change for metal-ligand dissociation decreases.[7]

Cobaltocene (Figure 2.1 c) is a purple crystalline solid that has an electron count of 19. This makes it unstable, according to the 18 e^- rule and its easily oxidized to the cobaltocenium ion ($CoCp_2^+$) upon exposure to air as shown in Scheme 2.1. The cobaltocenium ion is a black solid that has an electron count of 18 valence electrons.[8] Nickelocene (Figure 2.1 b) appears as green crystals and have the highest electron count (20 vacant electrons).[9] Nickelocene is a practical source of fragment NiCp and its protonation leads to a triple-decker sandwich $(Ni_2Cp_3)^+$. Ruthenocene (Figure 2.1 d) is a pale yellow and volatile solid.[10] It consists of ruthenium ion between cyclopentadienyl rings with 18 valence electron count.

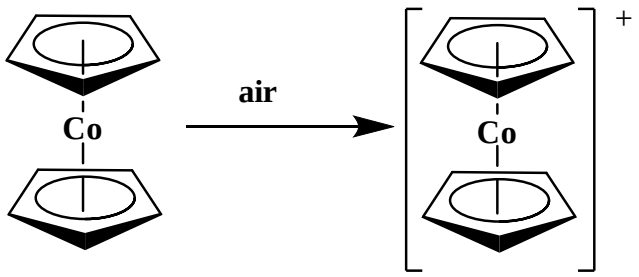

Scheme 2.1: Oxidation reaction of cobaltocene to cobaltocenium ion

The bonding in Cp-ligands is generally *via* all 5 carbon atoms to a metal centre (η5-coordination, π-complexes). In rare cases, the Cp unit can bond through three carbon atoms, like in $[(\eta^3\text{-Cp})WCp(CO)_2]$; or through one carbon atom, as in $[(\eta^1\text{-Cp})FeCp(CO)_2]$. However, half-sandwich compound (3-legged piano stool geometrics) have cyclic poly-hapto-ligand which is bound to an MLn center, where M is the metal and Ln represent the unidentate ligand (Figure 2.2).[3] The properties and utilities of these metallocenes can be enhanced or altered

through derivatization, either through substitution, on either one or both cyclopentadienyl rings, with groups such as alkyl, aryl or halogens.[11,12]

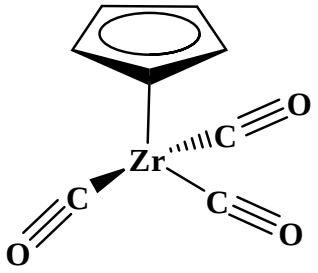

Figure 2.2: Structure of a half-sandwich metallocene

2.2 Carbon-based nanomaterial

Carbon-based materials have created a broad interest in materials science for decades.[13] Carbon is an extremely light and versatile material. It can act as an insulator, a conductor or a semi-conductor. The two common forms of carbon are diamond and graphite (Figure 2.6 a and b) were known in 1770s, however, nowadays it is known that there is a whole family of carbon-based materials.[14] Diamond is hard and transparent whereas graphite is very soft and opaque. Both of these structures are allotropes of carbon. They differ in the structure or the hybridisation of the carbon atoms, for example graphite is sp^2-hybridised while the hybridisation in diamond is sp^3.[15]

The first carbon allotrope that was discovered after the two allotropes of carbon; diamond and graphite was the C_{60} fullerene (Figure 2.3 d-f).[16,17] It was named buckmisterfullerene because of its resemblance to geodesic spheres. The C_{60} fullerene is a hollow and cage-like buckminsterfullerene molecule. Its structure consists of 60 carbon atoms in a number of five-membered ring separated by six-membered rings.[17] The other fullerene is C_{70} which has spherical carbon structure but slightly elongated to resemble a rugby ball. C_{70} is more stable than C_{60} because it consists of more carbon atoms than C_{60}.[18] For fullerene to be formed, they require the C-C bond interaction through bent sp^2 hybridized carbon atoms.[19] In brief there are many forms of fullerenes, they go up to and beyond C_{120}.[20] They are used in solar cells,[21,22] hydrogen storage media,[23] as an antioxidant for polymers,[24] hardening agents for carbides[25] and used for drug and gene delivery in medicine.[26]

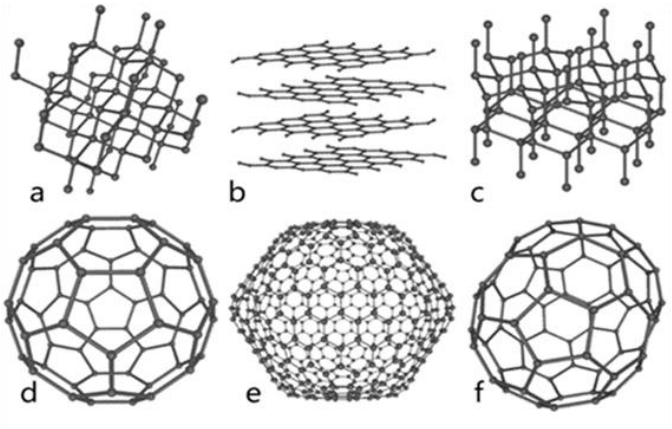

Figure 2.3: The allotropes of carbon (a) diamond, (b) graphite, (c) lonsdalieteans (d-f) buckminsterfullerenes[15]

Carbon is capable of producing other SCNMs that are known such as carbon helices, carbon nanofoams, carbon nanofibers, carbon nanocones, carbon nanohorns, carbon nanospheres, carbon nanotubes carbon nanocoils and carbon nano-onions (Figure 2.4). Carbon helices (Figure 2.4 a) were first synthesised in 1953.[27] Their synthesis was done at a lower temperature of between 250 to 700 °C and was used in the synthesis of novel catalyst support.[27] Carbon nanofoams were discovered by Rode and co-workers.[28] They consist of a low-density cluster-assembly of carbon atom strung together in a loose three-dimensional web (Figure 2.4 b). Similar conditions of synthesizing carbon nanotubes (CNTs) are also used in the synthesis of nanofoam.[28,29]

Carbon nanofibers have graphitic sheets which may be stacked perpendicular to the growth axis or at an angle to the growth axis[30] (Figure 2.4 c). They are differentiated into two *i.e.* platelet type and herringbone type.[31] Platelet has fibrous carbon layers which are perpendicular to fibre axis while for the herringbone, the layers are nested inside one another at an angle. Their diameters range between 150 and 300 nm while their lengths range from 10 nm to a few centimetres. They are mainly synthesized using the chemical vapour deposition (CVD) method[29] in the presence of a catalyst. During their synthesis, the catalyst plays an important role, since it controls the type of nanofibers to be obtained. Nanofibers are used in various composite materials[32] for different applications. A common confusion arises when it comes to the distinction between CNTs and nanofibers since they are both elongated carbon nanostructures. However, CNTs are hollow and many times smaller in size.

Carbon nanocones have curved walls (Figure 2.4 d). The thickness of the cone walls varies between 10 and 30 nm.[33] They are synthesized by decomposition of the hydrocarbons (hydrogen gas + methane gas) and argon using the plasma-enhanced CVD[34] or microwave plasma – assisted CVD.[35] Carbon nanocones occur on the surface of natural graphite and are stable at high temperature. They have potential application as drug delivery[36] agents. Carbon nanohorns have a single wall with horn-like tubes (Figure 2.4 e). Their diameters range between 3 and 25 nm, have lengths between 20 and 150 nm.[37] They can be synthesized using the arc discharge method.[38] They are used in gas storage,[39] photovoltaics and photoelectrochemical cells[40] and also as catalyst support because of their high porosity.[41]

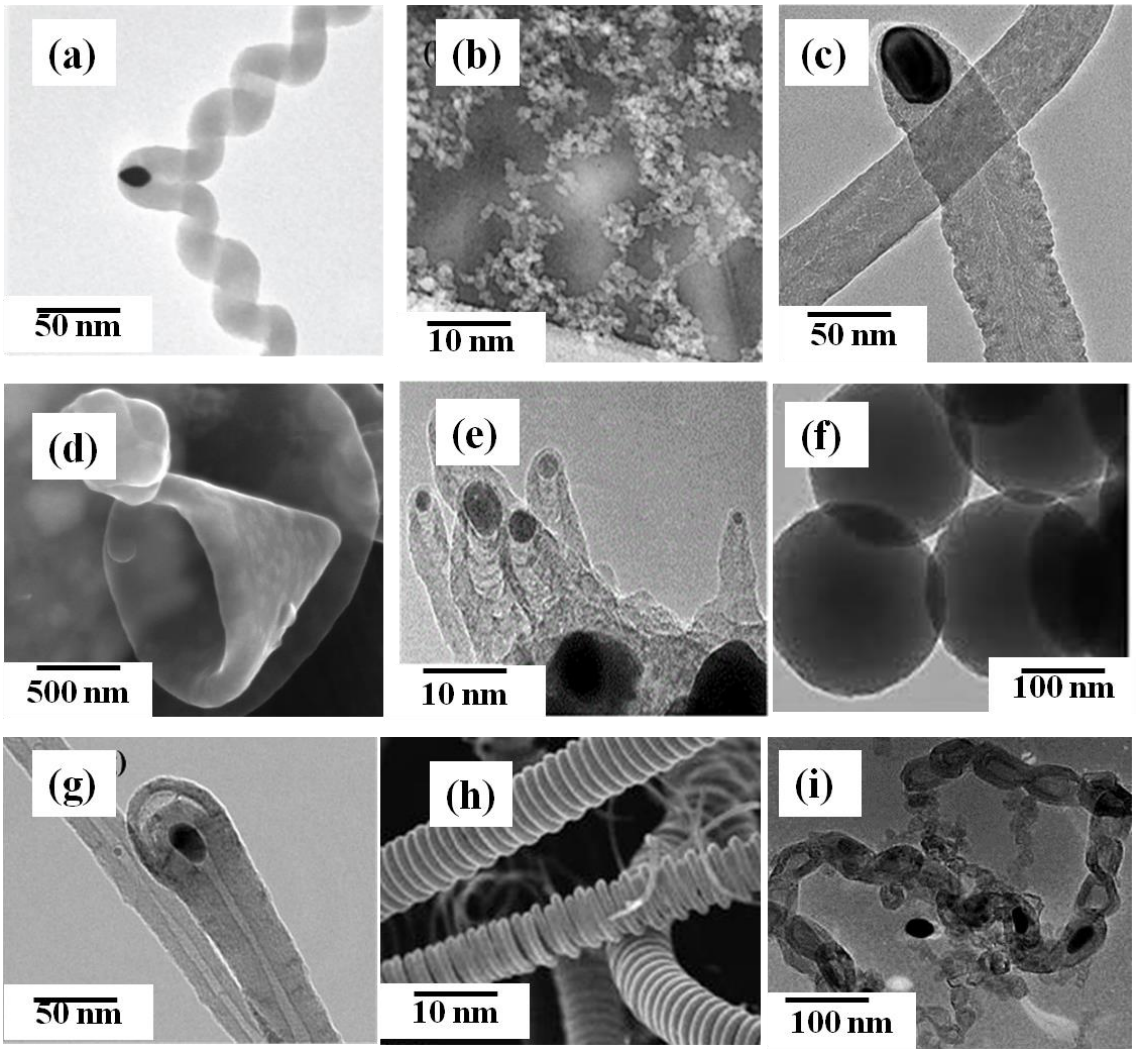

Figure 2.4: Types of SCNMs: (a) carbon helice,[27] (b) carbon nanofoam,[42] (c) carbon nanofiber,[43] (d) carbon nanocones,[33] (e) carbon nanohorns,[44] (f) carbon nanospheres,[45] (g) carbon nanotubes,[46] (h) carbon nanocoils[47] and (i) carbon nano-onions[48]

Carbon nanospheres (CSs) have solid core or hollow shell structure or a soccer ball shape (Figure 2.4 f).[45] They can either be crystalline or semi-crystalline because they have more than one carbon layer forming the outer carbon layer. Their diameters range between 2 and 10 000 nm. Carbon spheres with diameter less than 1000 nm tend to fuse together forming bead- or necklace-like structure called accretion.[49] Their classification is based on diameter, arrangement of carbon layers and also in terms of surface morphology. Those that are classified in terms of diameter are categorised into three: well-graphitised spheres, less-graphitised spheres and carbon beads.[49] Well-graphitised spheres have diameters between 2 and 20 nm. Less-graphitised has diameters between 50 and 1000 nm. Carbon beads have a diameter of 1000 nm and more.[49] Structurally, they can be classified as hollow, core-shell or solid (Figure 2.5). Their structural morphology depends on how the spheres have been synthesized.[50]

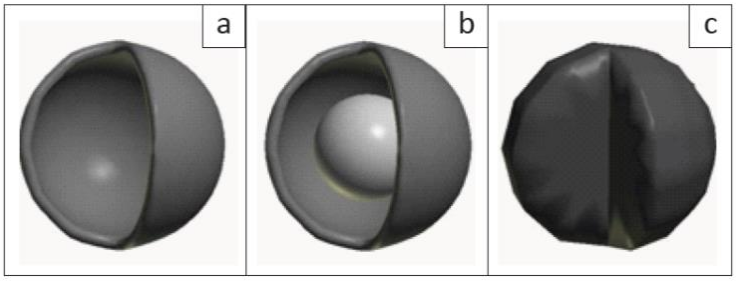

Figure 2.5: An image of (a) hollow, (b) core-shell and (c) solid spheres[51]

Hollow spheres are synthesized by the templating method. During the templating method, the spherical materials such as micelle, silica or metal nanoparticle are covered with a carbon source. These hollow CSs were reported by Wang *et al.*,[52] where by a carbon source of benzene was used. They have also been synthesized using pyrolysis, a medial-reduction route and solvothermal methods subsequently. At high temperature, the carbon source breaks down into carbon atoms and forms core-shell spheres (Figure 2.5 b). Wang *et al.*[53] had synthesized solid carbon sphere with a diameter of approximately 210 nm using the thermal decomposition of CH_4 and a metal oxide catalyst. Carbon layers of these sphere are arranged into three ways: concentric, random and radial[54] (Figure 2.6).

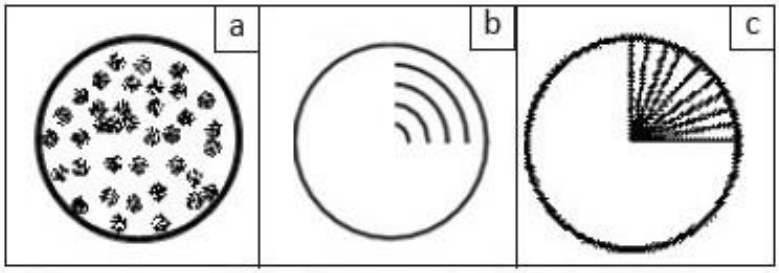

Figure 2.6: An image indicating (a) random, (b) concentric and (c) radial layer orientations in carbon nanospheres[51]

The synthesis of nanospheres is similar to that of the CNTs which is discussed in section 2.2.5.[49] They can be functionalized[55] and also be doped with boron or nitrogen in order to enhance their electric properties.[56] Spheres that have been functionalized and doped are more reactive and have numerous applications. For example they have been used in drug delivery,[57] catalyst support materials,[58] composite,[59] hydrogen storage[60] and fuel cell electrodes.[61] This is because of their low density, thermal stability and electronic properties.[62] The current work has been focused on carbon nanotubes and nanospheres and herein SCNMs will be referring to these structures.

2.2.1 Carbon nanotubes

CNTs are allotropes of carbon composed of a cylindrical nanostructure.[63] CNTs are members of the fullerene structural family. They are tubular in shape. Their name is derived from their long, hollow structure with the walls formed by one-atom-thick sheets of carbon, called graphene. These sheets are rolled at specific and discrete angles and the combination of the rolling angle and radius dictates the CNTs properties; for example, whether the individual CNTs shell is a conductor or semiconductor.[63] They come in different length, diameters and functional group content. They have length-to-diameter ratios of up to 1000 nm and they are considered as one-dimensional structures.

2.2.2 Discovery of CNTs

CNTs dates as far back as 1952 when they were reported in a publication by L.V. Radushkevich and V.M. Lukyanovich in the Soviet Journal of Physical Chemistry.[64] However, their work was not able to be conveyed since their publication appeared in Russian language and this was during the cold War when the Soviets had limited accessibility to the press. Thus, many

publications have suggested that it was Sumio Iijima in 1991 that made the discovery of these hollow, nanometre-sized tubes consisting of graphene carbon.[65] Iijima made the discovery in a serendipitious way when he viewed the CNTs that had formed in the soot under the transmission electron microscope while analysing the graphite carbons that he had made by the arc-discharge apparatus.

In 1992, Ebbesen and Ajayan[66] synthesized graphitic nanotubes using arc-discharge technique, under helium atmosphere. Again in that year Saito *et al.*[67] discovered electronic-structure of chiral graphene tubules. In 1993, Iijima[63] reported the growth process of single-walled carbon nanotubes. Since then, great advancements have been made in carbon nanotubes research. Among other people who made some of these pioneer advancements include, Bethune *et al.*[68] who used an arc discharge method in order to produce single-walled carbon nanotubes using cobalt/nickel catalyst.

As years passed, the research on nanotubes got more interesting; in 1995, boron nitride carbon nanotube were synthesized by Chopra *et al*.[69] In 1996, Kroto obtained the Nobel Prize for discovering the fullerenes.[70] Dai *et al.*[71] in 1996 synthesized single-walled nanotubes using laser-vaporized methods from nickel and cobalt mixture. Since then the preparation of high quality CNTs with high yield and with ease has been the goal of many research endeavours.

2.2.3 Structural features and classification of CNTs

CNTs are categorized as single-walled carbon nanotubes (SWCNTs), double-walled carbon nanotubes (DWCNTs) and multiwalled carbon nanotubes (MWCNTs) as shown in Figure 2.7.

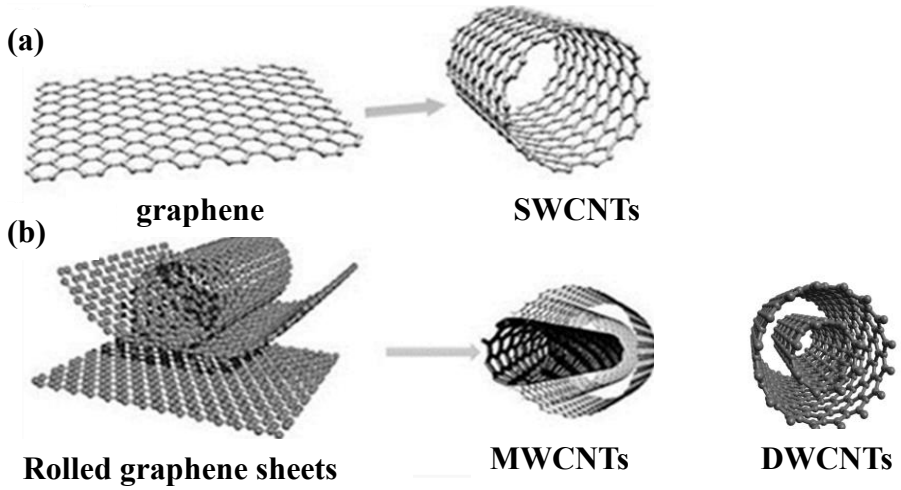

Figure 2.7: Illustration of CNTs categorised on the number of cylindrical tubes: (a) SWCNTs and (b) MWCNTs and DWCNTs[46]

SWCNTs have a single layer of graphene (Figure 2.7 a) and have higher stability.[63] The diameters of SWCNTs are less than 0.4 nm and have lengths of a thousand times long.[72] They have more defined and crystalline structures however, it is difficult to synthesize them as it requires proper control over growth and atmospheric condition. During their synthesis, catalysts are required. They are synthesized at a higher temperatures of about 900 – 1200 °C.[72] The way in which their graphene sheet is rolled-up into a tubular sheet is defined by equation 1:

$$C_h = na_1 + ma_2 \qquad (1)$$

Where C_h represent the chiral vector and a_1 and a_2 represent lattice vectors.[73,74] The integer values (*n* and *m*) denote the number of unit vectors along two directions in the crystal lattice of graphene (Figure 2.8).

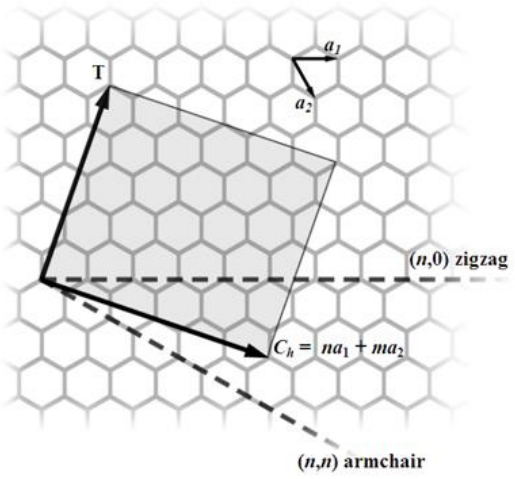

C_h = chiral vector

n = integer value

m = integer value

a_1 and a_2 = lattice vectors

T = tube axis

Figure 2.8: An illustration of the carbon nanotubes naming scheme (n,m)[75]

These indices are integers which represent a unit vector along two directions in a honeycomb style crystals lattice of graphene.[76] When integer m = 0, the shape of the crystal lattice takes a *zigzag* shape thus the CNTs are called *zigzag* CNTs and have a chiral angle of 0º.This is seen when two opposite C-C bonds of each hexagon are parallel to the tube axis. When m and n are equal, the nanotubes are called *armchair* CNTs and the chiral angle is 30º. When n is not equal to m, CNTs are generally referred to as *chiral*, with a chiral angle between 0º and 30º.[73] The different conformations are shown in Figure 2.9. These integers have been of great importance when it comes to theoretical calculations of physical properties and mechanical properties of CNTs. The physical properties have been shown to be dependent on the direction of the chiral vector.[77] The C-C bonds lies at an angle to the axis of the tube.[73]

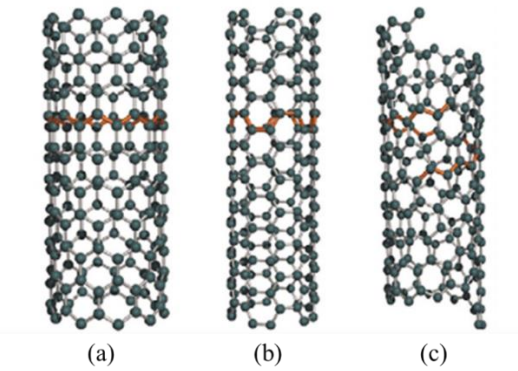

Figure 2.9: Illustration of the three helicities graphical structures of: (a) zigzag, (b) arm-chair and (c) chiral[75]

DWCNTs and MWCNTs are composed of two and multilayer respectively of graphene (Figure 2.7 b).[46] Their diameters range between 5 and 100 nm. They are synthesized at higher temperature of between 600 and 900 °C. MWCNTs were first discovered after the SWCNTs were observed. Individual CNTs naturally align themselves into "ropes" held together by van der Waals force and mostly by pi-stacking.[78] MWCNTs are divided into two models, *i.e.* the Russian Doll model and Parchment or Scroll model.[79] Russian Doll model consist of concentric SWCNTs which are combined one inside the other concentrically. These concentric SWCNTs have different diameters. Parchment or Scroll model consist of one graphene sheet which is rolled-up on itself like a scroll. The distance between graphite layers of MWCNTs is 3.4 Å.[80] Figure 2.10 illustrates the cross-sectional cutting of the CNTs.[79]

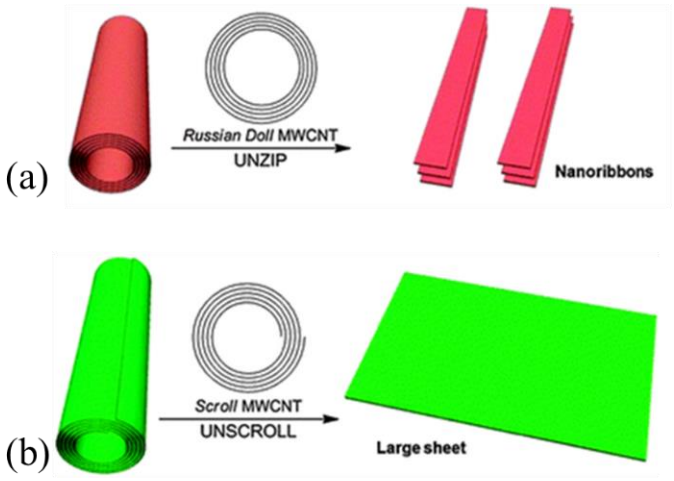

Figure 2.10: 3D and end-on representation of (a) Russian doll and (b) scroll MWCNTs models[79]

When the CNTs are characterized by scanning electron microscope, they appear as one plane whereas SWCNTs appears as two planes. MWCNTs appear in more than two planes which can be viewed as a series of parallel lines (Figure 2.11). Sometimes MWCNTs have more complex array forms due to concentric nanotubes which contain different structures.[81]

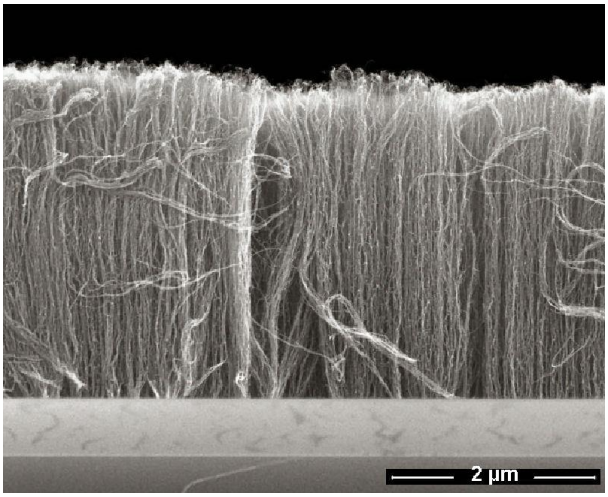

Figure 2.11: Aligned MWCNTs[81]

2.2.4 Properties of CNTs

CNTs have different types of properties which makes them to be suitable in many applications including electrical,[82] mechanical[83] and thermal application.[84]

2.2.4.1 Electrical properties

The electrical properties of CNTs are governed by the arrangement of carbon atoms on the tubes. CNTs can either be conducting or semi-conducting and the degree of conductivity depends upon their diameter and chiral vector.[82] Investigations of electrical properties of nanotubes have been focused solely on SWCNTs, because they have similar electronic band structures to graphene.[85] For graphene and metallic SWCNTs, the valence band and the conduction band are reported to touch at specific points in the reciprocal space, but for semiconducting SWCNTs the conduction band and the valence band do not touch. Generally, CNTs are conductive if *n* and *m* is a multiple of 3, otherwise they are semiconductors.[79] The semiconducting SWCNTs are candidates for applications such as transistor devices,[86] while conducting SWCNTs can be used in field emission devices.[87,88] The electrical properties of MWCNTs are difficult to predicate because they consist of different SWCNTs with different helicities. *Zigzag* nanotubes are semi-conducting while the armchair nanotubes are metallic.[88] The functionalization and doping of MWCNTs with nitrogen or boron atoms enhance their electrical properties.[88]

2.2.4.2 Mechanical property

Mechanical properties of CNTs, such as tensile strength, traction resistance, Young's modulus among others, have been determined by both theoretical calculations and experimental investigations. These investigations have shown that CNTs are stronger than diamond and have the highest Young's modulus and tensile strength of all materials.[83] The strength of CNTs is created by the hybridization of C-C bonds between the hexagonal carbon rings. The estimated Young's modulus for CNTs is 1060 GPa which is five times higher than that of steel.[89] Tensile strengths of 150 GPa and a traction resistance of 250 GPa have been reported. This is because of stronger and shorter length of sp^2 hybridized bonds, similar to those of graphene which relatively makes them stronger than sp^3 hybridized bonds, and hence this determines the tensile strength of CNTs.[89]

When the mechanical stability is high, it allows the CNTs to resist alteration of the surface area of the exposed and the existence of large microspores is avoided which limits the accessibility of the substrate to the active site. Magnetic properties of CNTs are promoted by the incorporation of a metal in the tube, which makes them susceptible to a magnetic field. The metals which have been incorporated include iron,[90] nickel[91] and cobalt[92] this makes the CNTs ferromagnetic. CNTs are flexible and highly elastic but MWCNTs are not as elastic as SWCNTs, as shown by Cheng *et al*.[93] Their elasticity modulus and stiffness may be a result of C=C (sp^2) bonds which are relatively shorter and stronger than sp^3 bonds.[94]

2.2.4.3 Thermal properties

Thermal conductivity and thermal expansion as properties have been investigated for both SWCNTs and MWCNTs. These are important when it comes to the technological applications of CNTs.[84,95] It has been shown that microscale electrical gadgets have a problem with thermal management and dissipation and therefore improving such material is required.[96] The thermal conductivity and thermal expansion investigations are done using graphite as reference. Graphite and diamond have high thermal conductivities, so it is expected that CNTs will be no exception.[97] Indeed this is the case as CNTs have been shown to have thermal conductivities as high as 3500 Wm^{-1} K^{-1}, which is higher than that of copper, known for its exceptional conductivity.[98] However, thermal expansions of CNTs have been found to differ from those of graphite and carbon nanofibers.[98] CNTs have high thermal expansion while graphite and carbon nanofibers have low thermal expansion.

2.2.5 Synthesis of CNTs

For over a decade of the study of CNTs, theoretically and experimentally techniques have been developed to produce CNTs in sizable quantities. Such techniques include, arc discharge,[99] laser ablation and chemical vapour deposition. Among factors considered in choosing a synthesis technique are cost effectiveness, yield/quantity and quality of CNTs. Most of these processes take place in vacuum or with process gases. In the subsequent section these synthesis techniques are discussed individually in more detail.

2.2.5.1 Arc discharge method

Arc discharge method was originally used for producing C_{60} fullerenes by Kratschmer *et al.*[100] however, recent investigations have shown that this technique can be used to synthesize CNTs. Subrahmanyam *et al.*[101] had shown that arc discharge is useful in synthesizing pure, B- and N-doped graphene. The same method had also been employed by Kroto *et al.*[19] and Iijima[65] to produce buckminsterfullerene and CNTs, respectively. It is accomplished by producing plasma between the two graphite electrodes, employing a high current power and low voltage supply. CNTs are developed through arc-vaporization of two carbon rods (anode and cathode) as shown in Figure 2.12.[99] The two carbon rods are placed end to end with a distance of approximately 1 mm apart in an enclosure filled with inert gas for instance argon or helium at low pressure between 50 and 700 mbar.[102] The inert atmosphere prevents oxidation of the graphite rods. A metal catalyst is added as a mixture with graphite powder in the anode. The formation of CNTs occurs when the electrodes are brought together and struck by a high arch subliming the carbon in the electrode, this plasma temperature reaches up to 3000 °C. Then the rod shaped tube sublimates settles on the cathode.

The inner core of the arch containing CNTs is much softer than outer grey, hard shell. The soft core also contains a mosaic of polyhedral particles and amorphous carbon. SWCNTs can also be formed using this method, however, they require greater selectivity and thus, a mixed metal catalyst is often used. Variable metal catalyst ratios of Fe, Co or Ni are incorporated in the anode.[103] The vaporization of carbon that occurs produces SWCNTs and other SCNMs.[63,104] The resultant SWCNTs are distributed as a fluffy web-like materials in the chamber. This makes it challenging to measure the diameter and length of the tubes because they congregate in "bundles". Varying the catalyst as well as carrier gas can alter both diameter and length of tubes formed. The main drawback of using arc-discharge method is small quantities of

products (CNTs) obtained and high cost.[105] The CNTs produced contains impurities in the form of metal catalyst residues and amorphous carbon (soot) and other SCNMs besides SWCNTs. This was shown by Qui *et al.*[106] when they synthesized highly graphitized carbon spheres using coal as a carbon source and Ni catalyst.

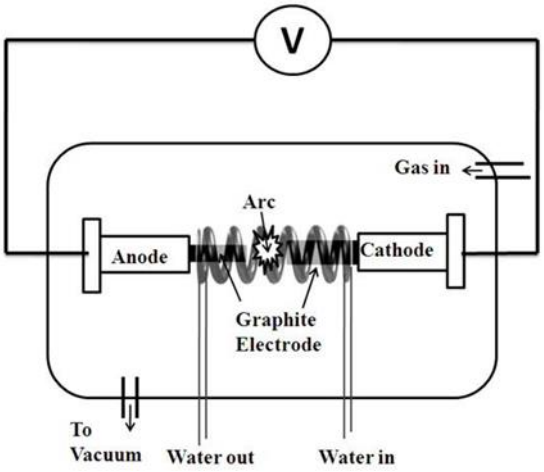

Figure 2.12: Schematic diagram of the arc-discharge[99]

2.2.5.2 Laser ablation method

Laser vaporization uses a pulsed-wave or continuous-wave to evaporate catalyst metal or graphite. The laser ablation is a very expensive method and it is mostly used for producing SWCNTs. It was first used by Guo *et al.*[107] in 1995. After a year it was further used by Thess *et al.*[108] in 1996 to produce SWCNTs with more than 70 wt% yield. In this technique a graphite target is placed in a quartz tube surrounded by a furnace. The graphite target is first mixed with metal catalyst in an inert atmosphere (helium or argon) at reduced pressure. Filling the oven with helium or argon gas helps to keep pressure at 500 torr. The furnace is required to heat up to a temperature of approximately 1200 °C (Figure 2.13).[107] A water-cooled surface may be included in the system. The soot is transferred by a constant flow of carrier inert gas to a water-cooled copper trap where it is collected. This condensation results in the formation of carbonaceous clusters which includes CNTs. Similar to direct arc discharge, laser ablation involves the vaporisation of graphite in an inert environment, however, in this case, better quality CNTs are obtained.[108-110] This is due to a laser having a better light intensity of 100 kW cm^{-2} relative to continuous source of 12 kW cm^{-2}.[111]

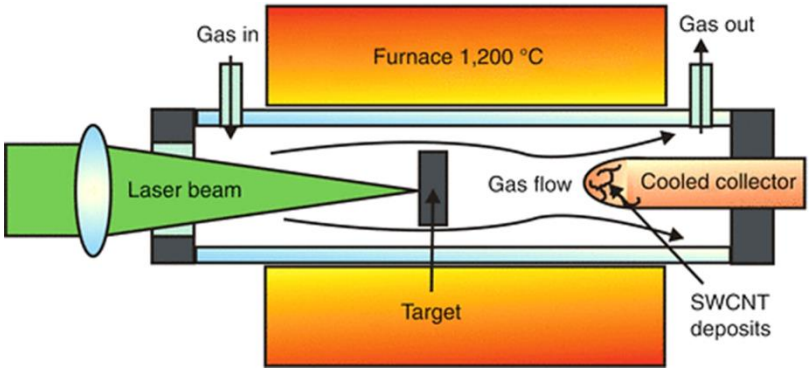

Figure 2.13: Laser ablation schematic diagram[111]

The major drawbacks of laser ablation include: its inability to increase the CNTs yield for large-scale production, complex instrumental set-up, and it is relatively costly. Another issue relates to the fact that the vaporization method grows CNTs in highly tangled forms, mixed with unwanted forms of carbon or metal species. Thus the CNTs produced are difficult to purify and manipulate.[112]

2.2.5.3 Chemical vapour deposition method

The main method for production of CNTs is the CVD method (Figure 2.14). Jose-Yacaman *et al.*[113] was the first person to produce the CNTs using the CVD. It is widely used because it produces high yields of CNTs in good quality. It also offers better growth control.[113] It can produce both SWCNTs and MWCNTs and other SCNMs with selectivity. This method relies on decomposition of carbon containing compounds on the surface of nanometer-sized transition metal particles that serve two main functions; act as catalysts for carbon source decomposition as well as, CNT formation sites.[114] There are different kinds of CVD methods, differentiated either by the heat source and the catalytic system. Those that are differentiated in terms of the heat source include plasma enhanced CVD (PECVD),[115] microwave plasma-assisted CVD (MPACVD),[116] hot wire CVD (HWCVD),[117] hot filament CVD[118] and thermal CVD.[119] The CVD is equipped with inert gas source, hydrocarbon source, temperature controller, quartz tube and exhaust.

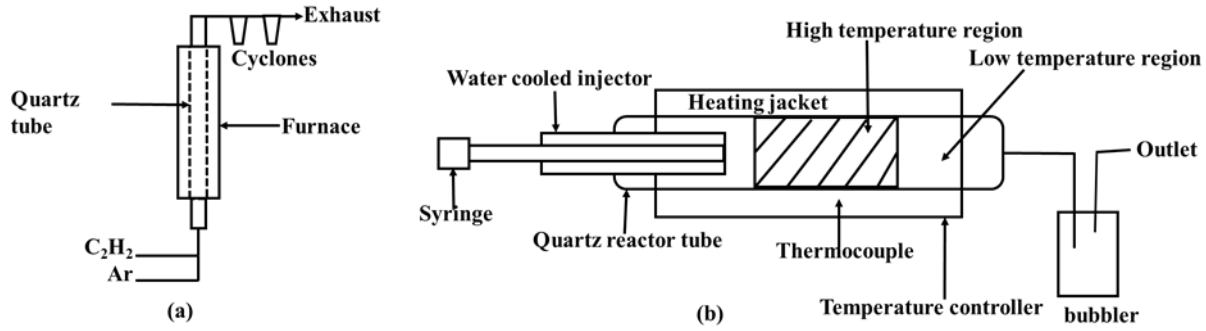

Figure 2.14: Schematic diagram of a simplified CVD setup (a) vertical and (b) horizontal.

The setup can be arranged in a horizontal or vertical fashion, with a quartz tube that is inserted into a hot oven (Figure 2.14).[120] The design of the horizontal CVD is such that the hot zone of the furnace is in the middle region and that is where growth would eventually take place. The carbon source is then passed through the quartz tube with a suitable inert carrier gas at a temperature of ~ 600 °C – 1100 °C in the presence of a catalyst. The catalyst can be introduced either as a liquid or gaseous form. The catalyst can be passed through the reactor with the carrier gas as a floating catalyst[121] or be placed in the reactor as a supported catalyst.[122] Alternatively, the catalyst can be deposited on a support material, that will increase catalyst surface area before it is coated on the quartz reactor.[114] Upon the decomposition of the reactants the CNTs form. The advantages of using the floating catalyst over supported catalyst can be summarized as follows: firstly, no support removal procedures are required after the reaction. Secondly, during the coating step, not all of the catalyst sticks onto the quartz wall. Thirdly, the floating catalyst method can introduce catalyst in liquid or gas form and all prepared catalyst can participate in the reaction.[120] CNTs produced by this method exhibit greater electrical properties, because they can be grown to significantly long lengths and are seldom found in bundles as in the previous methods.

A vertical CVD reactor works in more or less the same way as the horizontal CVD reactor, however, with this technique the inlet flows from the bottom-up (Figure 2.14 a). The products are collected during the reaction thus this makes this technique superior in the ease of product extraction. Moreover, vertical CVD has an added advantage of affordability to produce carbonaceous products on a large scale and that are fairly pure, thus minimizing purification.

The carbon source and catalyst mixture can also be introduced into the reactor by producing a fine mist. This latter method is known as spray pyrolysis.[123] With spray pyrolysis, the system consists of two-stage furnace system where the first furnace is for sublimation of the catalyst and carbon source into vapour as shown in Figure 2.15. The vapour is carried by a carrier gas either; helium, nitrogen, argon, hydrogen gas (or sometimes can be a mixture of hydrogen and argon gases) to the second furnace, which is at higher temperature (1100 °C).[124] The quartz reactor tube is then used to collect the SCNMs.

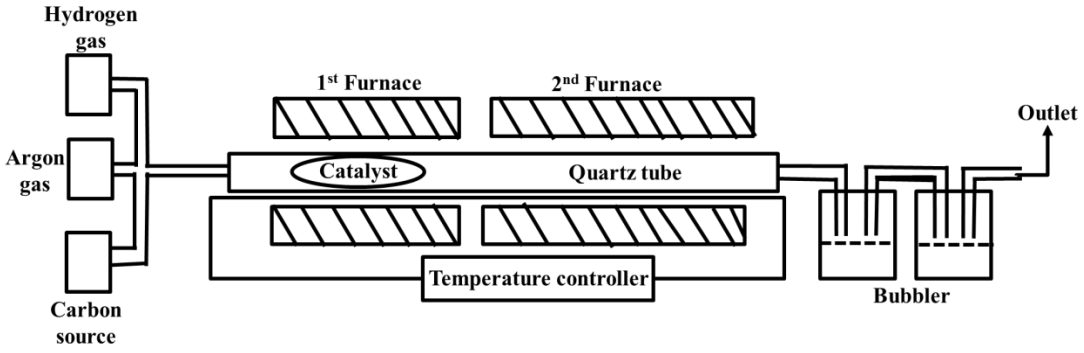

Figure 2.15: Schematic diagram of a two stage furnace pyrolysis set up[121]

Reactions at lower temperature from 600 to 900 °C are known to yield MWCNTs whereas those that are carried at higher temperature from 900 to 1200 °C yield SWCNTs. The CVD has advantages in that, it requires low power input, lower temperature range and allows for scale up of the process. Other advantages include, easy control of catalyst particles.[125] The main disadvantage of using the CVD is that the various parameters such as catalyst, carbon source, carrier gas, reaction temperature, and reaction time and flow rate need to be regulated to optimize quantity and quality, making the synthesis complex. Other disadvantages include the type of catalyst precursors that can be toxic *e.g.* nickel carbonyl, explosive such asdiborone tetrahydride, or corrosive such as tetrachlorosilane and also the by-products of the CVD reactions can be hazardous like carbon monoxide, hydrogen gas or hydrogen fluoride.[126]

2.2.6 Factors that affect CNTs growth in the CVD synthesis

2.2.6.1 Carbon source

One of the most important parameter in the synthesis of CNTs is a carbon source. It can be introduced in the furnace as a carrier gas or by injection or aerosol or held in the hot zone while heating. The carbon source can be any carbon containing material such as hydrocarbons. Liquid and gaseous hydrocarbons are commonly used. liquid hydrocarbons used are alkyls (butane[127] and ethane[128]) and aromatics (toluene,[129,130] benzene[131] and xylene[132]) while gaseous hydrocarbon that can be used are methane[133] and acetylene.[127,134] However, the common carbon source used for the production of CNTs is carbon monoxide. The disproportion reaction which occurs is given in equation 2:[135]

$$CO_{(g)} + CO_{(g)} \rightarrow C_{(s)} + CO_{2(g)} \qquad (2)$$

In equation (2), $C_{(s)}$ represent the CNTs. A range of hydrocarbon used in the synthesis of CNTs, have no significant effect on the properties of the CNTs. However, when the carbon source used contains a heteroatom (oxygen, nitrogen, or sulfur), the morphology, size and yield are affected. For example when benzene is used as a carbon source, its yields double size of the normal CNTs.[131] However, a carbon source of acetonitrile result in CNTs with bamboo morphology because of the presence of nitrogen.[136] The common heteroatoms used in the synthesis of CNTs are discussed in section 2.2.7. The carbon source works in conjunction with the catalyst. When the carbon source is not accompanied by the catalyst, carbon spheres are primarily formed.

2.2.6.2 Catalyst precursor

A Catalyst determines the product of a reaction. It can be used as a solid or liquid or in a gaseous phase. In 1993, Tibbets reported the use of ferrocene in the synthesis of carbon fibre.[137] Since then many reports has been using organometallics on the growth of SCNMs because they are volatile, air stable, relatively inexpensive and readily available.[121] Different types of catalyst have been investigated extensively in CVD. Common transition metals used are iron (Fe), nickel (Ni), cobalt (Co) and ruthenium (Ru). A study was done by Deck *et al.*[12] where they used a wide range of metallocenes or chlorides of (Fe, Co, Ni, Cr, Mn, Zn, Cd, Ti, Zr, La, Cu, V and Gd) on their suitability as CNTs catalysts and discovered that the three

elements suitable for the synthesis of CNTs were: Fe, Co, Ni. The elements; Ti, Cu, Gd produced nothing while the other elements produced soot.[12] The morphology, size and growth rate of CNTs is influenced by the choice of catalyst and it concentration.

The transition metals are also used as acetates,[138] halogen salts[139] or metal carbonyl[140] but mostly as metallocene because of the partially filled d-orbitals. In their elemental forms, these metals are used when supported by substrates such as MgO,[141] silicon,[142] quartz[143] and zeolites.[144] As halogen salts these metals have been used as MX_2 (where M = Fe, Co, Ni and X = Cl, Br). Organometallic compounds such as ferrocene,[145] $Fe(CO)_5$,[146] $W(CO)_5$,[145] arylferrocene ring substituents[147] and piano stool complexes[148] have been investigated.

The second most used organometallic complex is $Fe(CO)_5$ with the most common being ferrocene. $Fe(CO)_5$ is used in the industrial HiPCO process to synthesis CNTs.[135] This technique is for catalytic production of SWCNTs in a continuous-flow gas phase using CO as the carbon feedstock. The metal carbonyls have an advantage over elemental catalysts and metal halogens because they can act both as a catalyst and as a carbon source (in CO).

The nanoparticle size and distribution of the SCNMs can be also controlled by bimetallic catalyst.[133] This approach involves the use of two or more metals bonded to each other in metal clusters compound or the metal catalyst can be added in the synthesis as a mixture of two separate compound. Bimetallic catalyst has been reported to produce high yields of CNTs. This is caused by increase in their carbon solubility and development of well-dispersed metal clusters during CNTs synthesis.[133,149]

2.2.6.3 Injection rate

The injection rate plays an important role in reaction rate and also in the shape and size of the CNTs produced. Higher injection rate causes an increase in the reaction rate because the partial pressure of component in the gas phase is higher. This results in larger diameters of CNTs because of the increased rate of metal nanoparticles collision and coalescence. Mohlala *et al*.[150] showed that the injection rate has no effect on the morphology of CNTs when rate of 0.2 and 0.8 mL min^{-1} is used. However, they discovered that the yield of the product (CNTs) was influenced by lower injection rate. A lower injection rate formed more products while higher injection rate gave lower product yields.

2.2.6.4 Gas flow rate

The carrier gas influences the type of SCNMs produced in terms of rate of formation, diameter and length. The gas flow rates are important because they promote the elongation of the CNTs and also flush impurities out of the system. Fast flow rates prevent agglomeration and produce shorter CNTs.[151] Qiu *et al.*[152] reported that the higher the flow rate over coal gas, the higher the rate of formation of the SWCNTs. It had also been reported that higher flow rate causes a decrease in SWCNTs.[153] This is caused by insufficient carbon to metal nanoparticles.

2.2.6.5 Temperature

Growth temperatures play an important part in the synthesis of SCNMs. The temperature affects the kinetic energy (rate of collision and coalescence) of the nanoparticles inside the CVD. A wide range of temperatures have been investigated resulting indifferent SCNMs.[154] Lower growth temperature of less than 800 °C produce high amount of amorphous carbon while a high temperature above 900 °C produces lots of carbon spheres. Temperature range 800 – 900 °C has been reported to be the best for synthesizing good quality CNTs.[155] The choice of temperature used in the CVD methods influences the levels of amorphous carbon.[151] This was reported by Su *et al.*[151] when he observed that less amorphous carbon were produced at higher temperature of 1100 °C. Bai *et al.*[156] reported that preheating temperature in a two-phase CVD system also influences the formation rate of CNTs because of the way in which the catalyst decomposes which results in low carbon production. Temperature also affects the yield of SCNMs. Higher temperatures (1000 °C) tend to produce higher yield of SCNMs than lower temperature (800 °C) but necessarily for selective production of CNTs. This change in yield is caused by the kinetic energy of the metal nanoparticles in the CVD method. At higher temperature, the rate of collision and dissolution of carbon species increase, hence affecting the rate of nucleation and growth. It is shown that the temperature also affect the diameters of the CNTs, as shown by Kuwana *et al.*[157] and experimentally by Singh *et al.*[158] Higher temperatures tend to produce larger diameter and lower temperature produce smaller diameter CNTs.

2.2.7 Effect of introducing nitrogen

The introduction of heteroatom in reactions has been shown to modify the structure, yield and size of CNTs. Introducing heteroatoms in the lattice structure of the CNTs (often referred to as doping) alters the physical and chemical properties of CNTs. These distortions in the carbon fabric cause changes that allow CNTs to be suitable for various applications. During doping a precursor containing an element of choice is used. When the heteroatom is added, it usually replaces a carbon atom. Heteroatoms such as nitrogen have been included in the synthesis of SCNMs.[159]

Nitrogen can be added as part of the catalyst ligand, part of the carbon source or carrier gas. The addition of nitrogen has been shown to change morphology of the CNTs, giving rise to a bamboo compartment. The 'bamboo compartments are situated in the inner walls of the CNTs as shown in Figure 2.16.[136] Bamboo compartments are sometimes seen in the pristine-CNTs and have been reported to occur due to fluctuation in the carbon concentration in the metal catalyst.[160] The number of bamboo compartments in the CNTs, depend on the concentration of nitrogen incorporated. The greater the number of bamboo compartments and shorter the distance between the compartments, the greater the concentration of nitrogen.[161] N-CNTs have larger inner diameter whilst their outer diameter are small. Other than bamboo structure, nitrogen doping has been found to produce coiled or telephone cord-like CNTs.[162]

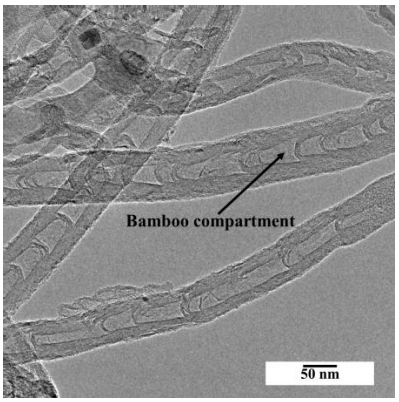

Figure 2.16: TEM image of bamboo-shaped CNTs as a result of N-doping[136]

The configuration of nitrogen atoms in N-CNTs is better explained by different models, namely pyrrole-like, pyridine-like and graphitic-nitrogen configuration. In pyrrole-like configuration, the nitrogen is situated in a five-membered ring whilst in the pyridine-like; nitrogen is

connected to two atoms within a six-membered ring. In graphitic-nitrogen configuration, the nitrogen atom replace the graphitic carbon atom.[163] Figure 2.17 represent a diagram of different configurations.

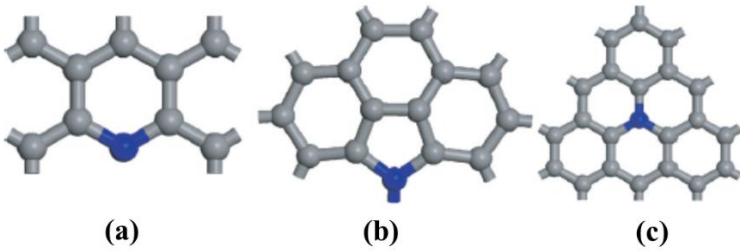

Figure 2.17: Different ways in which nitrogen is incorporated into the carbon structure (a) pyridine-like, (b) pyrrole-like and (c) graphitic-nitrogen configuration[163]

These configurations have different hybridization of nitrogen atom which takes part in investigation of the electrical properties of N-CNTs. Pyrrole-like configurations have a sp^3 hybridized. Pyridine-like and graphitic-nitrogen configuration are sp^2 hybridized because the nitrogen atom is coordinated to two atoms.[163]. N-CNTs are less mechanical[164] and less thermally[48] stable when compared to their undoped counterpart

Nitrogen-doping is divided into two categories, (i) "in situ"-doping which is done directly during the synthesis of porous carbon nanostructure materials, (ii) post-doping, which occurs during the post-treatment of pre-synthesized carbon materials with a nitrogen-containing precursor such as nitric acid. The post-doping reaction is performed in nitric acid at high temperatures (600 – 900 °C).[165] Nitrogen doping of CNTs leads to *n*-type semiconductor behaviour because of the incorporation of nitrogen into CNTs which enhances conductivity. Nitrogen has been reported to increase the conductivity and improve the transport and field emission properties of the CNTs. The N-CNTs are normally used as support for nanoparticles of Pt-Ru in fuel cells due to the altered properties from the inclusion of nitrogen.[50,165]

2.2.8 CNTs growth mechanism

The CNTs growth occurs in a series of steps. The two most possible growth mechanisms are the vapour-solid-solid (VSS)[166] and the vapour-liquid-solid (VLS) mechanism.[167] In the VSS mechanism, carbon vapours are believed to precipitate on the surface of the metal as a solid and CNT growth propagates in the solid state. In the VLS mechanism, carbon is believed to

undergo condensation from the vapour phase before the solid state. Although the exact mechanism by which CNTs grow is still unclear, they have been shown to follow two growth models, *i.e*. the tip- and base-growth mechanisms.[72] These mechanisms depend on reaction conditions and also between the interaction of the metal catalyst particle and the support. Tip-growth mechanism is expected to occur when the catalyst-support is weak while the base-growth mechanism is expected when the catalyst interaction is strong. When the catalyst-interaction is weak, the CNTs will lift the catalyst as it grows vertically whereas with the base-growth mechanism, catalyst-support interaction are strong, therefore, the CNTs will lift the catalyst as it grows horizontally.[114,168] Both of these growths are achieved by the presence of more than one catalyst dot during their growth.[169-171]

2.2.8.1 Tip-growth mechanism

Tip-growth mechanism is similar to the floating-catalyst CVD method which is illustrated in Figure 2.18. According to Amelinckx *et al*.[172] tip-growth mechanism occurs when the small particle is situated on a support (larger metal particle). The smaller particles are forced out from the support. The process of extrusion of the smaller metal particle from the larger metal particle is driven by the carbon deposition onto the surface of the metal particle. This dissolution of carbon takes place at high temperature. The growth process continues until the metal catalyst is completely coated with graphene sheets. An increase in outer diameter of the tubes is observed as the graphene sheet is continuously deposited (Figure 2.18).[172]

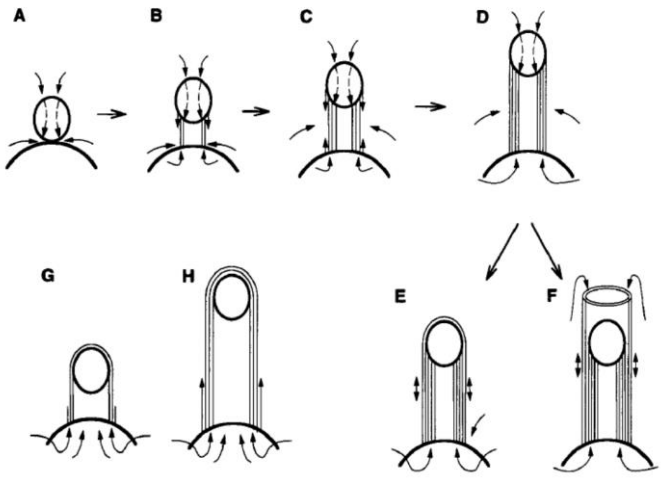

Figure 2.18: Schematic illustration of the tip-growth mechanism in floating-catalyst CVD method[172]

2.2.8.2 Base-growth mechanism

Base-growth mechanism is favoured over tip-growth mechanism when the interaction between the catalyst and the support is strong. The higher strength of this interaction is characterized by the location of the metal catalyst at the bottom of the CNTs. In 2005, Puretzky *et al.*[173] reported an *in situ* measurement and modelling of base-growth mechanism. It occurs mostly in the CVD growth of CNTs over a supported catalyst. The mechanism happens by the decomposition of the carbon source into graphitic flakes on the surface of the supported metal catalyst parallel to the metal particles (Figure 2.19). This results in the formation of the hemispherical graphene cap on the surface of the metal catalyst like a *yarmulke*.[71,174] Upon this catalyst the carbon can be continually deposited until the catalyst is deactivated and forms a carbon capsule. The diameter of the CNTs is equivalent to the circumference of the metal particle from which they emerge. During the synthesis of CNTs other SCNMs of amorphous carbon may form, hence this lowers the product purity and therefore purification becomes relevant.[110,175]

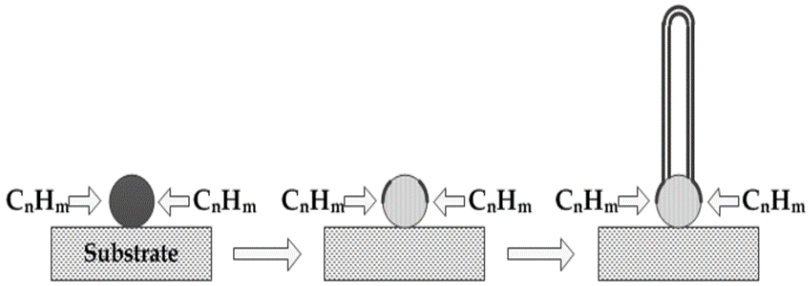

Figure 2.19: Base-growth mechanism of carbon nanotubes[176]

2.2.9 Purification of the CNTs

Purification enables the exploitation of the applications and properties of carbon nanotubes. Different types of purification methods are discussed in the following subsections.

2.2.9.1 Acid refluxing

This purification involves the treatment of CNTs with strong acid such as nitric acid (HNO_3), sulphuric acid (H_2SO_4) and hydrochloric acid (HCl) or combination of these acids.[177] During the purification process, the CNTs are sonicated in an acidic solution to expose the metal

catalyst particles and thereafter refluxed for several hours to dissolve the metal. After refluxing, CNTs are then washed with ethanol or acetone for neutralization. This is then followed by drying the CNTs in the oven. Strong acids such as sulphuric acid and concentrated nitric acid usually breaks the CNTs into shorter pieces and surface etching, however, these approach leads to a greater degree of purification. CNTs purified with acids are normally more disordered than as-synthesized CNTs and this can be confirmed by Raman spectroscopy.[178-180]

2.2.9.2 Surfactant aided sonication, filtration and annealing

The acid treated CNTs usually are entangled together and sometimes have trapped the impurities such as catalyst particles and carbon particles. These impurities are very difficult to remove by filtration therefore surfactant-aided sonication is performed. Sonication is mostly done to promote the dispersion of CNTs and also to further improve the CNTs solubility. Widely used surfactants are anionic surfactant, sodium dodecylbenzene sulfonate (SDBS) with methanol or ethanol as organic solvent.[181,182] SDBS and organic solvent are usually preferred because during the sonication of CNTs, they cause the CNTs to take longer time to settle down which indicates a good suspension. After sonication the solution of CNTs and surfactant are then filtered with an ultra-filtration unit[183] and annealed at 1273 °C in nitrogen gas (N_2) for 4 hrs.[184] Annealing is powerful in optimizing the structure of CNTs by increasing thermal stability and mechanical strength.[185] Graphite is known to be stable even at 3000 °C and higher temperatures tend to cause evaporation of the metal particles. Therefore, annealing is capable of removing metal nanoparticles in the hollow core or at the tip of CNTs.

2.2.9.3 Oxidation in air

This purification involves the oxidation of the sample in air which results in the elimination off amorphous carbon. This is achieved upon the subjection of CNTs to high temperatures (but below 700 °C) in air. The amorphous carbons and other less stable SCNMs such as fullerenes are removed thus leaving behind the pure CNTs. This is because these impurities are less thermally stable and hence oxidized at a faster rate and at lower temperatures (200 °C) than CNTs. However, this can also lead to a decrease in production yield as some of the CNTs can also be oxidized at higher temperatures. Hence, oxidations can result to CNTs damage and loss. In order to prevent this, the temperature has to be controlled. This can be achieved either by using isothermal or dynamic oxidation (Figure 2.20).[186]

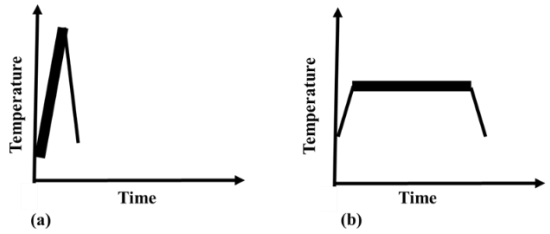

Figure 2.20: Comparison of (a) dynamic oxidation with (b) conventional isothermal (static) oxidation[186]

During the dynamic oxidation, CNTs are put through a constantly increasing temperature such as 10 °C min^{-1} in the presence of air while isothermal oxidation is subjected to constant temperature (Figure 2.20 b). Dynamic oxidation requires smaller oxidation time (<1.5 hr) when compared to the isothermal oxidation (<5 hr). The smaller oxidation time helps in minimizing contributions of catalytic effects. CNTs that are purified using dynamic oxidation method tend to have higher purity compared to those that are purified using isothermal oxidation. CNTs purified using these methods are more graphitic when compared with those which are purified by acid and basic treatment, which are more disordered. A positive note of this draw-back is that the thermal treatment results in the rearrangement of CNTs which ultimately results in more ordered and crystalline CNTs.[186,187]

2.2.10 Functionalization of CNTs

The lack of solubility of CNTs in aqueous media has been a major technical barrier for biological and biomedical applications and to tackle this problem, functionalization is done with certain groups, such as ester groups, amides or carboxylic acids.[188-190] Many applications of CNTs require them to be dispersible in water or polar solvents and to be compatible with polymer matrices. Functionalization modifies the physical and chemical properties of the CNTs.

Functionalization can be classified into two categories *e.g.* covalent and non-covalent functionalization. Covalent functionalization requires formation of covalent bond among various functional groups on the sidewalls sites and on the tips of CNTs.[191] It is irreversible and interferes with the electronic properties of CNTs which cause permanent loss of double bond. Covalent functionalization can be accomplished by fluorination, diazonium salt and

cycloaddition.[192] Non-covalent functionalization is based on attraction of the hydrophobic end of an adsorbed molecule to CNTs walls.[193] It can be executed in ionic liquids. Non-covalent functionalization does not interfere with the electronic properties of CNTs, since it doesn't interfere with the covalent network of CNTs. Their main drawback is that it is hard to control functionalization system.

2.2.11 Structural and morphological characterization of CNTs

Carbon nanotubes can be characterized using a range of techniques such as transmission electron microscopy (TEM), scanning electron microscopy (SEM), electron dispersive X-ray spectroscopy (EDX), thermogravimetric analysis (TGA), Raman spectroscopy and Brunauer, Emmett and Teller (BET) analysis.

2.2.11.1 Transmission electron microscopy

TEM is usually used for size and structure verification which provides data on parameters such as diameter (inner- and outer-diameter), length, viewing the number of layers and the nature of the apex, *i.e.* whether they are open or close and presence of impurities such as metal in the structure.[194] TEM also enables determination of the quality of the CNTs structure, amorphous material in and around the CNTs, and coordination between the CNTs and support material.[195]

TEM consists of three systems namely: an illumination, imaging and image translating system. The illumination consists of two units, *i.e.* the condenser and electron gun.[196] The electron gun is the source of electrons while the condenser is capable of controlling the beam incident onto the sample (Figure 2.21 a). The electron gun is made up of three components: filament, Whenhelt cap and an anode. The filament appears in a form of a pure tungsten wire. It is connected to the negative power supply. During the passing of electric current, it turns up to be very hot and emit electrons. These emitted electrons are further pumped between the filament and an anode and the sample is then illuminated.[196,197] The imaging system comprises of projector and objective lenses. The lenses allow the electron wave distribution to be correctly positioned onto the viewing system. The image translating system uses charge device camera (CCD) to convert the electron image into visible light image.[197] HRTEM is the most powerful instrument that reveals the diameters of the single-wall and multi-wall CNT, the number of walls (Figure 2.21 b)[198] and the distance between the walls.[199]

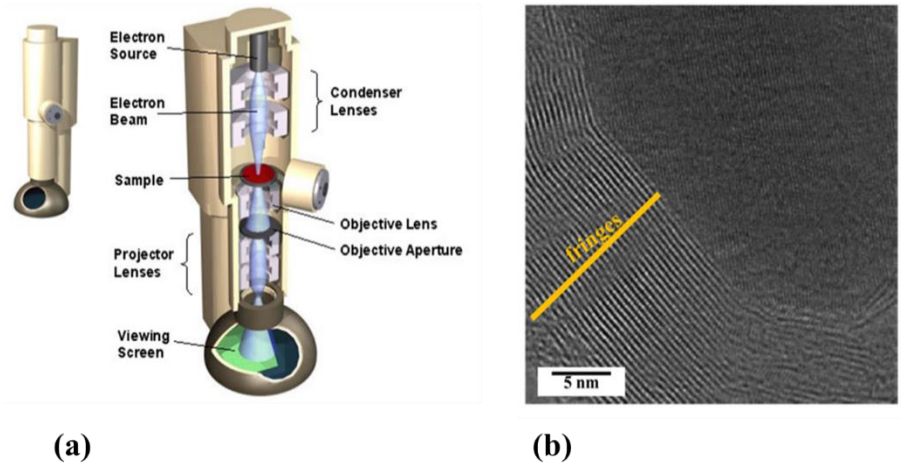

Figure 2.21: (a) Schematic diagram of TEM spectrometer[200] and (b) HRTEM image of the carbon encapsuled iron particles[198]

2.2.11.2 Scanning electron microscopy

SEM is used for the surface morphology studies and the presence of impurities. It also gives information on the surface, alignment of CNTs and also, their crystallinity.[201] The advantage for using SEM is that it requires minimal sample preparation and also it is relatively easy to use. It is capable of producing three-dimensional image.[201] It operates in the same way as TEM. The surface of a sample is scanned using focused beam and produces a diversity of signals at the surface (Figure 2.22 a). The high-energy electrons are then emitted from the sample and are converted into a tiny current that is amplified to produce a signal voltage. The signal is further passed onto a cathode-ray tube (CRT) or cathode lenses and the image is formed as shown in Figure 2.22 b.[202]

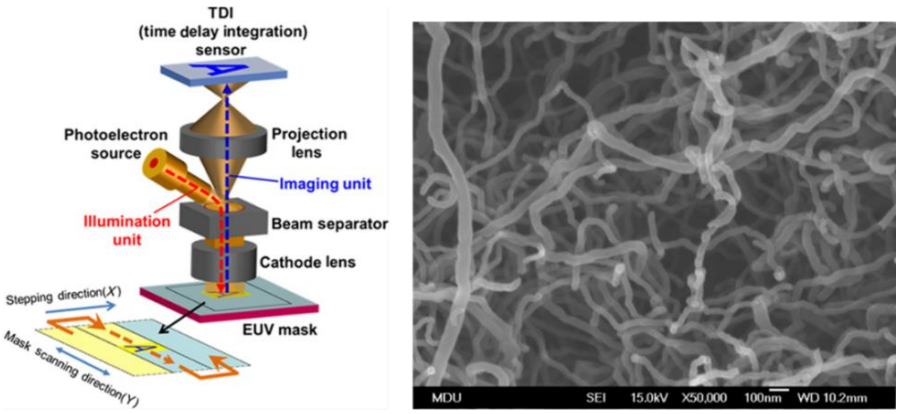

Figure 2.22: (a) Schematic diagram of SEM spectrometer[202] and (b) SEM image of the CNTs[203]

2.2.11.3 Electron dispersive X-ray spectroscopy

EDX allows the investigation of the elemental composition of a small scanned region of SCNMs from SEM. The presence of other elements, such as nitrogen, sulfur and phosphorus can be evaluated when dopants are used (from catalyst with heteroatoms).[204] EDX depend on the interaction between incident electron beam and the sample. These interactions give rise to X-rays characteristic of the elemental composition of the sample. The emitted characteristic X-rays follow the fundamental principle that each element has a unique atomic structure creating a unique set of its X-ray spectrum as represented in Figure 2.23.[205]

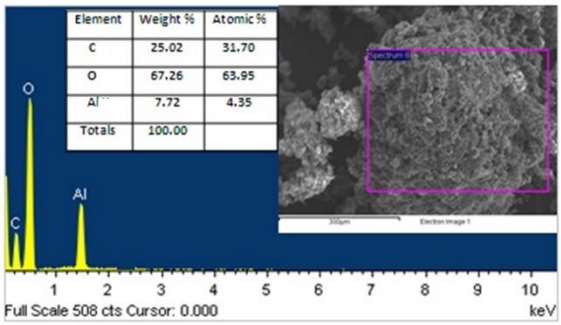

Figure 2.23: EDX spectrum and image of the CNTs[206]

2.2.11.4 Raman spectroscopy

Raman spectroscopy is a fast, convenient and non-destructive analysis technique. It is able to study liquid, solid and gaseous samples. It consists of laser source, sample illumination system, light collection optics, wavelength selector and detector. The sample is illuminated with laser source. It uses monochromatic light from laser source during inelastic scattering. Inelastic scattering refers to changes of frequency of photons in monochromatic light when it interact with a sample.[207] The sample absorbs the photons and then reemits them. The absorbed photons cause a transformation of electrons from low-energy state to high-energy state. The reemitted photon's frequency is shifted up or down as compared to the original monochromatic light (Raman effect). This shift gives information about rotational and vibrational frequency in molecules. Scattered lights are brought together by a lens and are sent to the wavelength selector in order to obtain a spectrum of a sample.[207]

The laser beam is regards as an oscillating electromagnetic wave which consist of electrical vector when it interacts with the sample, it causes electric dipole moment which changes the molecule. This deformation of molecule causes it to vibrate with characteristic frequency. The vibration is called nuclear displacement. In other words, the monochromatic light excites the molecules and convert it to oscillating dipoles which emit light into three different frequencies *i.e.* Rayleigh scattering, stokes and anti-stokes (Figure 2.24 a).[207] Rayleigh scattering occurs when a molecule which is Raman-inactive absorbs a photon. The molecule become excited and goes back to same frequency as an excitation source. Stokes occurs when the Raman-active molecule absorbs a photon (at a ground vibration level ($\nu = 0$). Some of the photon's energy is moved to Raman-active mode and the scattering light frequency's reduced. It normally occurs when the scattering radiation has lower frequency than the excitation radiation. Anti-stokes occurs when a photon is being absorbed by a Raman-active molecule, during their time of interaction, they are in the vibration state.[208] The excess energy is released from the Raman-active mode and the molecule goes back to their ground state vibrational mode. Their scattering radiations have a higher frequency when compared to the source radiation.

Raman spectroscopy is capable of analysing amorphous carbon, graphene sheet, activated carbon, carbon platelets, SWCNTs and MWCNTs.[209] MWCNTs possess a discrete Raman fingerprint and several bands are perceived which are controlled by the type of laser used. G-band (tangential modes – 1580 cm^{-1}) is represented by the first order Raman scattering. It

measures on how the carbon bond structure could deviate from ideal graphite sp^2 hybrid structure. The disorder-induced D-band is found around 1450 cm^{-1}.[210]

This technique can be used to quantify the relative fraction of impurities in the measured CNTs sample by using the ratio of disorder to graphitic band (D/G band) under fixed laser power density. It is used to assess molecular motion and fingers printing species. Its routine energy ranges from 200 – 4000 cm^{-1}.[211,212] The most used characteristic features are lower-frequency peak < 200 cm^{-1} (which represent the radial breathing mode), 1340 cm^{-1} (residual ill-organized graphite which is normal called D-line), 1500 and 1600 cm^{-1} (G-line) and a second order which is found between 2450 and 2650 $cm^{-1}$is assigned to the G′ mode (Figure 2.24 b).[211] The CNTs quality is recognized by the I_D/I_G ratio, where I_G represents the intensity of the G band whereas the I_D represents the intensity of the D band. The lower, the I_D/I_G ratio, higher the graphitic structural quality of the CNTs produced.[213]

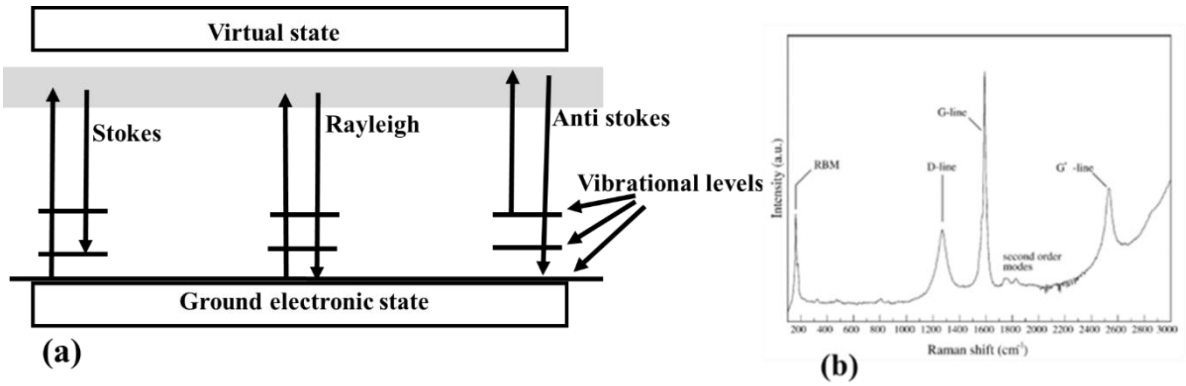

Figure 2.24: (a) Energy diagram for Raman and Rayleigh scattering[214] and (b) Raman spectrum showing the most characteristic features of CNTs: radial breathing mode (RBM) D-band and G'-band[211]

2.2.11.5 Thermogravimetric analysis

Thermogravimetric analysis (TGA) is used in the CNTs analysis in order determine the thermal stability. This is performed by monitoring the weight loss that occurs during the heating.[215] TGA consist of a thermobalance (microbalance), furnace, carrier gas system and a computer system (data acquisition and data processing).[207] A known mass (1 – 100 mg) of the CNTs sample is inserted in a crucible hanged from the micro-balance (Figure 2.25 a). It is loaded in the oven or furnace. The sample in the furnace is heated from ambient temperature up to 1000

°C at a heating rate between 0.1 to 100 °C min^{-1}. All of this is performed in the presence of air or inert gas (He, Ar or N_2) in order to prevent undesired reaction.[216] During the heating of the sample, the mass of the sample changes which cause a deflection of the beam. The deflection of the beam inserts a light shutter between the photodiode and lamp and produces current. The amplified photodiode current is monitored and transformed into weight-loss by the data processing system (thermocouple).[215,216]

The weight loss of the sample is represented in the form of a curve and their derivative weight loss curve is used to determine the actual temperature where the weight loss occurs. Oxidation temperature is affected by the length of carbon-carbon bond of the CNTs. Thermal stability is derived from oxidation temperature of the sample. TGA provides information about the amount of amorphous carbon, metal content and CNTs based on oxidation temperature. Initially any moisture or solvent will be evaporated at an oxidation temperature of 25-120 °C while amorphous carbon will be oxidized at 300-400 °C.[215] The oxidative temperature of about 500 to 600 °C is characteristic of SWCNTs and at 640 to 790 °C of pure MWCNTs (for instance Figure 2.25 b). The mass of the sample remaining after 790 °C indicate the metal content present in the sample.[216]

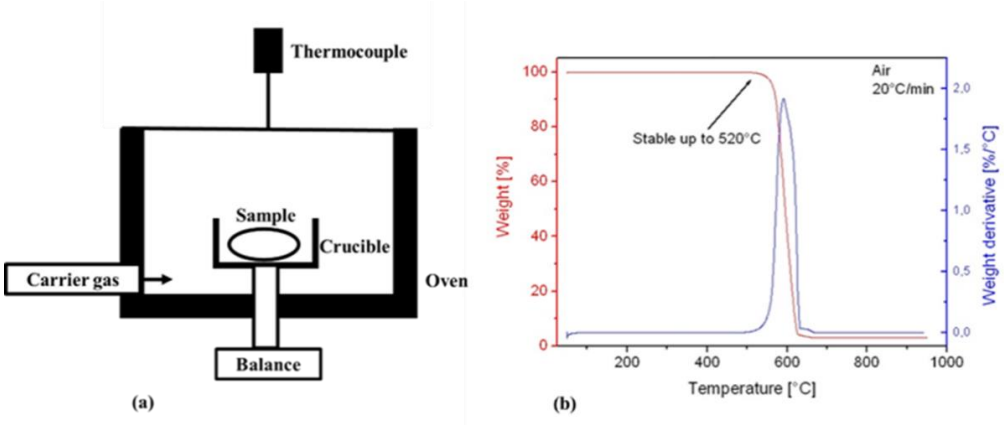

Figure 2.25: (a) Schematic diagram of how the TGA operates and (b) TGA thermogram of the MWCNTs [217]

2.2.11.6 Brunauer, Emmett and Teller analysis

Brunauer, Emmett and Teller analysis (BET) is used for the determination of the surface area and porosity. Surface area is the total sum of the surface area of individual particulates constituting the material.[218] Pore volume is the size of empty spaces in a material. The amount

of gas adsorbed at a given pressure allows determination of the surface area. BET theory involves extension of the Langmuir theory. Langmuir theory is based on monolayer molecular adsorption and multilayer adsorption. BET theory ignores inhomogeneities of the surface and lateral adsorbate-absorbate interactions. Before the CNTs are characterized using the BET method, they are firstly degassed in order to remove moisture. BET mostly uses nitrogen gas because it is readily available and it strongly interacts with many solid surface.

The BET equation is expressed by:

$$\frac{1}{V[\left(P_o/P\right)-1]} = \frac{C-1}{V_m\,C}\left(\frac{P}{P_o}\right) + \frac{1}{V_m\,C} \qquad (3)$$

In equation 3, V represent quantity of adsorbed gas, P and P_o represent the saturation and equilibrium pressure of the adsorbates, C represent the BET constant and V_m represent the quantity of the monolayer adsorbed gas. This method is used to calculate the surface area of the solid. V and P/P_o are measured by the BET analyser and V_m relates to surface area (it is converted to area). CNTs have a surface area of 264.08 $m^2\ g^{-1}$ and pore volume of 2.419 $cm^3\ g^{-1}$.[219]

2.2.12 Current and potential application of CNTs

The remarkable properties of CNTs have led to their use in composites,[220] energy storage,[221] fuel cells,[222] catalyst support[223] and drug delivery agents in medicine.[224]

2.2.12.1 Composites

CNTs are the strongest and stiffest known material in terms of tensile strength and elastic modulus, therefore, they are used as composite nanofibers in polymers to enhance the mechanical, electrical and thermal properties of the bulk materials.[225] The composite are used in bullet-proof vests. It has been reported, that functionalized-CNTs are also capable of improving tensile strength.[220] During the synthesis of the composite, the CNTs are mixed with the solution of the polymer and the solvent is removed by evaporation. Then the CNTs are pre-treated in order to enhance solubilisation.

2.2.12.2 Energy storage

SCNMs have been used in energy production and have a potential application in energy storage.[221] There are two elements that can be stored in CNTs, *i.e.* hydrogen[226,227] and lithium[228] and hence their use in capacitor[229] and solar cells.[230,231] They have been used as anodes in lithium ion based batteries and because of their small diameters they have a potential application in hydrogen storage.[227] They have also been used to make ideal vessel (storage vessels for hydrogen gas).[232] This is due to their high surface and abundant pore volume which potentially leads to CNTs being good adsorbents.

2.2.12.3 Fuel cells

Fuel cells have been used as a source of renewable energy and are a major subject for many researchers. The main fuel cell source is hydrogen gas because it is easily available unlike fossil-based power sources.[222] Major components of fuel cells are membrane, catalyst, catalyst support, catalyst layer, gas diffusion layer, and current collector. There are various fuel cell technologies such as proton exchange membrane fuel cells (PEMFCs),[233] alkaline fuel cells (AFCs),[234] direct methanol fuel cell (DMFCs),[235] phosphoric acid fuel cells (PAFCs),[236] and solid oxide fuel cells (SOFCs).[237] PEMFCs use a thin proton as a membrane.[62] AFCs use potassium hydroxide as an electrolyte. DMFCs use a membrane as electrolyte together with methanol at the anode. PAFCs use acidic electrolytes. SOFCs use solid ceramic electrolyte. Out of all the fuel cells, PMEFCs are advantageous because they can operate at low temperature and they do not need to be run when there is no demand for electricity.

The performances of these fuel cells are improved by using CNTs as the catalyst support. CNTs increase the reaction kinetics and the rate of oxygen reduction reaction. In order for the CNTs to be used as a catalyst supporter, a surface area of 500 m^2 g^{-1} for the MWCNTs and 1500 m^2 g^{-1} for the SWCNTs is required.[238] The good properties of the catalyst support, such as high surface area, low resistance, and high mechanical strength and chemical stability, are essential for catalytic electrodes.[239] Some of the challenges about using fuel cell technology are the cost of fuel cell (because of waste management and platinum catalyst loading).

2.2.12.4 Catalyst support

Catalyst is a substance which is used in small amount in order to increase the reaction rate. They can be loaded on another material which has a high surface area so that it can serve as a support and form a supported catalyst of a system. The supported catalyst is used to control porous structure, assist in catalysis and to improve mechanical strength.[223] CNTs have large surface area which enable them to be easily loaded with metal on their surface.[240] Metals such as palladium and platinum had been used for loading. Mostly palladium is used because it is less sensitive to water or oxygen[241] and it is relatively cheaper compared to platinum and other platinum group metals (PGMs). The challenge of making supported nanoparticle is to avoid agglomeration. The examples of catalyst support are Ni/CNTs and Pt/CNTs catalyst.[192,241]

2.2.12.5 Medicine

In medicine, CNTs have been shown to have a potential to act as a tool for cancer diagnosis[242] and therapy.[224] Polyphosphazene platinum is one of the anticancer drug which is given with nanotubes.[243] It has been reported to show enhanced permeability and retention in the brain as a result of controlled lipophilicity of nanotubes. CNTs have been also tested for drug delivery to the system *e.g.* Hydro-gel (gelatin CNTs mixture) which is used as a carrier system for biomedicals.[244] In tablet manufacturing, CNTs are used as glodants or lubricants because of their nanosize and sliding nature of graphite layer which are bound with van der Waals forces.[245] CNTs have been used to manipulate genes in the process of bioimaging genomes[246] and tissue engineering.[247] In biology CNTs can be functionalised with a biomedical such as a protein or lipid.[248] These modified CNTs can be used to mimic certain biological processes depending on biomolecule attached onto the wall of the CNTs.

2.2.12.6 Field emission device

CNTs are used in field emission device because they contain metal which act as an emission source[249] and can operate at lower voltage. They have high mechanical strength and high chemical stability.[250] Their fabrication process is simple and they are anticipated to create field emission devices with low power usage and low cost. CNTs doped with nitrogen displays some interesting electronic properties.[251] Due to their electrical properties, they can be used in field emission display[252,253] and field emission lamps.[254]

2.3 References

1. S. A. Miller, J. A. Tebboth and J. F. Tremaine, *Journal of the Chemical Society*, 1952, 4, 632-635.
2. J. D. Dunitz and L. E. Orgel, *Nature*, 1953, 171, 121-122.
3. T. J. Johnson, K. Folting, W. E. Streib, J. D. Martin, J. C. Huffman, S. A. Jackson, O. Eisenstein and K. G. Caulton, *Inorganic Chemistry*, 1995, 34, 488-499.
4. S. Harder and M. H. Prosenc, *Angewandte Chemie International Edition in English*, 1994, 33, 1744-1746.
5. T. J. Kealy and P. L. Pauson, *Nature* 1951, 168, 1039-1040.
6. L. Pauling, *The Nature of the Chemical Bond*, Cornell University Press Ithaca, New York, 1960, vol. 3, p. 175.
7. W. B. Jensen, *Journal of Chemical Education*, 2005, 82, 28.
8. C. Famiglietti and E. J. Baerends, *Chemical Physics*, 1981, 62, 407-421.
9. P. Seiler and J. D. Dunitz, *Acta Crystallographica Section B*, 1980, 36, 2255-2260.
10. E. R. Lippincott and R. D. Nelson, *Spectrochimica Acta*, 1958, 10, 307-329.
11. S. Barlow and S. R. Marder, *Chemical Communications*, 2000, 1555-1562.
12. C. P. Deck and K. Vecchio, *Carbon*, 2006, 44, 267-275.
13. A. H. Castro Neto, *Materials Today*, 2010, 13, 12-17.
14. D. Cox, K. Reichmann and A. Kaldor, *Journal of Chemical Physics*, 1988, 88, 1588-1597.
15. D. Sederberg, L. Bryan and N. Giordano, *Nature*, 2009, 1, 8-25.
16. H. W. Kroto, J. R. Heath, S. C. O'Brien, R. F. Curl and R. E. Smalley, *Nature* 1985, 318, 162-163.
17. H. Kroto and K. McKay, *Nature*, 1988, 331, 328-331.
18. H. D. Beckhaus, S. Verevkin, C. Ruechardt, F. Diederich, C. Thilgen, H. U. ter Meer, H. Mohn and W. Mueller, *Angewandte Chemie International Edition*, 1994, 106, 1033-1035

19. H. W. Kroto, J. R. Heath, S. C. O'Brien, R. F. Curl and R. E. Smalley, *Journal of Astrophysics*, 1987, 314, 352-355.

20. K. Komatsu, K. Fujiwara, T. Tanaka and Y. Murata, *Carbon*, 2000, 38, 1529-1534.

21. C. J. Brabec, S. Gowrisanker, J. J. Halls, D. Laird, S. Jia and S. P. Williams, *Advanced Materials*, 2010, 22, 3839-3856.

22. B. C. Thompson and J. M. Frechet, *Angewandte Chemie International Edition*, 2008, 47, 58-77.

23. Y. Zhao, Y.-H. Kim, A. C. Dillon, M. J. Heben and S. B. Zhang, *Physical Review Letters*, 2005, 94, 155504.

24. E. B. Zeinalov and G. Koßmehl, *Polymer Degradation and Stability*, 2001, 71, 197-202.

25. S. D. Kushch, N. S. Kuyunko, P. A. Vityaz', A. I. Komarov and V. I. Komarova, *Russian Journal of General Chemistry*, 2010, 80, 1086-1090.

26. R. Bakry, R. M. Vallant, M. Najam-ul-Haq, M. Rainer, Z. Szabo, C. W. Huck and G. K. Bonn, *International Journal of Nanomedicine*, 2007, 2, 639-649.

27. W. R. Davis, R. J. Slawson and G. R. Rigby, *Nature*, 1953, 171, 756-756.

28. A. V. Rode, E. G. Gamaly and B. Luther-Davies, *Applied Physics A*, 2000, 70, 135-144.

29. Y. Zhang and X. Sun, *Advanced Materials*, 2007, 19, 961-964.

30. M. Endo and H. W. Kroto, *Journal of Physical Chemistry*, 1992, 96, 6941-6944.

31. A. Chambers, C. Park, R. T. K. Baker and N. M. Rodriguez, *Journal of Physical Chemistry B*, 1998, 102, 4253-4256.

32. E. Hammel, X. Tang, M. Trampert, T. Schmitt, K. Mauthner, A. Eder and P. Potschke, *Carbon*, 2004, 42, 1153-1158.

33. http://sem.elte.hu/en/index.php?p=introductory_images#11, (accessed 11 March 2015).

34. Z. L. Tsakadze, I. Levchenko, K. Ostrikov and S. Xu, *Carbon*, 2007, 45, 2022-2030.

35. N. Shang, W. I. Milne and X. Jiang, *Journal of the American Chemical Society*, 2007, 129, 8907-8911.

36. K. Ajima, M. Yudasaka, T. Murakami, A. Maigné, K. Shiba and S. Iijima, *Molecular Pharmaceutics*, 2005, 2, 475-480.

37. C. Cioffi, S. Campidelli, C. Sooambar, M. Marcaccio, G. Marcolongo, M. Meneghetti, D. Paolucci, F. Paolucci, C. Ehli, G. M. A. Rahman, V. Sgobba, D. M. Guldi and M. Prato, *Journal of the American Chemical Society*, 2007, 129, 3938-3945.

38. N. Sano, J. Nakano and T. Kanki, *Carbon*, 2004, 42, 686-688.

39. E. Bekyarova, K. Murata, M. Yudasaka, D. Kasuya, S. Iijima, H. Tanaka, H. Kahoh and K. Kaneko, *Journal of Physical Chemistry B*, 2003, 107, 4681-4684.

40. G. Rotas, A. S. D. Sandanayaka, N. Tagmatarchis, T. Ichihashi, M. Yudasaka, S. Iijima and O. Ito, *Journal of the American Chemical Society*, 2008, 130, 4725-4731.

41. Y. Shao, G. Yin and Y. Gao, *Journal of Power Sources*, 2007, 171, 558-566.

42. A. V. Rode, S. T. Hyde, E. G. Gamaly, R. G. Elliman, D. R. McKenzie and S. Bulcock, *Applied Physics A*, 1999, 69, 755-758.

43. http://www.microphase.jp/e/e_data0107.html, (accessed 11 March 2015).

44. J. Geng, C. Ducati, D. S. Shephard, M. Chhowalla, B. F. Johnson and J. Robertson, *Chemical Communications*, 2002, 1, 1112-1113.

45. P. Zhang, Z.-A. Qiao and S. Dai, *Chemical Communications*, 2015, 51, 9246-9256.

46. http://www.bo.imm.cnr.it/site/book/export/htmml/537, (accessed 11 March 2015).

47. D. Fejes and K. Hernadi, *Materials*, 2010, 3, 2618.

48. M. Glerup, J. Steinmetz, D. Samaille, O. Stéphan, S. Enouz, A. Loiseau, S. Roth and P. Bernier, *Chemical Physics Letters*, 2004, 387, 193-197.

49. P. Serp, R. Feurer, P. Kalck, Y. Kihn, J. L. Faria and J. L. Figueiredo, *Carbon*, 2001, 39, 621-626.

50. R. Chetty, S. Kundu, W. Xia, M. Bron, W. Schuhmann, V. Chirila, W. Brandl, T. Reinecke and M. Muhler, *Electrochimica Acta*, 2009, 54, 4208-4215.

51. N. J. Coville, S. D. Mhlanga, E. N. Nxumalo and A. Shaikjee, *South African Journal of Science*, 2011, 107, 01-15.

52. Y. Wang, F. Su, J. Y. Lee and X. Zhao, *Chemistry of Materials*, 2006, 18, 1347-1353.

53. Z. Wang and Z. Kang, *Carbon*, 1997, 35, 419-426.

54. M. Inagaki, *Carbon*, 1997, 35, 711-713.

55. H. P. Boehm, *Carbon*, 2002, 40, 145-149.

56. F. Ma, H. Zhao, L. Sun, Q. Li, L. Huo, T. Xia, S. Gao, G. Pang, Z. Shi and S. Feng, *Journal of Materials Chemistry*, 2012, 22, 13464-13468.

57. B. R. Selvi, D. Jagadeesan, B. S. Suma, G. Nagashankar, M. Arif, K. Balasubramanyam, M. Eswaramoorthy and T. K. Kundu, *Nano Letters*, 2008, 8, 3182-3188.

58. E. Auer, A. Freund, J. Pietsch and T. Tacke, *Applied Catalysis A: General*, 1998, 173, 259-271.

59. X. Wang, P. Hu, Y. Fangli and L. Yu, *Journal of Physical Chemistry C*, 2007, 111, 6706-6712.

60. J. Jiang, Q. Gao, Z. Zheng, K. Xia and J. Hu, *International Journal of Hydrogen Energy*, 2010, 35, 210-216.

61. Z. Wen, Q. Wang, Q. Zhang and J. Li, *Electrochemistry Communications*, 2007, 9, 1867-1872.

62. X. Chen, K. Kierzek, Z. Jiang, H. Chen, T. Tang, M. Wojtoniszak, R. J. Kalenczuk, P. K. Chu and E. Borowiak-Palen, *Journal of Physical Chemistry C*, 2011, 115, 17717-17724.

63. S. Iijima and T. Ichihashi, *Nature*, 1993, 363, 603-605.

64. L. V. Radushkevich and V. M. Luk'yanovich, *Zhurnal Fizicheskoi Khimii*, 1952, 26, 88-95.

65. S. Iijima, *Nature* 1991, 354, 56-58.

66. T. Ebbesen and P. Ajayan, *Nature*, 1992, 358, 220-222.

67. R. Saito, M. Fujita, G. Dresselhaus and M. S. Dresselhaus, *Applied Physics Letters*, 1992, 60, 2204-2206.

68. D. S. Bethune, C. H. Klang, M. S. de Vries, G. Gorman, R. Savoy, J. Vazquez and R. Beyers, *Nature*, 1993, 363, 605-607.

69. N. G. Chopra, R. J. Luyken, K. Cherrey, V. H. Crespi, M. L. Cohen, S. G. Louie and A. Zettl, *Science*, 1995, 269, 966-967.

70. I. W. Locke, A. D. Darwish, H. W. Kroto, K. Prassides, R. Taylor and D. R. M. Walton, *Chemical Physics Letters*, 1994, 225, 186-190.

71. H. Dai, A. G. Rinzler, P. Nikolaev, A. Thess, D. T. Colbert and R. E. Smalley, *Chemical Physics Letters*, 1996, 260, 471-475.

72. M. Endo, T. Hayashi, Y. Ahm Kim, M. Terrones and M. S. Dresselhaus, *The Royal Society*, 2004, 362, 2223-2238.

73. M. S. Dresselhaus, G. Dresselhaus and R. Saito, *Carbon*, 1995, 33, 883-891.

74. N. Hamada, S.-i. Sawada and A. Oshiyama, *Physical Review Letters*, 1992, 68, 1579.

75. V. Choudhary and A. Gupta, *Polymer-Carbon Nanotubes Nanocomposites*, 2011, 4, 203-245.

76. I. Mönch, A. Meye, A. Leonhardt, K. Krämer, R. Kozhuharova, T. Gemming, M. P. Wirth and B. Büchner, *Journal of Magnetism and Magnetic Materials*, 2005, 290–291, 276-278.

77. M. L. Terranova, V. Sessa and M. Rossi, *Chemical Vapour Deposition*, 2006, 12, 315-325.

78. C. Laurent, E. Flahaut, A. Peigney and A. Rousset, *New Journal of Chemistry*, 1998, 22, 1229-1237.

79. C. H. A. Wong and M. Pumera, *Physical Chemistry Chemical Physics*, 2013, 15, 7755-7759.

80. M. Dresselhaus, G. Dresselhaus and A. Jorio, *Annual Review of Material Research*, 2004, 34, 247-278.

81. P. Mahanandia, J. J. Schneider, M. Engel, B. Stühn, S. V. Subramanyam and K. K. Nanda, *Beilstein Journal of Nanotechnology*, 2011, 2, 293-301.

82. Z. Spitalsky, D. Tasis, K. Papagelis and C. Galiotis, *Progress in Polymer Science*, 2010, 35, 357-401.

83. J. P. Lu, *Physical Review Letters*, 1997, 79, 1297.

84. J. Hone, M. C. Llaguno, M. J. Biercuk, A. T. Johnson, B. Batlogg, Z. Benes and J. E. Fischer, *Applied Physics A*, 2002, 74, 339-343.

85. G. D. Nessim, *Nanoscale*, 2010, 2, 1306-1323.

86. S. Huang, X. Cai and J. Liu, *Journal of the American Chemical Society*, 2003, 125, 5636-5637.

87. S. Ravindran, S. Chaudhary, B. Colburn, M. Ozkan and C. S. Ozkan, *Nano Letters*, 2003, 3, 447-453.

88. C. Li and T.-W. Chou, *International Journal of Solids and Structures*, 2003, 40, 2487-2499.

89. J. P. Salvetat, J. M. Bonard, N. H. Thomson, A. J. Kulik, L. Forró, W. Benoit and L. Zuppiroli, *Applied Physics A*, 1999, 69, 255-260.

90. A. Leonhardt, S. Hampel, C. Mueller, I. Moench, R. Koseva, M. Ritschel, D. Elefant, K. Biedermann and B. Buechner, *Chemical Vapour Deposition*, 2006, 12, 380-387.

91. S. Hampel, A. Leonhardt, D. Selbmann, K. Biedermann, D. Elefant, C. Müller, T. Gemming and B. Büchner, *Carbon*, 2006, 44, 2316-2322.

92. R. Kozhuharova, M. Ritschel, I. Mönch, T. Mühl, A. Leonhardt, A. Graff and C. M. Schneider, *Fullerenes, Nanotubes and Carbon Nanostructures*, 2005, 13, 347-353.

93. H. Cheng, F. Li, G. Su, H. Pan, L. He, X. Sun and M. Dresselhaus, *Applied Physics Letters*, 1998, 72, 3282-3284.

94. U. Weissker, S. Hampel, A. Leonhardt and B. Buechner, *Materials*, 2010, 3, 4387-4427.

95. R. S. Ruoff and D. C. Lorents, *Carbon*, 1995, 33, 925-930.

96. S. Basu, Y. Chen and Z. Zhang, *International Journal of Energy Research*, 2007, 31, 689-716.

97. M. J. McAllister, J.-L. Li, D. H. Adamson, H. C. Schniepp, A. A. Abdala, J. Liu, M. Herrera-Alonso, D. L. Milius, R. Car, R. K. Prud'homme and I. A. Aksay, *Chemistry of Materials*, 2007, 19, 4396-4404.

98. D. L. Ellis and D. L. McDaniels, *Thermal Conductivity and Thermal Expansion of Graphite Fiber/Copper Matrix Composites*, Metallurgical and Materials Transactions A, Washington, DC, 1991, vol. 24, pp. 43-52.

99. V. Choudhary, B. P. Singh and R. B. Mathur, *Syntheses and Applications of Carbon Nanotubes and Their Composites*, Intech Open Science, Dr Satoru Suzuki edn., 2013, vol. 10, ch. 9, pp. 193-222.

100. W. Kratschmer, L. D. Lamb, K. Fostiropoulos and D. R. Huffman, *Nature*, 1990, 347, 354-358.

101. K. Subrahmanyam, L. Panchakarla, A. Govindaraj and C. Rao, *Journal of Physical Chemistry C*, 2009, 113, 4257-4259.

102. Y. Li, S. Xie, W. Zhou, D. Tang, Z. Liu, X. Zou and G. Wang, *Carbon*, 2001, 39, 1429-1431.

103. J. Prasek, J. Drbohlavova, J. Chomoucka, J. Hubalek, O. Jasek, V. Adam and R. Kizek, *Journal of Materials Chemistry*, 2011, 21, 15872-15884.

104. Y. Saito, T. Yoshikawa, M. Okuda, N. Fujimoto, K. Sumiyama, K. Suzuki, A. Kasuya and Y. Nishina, *Journal of Physics and Chemistry of Solids*, 1993, 54, 1849-1860.

105. X. Zhao, M. Ohkohchi, H. Shimoyama and Y. Ando, *Journal of Crystal Growth*, 1999, 198–199, 934-938.

106. J. Qiu, Y. Li, Y. Wang, C. Liang, T. Wang and D. Wang, *Carbon*, 2003, 41, 767-772.

107. T. Guo, P. Nikolaev, A. G. Rinzler, D. Tomanek, D. T. Colbert and R. E. Smalley, *Journal of Physical Chemistry*, 1995, 99, 10694-10697.

108. A. Thess, R. Lee, P. Nikolaev, H. Dai, P. Petit, J. Robert, C. Xu, Y. H. Lee, S. G. Kim, D. T. Rinzler and G. E. Colbert, *Science* 1996, 273, 483-487.

109. E. Muñoz, W. K. Maser, A. M. Benito, M. T. Martínez, G. F. de la Fuente, Y. Maniette, A. Righi, E. Anglaret and J. L. Sauvajol, *Carbon*, 2000, 38, 1445-1451.

110. W. K. Maser, E. Muñoz, A. M. Benito, M. T. Martínez, G. F. de la Fuente, Y. Maniette, E. Anglaret and J. L. Sauvajol, *Chemical Physics Letters*, 1998, 292, 587-593.

111. S. Henley, J. Anguita and S. R. Silva, *Encyclopedia of Nanotechnology*, ed. B. Bhushan, Springer Netherlands, 2012, pp. 2615-2621.

112. M. Terrones, N. Grobert, J. Olivares, J. Zhang, H. Terrones, K. Kordatos, W. Hsu, J. Hare, P. Townsend and K. Prassides, *Nature*, 1997, 388, 52-55.

113. M. José-Yacamán, M. Miki-Yoshida, L. Rendón and J. G. Santiesteban, *Applied Physics Letters*, 1993, 62, 202-204.

114. S. B. Sinnott, R. Andrews, D. Qian, A. M. Rao, Z. Mao, E. C. Dickey and F. Derbyshire, *Chemical Physics Letters*, 1999, 315, 25-30.

115. B. E. Huff and F. Moghadam, *Google Patents*, 1999, US5872064 A, 08/891,268.

116. S. Hiromu, T. Keiichirou, N. Yoshiki and F. Naoji, *Japanese Journal of Applied Physics*, 1990, 29, 34.

117. A. C. Dillon, A. H. Mahan, P. A. Parilla, J. L. Alleman, M. J. Heben, K. M. Jones and K. E. H. Gilbert, *Nano Letters*, 2003, 3, 1425-1429.

118. Z. P. Huang, J. W. Xu, Z. F. Ren, J. H. Wang, M. P. Siegal and P. N. Provencio, *Applied Physics Letters*, 1998, 73, 3845-3847.

119. A. Szabo, C. Perri, A. Csato, G. Giordano, D. Vuono and J. B. Nagy, *Materials*, 2010, 3, 3092-3140.

120. W. I. Milne, K. B. K. Teo, G. A. J. Amaratunga, P. Legagneux, L. Gangloff, J. P. Schnell, V. Semet, V. T. Binh and O. Groening, *Journal of Material Chemistry*, 2004, 14, 933-943.

121. V. O. Nyamori, S. D. Mhlanga and N. J. Coville, *Journal of Organometallic Chemistry*, 2008, 693, 2205-2222.

122. S. D. Mhlanga, K. C. Mondal, R. Carter, M. J. Witcomb and N. J. Coville, *South African Journal of Chemistry*, 2009, 62, 67-76.

123. R. Kamalakaran, M. Terrones, T. Seeger, P. Kohler-Redlich, M. Rühle, Y. A. Kim, T. Hayashi and M. Endo, *Applied Physics Letters*, 2000, 77, 3385-3387.

124. V. Ivanov, A. Fonseca, J. B. Nagy, A. Lucas, P. Lambin, D. Bernaerts and X. B. Zhang, *Carbon*, 1995, 33, 1727-1738.

125. K. Mukhopadhyay, A. Koshio, T. Sugai, N. Tanaka, H. Shinohara, Z. Konya and J. B. Nagy, *Chemical Physics Letters*, 1999, 303, 117-124.

126. Y. C. Choi, Y. M. Shin, Y. H. Lee, B. S. Lee, G.-S. Park, W. B. Choi, N. S. Lee and J. M. Kim, *Applied Physics Letters*, 2000, 76, 2367-2369.

127. B. C. Satishkumar, A. Govindaraj and C. N. R. Rao, *Chemical Physics Letters*, 1999, 307, 158-162.

128. G. Gulino, R. Vieira, J. Amadou, P. Nguyen, M. J. Ledoux, S. Galvagno, G. Centi and C. Pham-Huu, *Applied Catalysis A: General*, 2005, 279, 89-97.

129. M. S. Mohlala, X.-Y. Liu and N. J. Coville, *Journal of Organometallic Chemistry*, 2006, 691, 4768-4772.

130. M. S. Mohlala, X.-Y. Liu, M. J. Witcomb and N. J. Coville, *Applied Organometallic Chemistry*, 2007, 21, 275-280.

131. H. M. Cheng, F. Li, G. Su, H. Y. Pan, L. L. He, X. Sun and M. S. Dresselhaus, *Applied Physics Letters*, 1998, 72, 3282-3284.

132. A. Cao, H. Zhu, X. Zhang, X. Li, D. Ruan, C. Xu, B. Wei, J. Liang and D. Wu, *Chemical Physics Letters*, 2001, 342, 510-514.

133. A. M. Cassell, J. A. Raymakers, J. Kong and H. Dai, *Journal of Physical Chemistry B*, 1999, 103, 6484-6492.

134. Z. F. Ren, Z. P. Huang, J. W. Xu, J. H. Wang, P. Bush, M. P. Siegal and P. N. Provencio, *Science*, 1998, 282, 1105-1107.

135. P. Nikolaev, M. J. Bronikowski, R. K. Bradley, F. Rohmund, D. T. Colbert, K. A. Smith and R. E. Smalley, *Chemical Physics Letters*, 1999, 313, 91-97.

136. M. S. Meier, R. Andrews, D. Jacques, K. B. Cassity and D. Qian, *Journal of Materials Chemistry*, 2008, 18, 4143-4145.

137. G. G. Tibbetts, D. W. Gorkiewicz and R. L. Alig, *Carbon*, 1993, 31, 809-814.

138. Y. Murakami, Y. Miyauchi, S. Chiashi and S. Maruyama, *Chemical Physics Letters*, 2003, 377, 49-54.

139. R. Tenne, *Angewandte Chemie International Edition*, 2003, 42, 5124-5132.

140. Y. Li, J. Liu, Y. Wang and Z. L. Wang, *Chemistry of Materials*, 2001, 13, 1008-1014.

141. B. C. Liu, S. C. Lyu, S. I. Jung, H. K. Kang, C. W. Yang, J. W. Park, C. Y. Park and C. J. Lee, *Chemical Physics Letters*, 2004, 383, 104-108.

142. K. Kakehi, S. Noda, S. Maruyama and Y. Yamaguchi, *Applied Surface Science*, 2008, 254, 6710-6714.

143. C. Singh, T. Quested, C. B. Boothroyd, P. Thomas, I. A. Kinloch, A. I. Abou-Kandil and A. H. Windle, *Journal of Physical Chemistry B*, 2002, 106, 10915-10922.

144. P. T. A. Reilly and W. B. Whitten, *Carbon*, 2006, 44, 1653-1660.

145. M. S. Mohlala, X.-Y. Liu, J. M. Robinson and N. J. Coville, *Organometallics*, 2005, 24, 972-976.

146. C. J. Lee, S. C. Lyu, H.-W. Kim, J. H. Lee and K. I. Cho, *Chemical Physics Letters*, 2002, 359, 115-120.

147. V. O. Nyamori, E. N. Nxumalo and N. J. Coville, *Journal of Organometallic Chemistry*, 2009, 694, 2222-2227.

148. V. O. Nyamori, M. D. Bala and D. S. Mkhize, *Journal of Organometallic Chemistry*, 2015, 780, 13-19.

149. J. E. Herrera, L. Balzano, A. Borgna, W. E. Alvarez and D. E. Resasco, *Journal of Catalysis*, 2001, 204, 129-145.

150. M. S. Mohlala and N. J. Coville, *Journal of Organometallic Chemistry*, 2007, 692, 2965-2970.

151. L. F. Su, J. N. Wang, F. Yu, Z. M. Sheng, H. Chang and C. Pak, *Chemical Physics Letters*, 2006, 420, 421-425.

152. J. Qiu, Y. An, Z. Zhao, Y. Li and Y. Zhou, *Fuel Processing Technology*, 2004, 85, 913-920.

153. A. Moisala, A. G. Nasibulin, D. P. Brown, H. Jiang, L. Khriachtchev and E. I. Kauppinen, *Chemical Engineering Science*, 2006, 61, 4393-4402.

154. M. Mazaheri, D. Mari, Z. R. Hesabi, R. Schaller and G. Fantozzi, *Composites Science and Technology*, 2011, 71, 939-945.

155. S. Maruyama, R. Kojima, Y. Miyauchi, S. Chiashi and M. Kohno, *Chemical Physics Letters*, 2002, 360, 229-234.

156. D. L. X. Bai, Y. Wang, and J. Liang, *Tsinghua Science Technology*, 2005, 10, 729.

157. K. Kuwana and K. Saito, *Carbon*, 2005, 43, 2088-2095.

158. C. Singh, M. S. P. Shaffer and A. H. Windle, *Carbon*, 2003, 41, 359-368.

159. C.-L. Sun, H.-W. Wang, M. Hayashi, L.-C. Chen and K.-H. Chen, *Journal of the American Chemical Society*, 2006, 128, 8368-8369.

160. M. Jung, K. Yong Eun, J.-K. Lee, Y.-J. Baik, K.-R. Lee and J. Wan Park, *Diamond and Related Materials*, 2001, 10, 1235-1240.

161. A. H. Nevidomskyy, G. Csányi and M. C. Payne, *Physical review letters*, 2003, 91, 105502.

162. M. Yudasaka, R. Kikuchi, Y. Ohki and S. Yoshimura, *Carbon*, 1997, 35, 195-201.

163. C. Ewels and M. Glerup, *Journal of Nanoscience and Nanotechnology*, 2005, 5, 1345-1363.

164. E. N. Nxumalo, V. P. Chabalala, V. O. Nyamori, M. J. Witcomb and N. J. Coville, *Journal of Organometallic Chemistry*, 2010, 695, 1451-1457.

165. R. Droppa Jr, P. Hammer, A. C. M. Carvalho, M. C. dos Santos and F. Alvarez, *Journal of Non-Crystalline Solids*, 2002, 299–302, 874-879.

166. J. Arbiol, B. Kalache, P. R. i Cabarrocas, J. R. Morante and A. F. i Morral, *Nanotechnology*, 2007, 18, 305606.

167. Y. M. Tairov, V. F. Tsvetkov and I. I. Khlebnikov, *Journal of Crystal Growth*, 1973, 20, 155-157.

168. S. Huang, M. Woodson, R. Smalley and J. Liu, *Nano Letters*, 2004, 4, 1025-1028.

169. M. J. Height, J. B. Howard, J. W. Tester and J. B. Vander Sande, *Journal of Physical Chemistry B*, 2005, 109, 12337-12346.

170. M. H. Kuang, Z. L. Wang, X. D. Bai, J. D. Guo and E. G. Wang, *Applied Physics Letters*, 2000, 76, 1255-1257.

171. Z. L. Wang and Z. C. Kang, *Philosophical Magazine Part B*, 1996, 74, 51-69.

172. S. Amelinckx, X. B. Zhang, D. Bernaerts, X. F. Zhang, V. Ivanov and J. B. Nagy, *Science* 1994, 265, 635-639.

173. A. A. Puretzky, D. B. Geohegan, S. Jesse, I. N. Ivanov and G. Eres, *Applied Physics A*, 2005, 81, 223-240.

174. P. J. F. Harris, *Carbon*, 2007, 45, 229-239.

175. N. M. Rodriguez, A. Chambers and R. T. K. Baker, *Langmuir*, 1995, 11, 3862-3866.

176. J. P. Gore and A. Sane, *Flame Synthesis of Carbon Nanotubes*, 2011, 6, 122–132.

177. P. X. Hou, S. Bai, Q. H. Yang, C. Liu and H. M. Cheng, *Carbon*, 2002, 40, 81-85.

178. T. W. Ebbesen, *Physics Today*, 1996, 49, 26-35.

179. A. G. Rinzler, J. Liu, H. Dai, P. Nikolaev, C. B. Huffman, F. J. Rodríguez-Macías, P. J. Boul, A. H. Lu, D. Heymann, D. T. Colbert, R. S. Lee, J. E. Fischer, A. M. Rao, P. C. Eklund and R. E. Smalley, *Applied Physics A*, 1998, 67, 29-37.

180. L. Yu, Z. Xiaobin, L. Junhang, H. Wanzhen, C. Jipeng, L. Zhiqiang, L. Ting, L. Fu, X. Guoliang, K. Xiaoxing, L. Lin and J. G. Herman, *Nanotechnology*, 2004, 15, 1645.

181. A. J. Blanch, C. E. Lenehan and J. S. Quinton, *Carbon*, 2011, 49, 5213-5228.

182. E. E. Tkalya, M. Ghislandi, G. de With and C. E. Koning, *Current Opinion in Colloid & Interface Science*, 2012, 17, 225-232.

183. K. B. Shelimov, R. O. Esenaliev, A. G. Rinzler, C. B. Huffman and R. E. Smalley, *Chemical Physics Letters*, 1998, 282, 429-434.

184. R. Andrews, D. Jacques, D. Qian and E. C. Dickey, *Carbon*, 2001, 39, 1681-1687.

185. W. Huang, Y. Wang, G. Luo and F. Wei, *Carbon*, 2003, 41, 2585-2590.

186. N. Dementev, S. Osswald, Y. Gogotsi and E. Borguet, *Journal of Materials Chemistry*, 2009, 19, 7904-7908.

187. S. Osswald, G. Yushin, V. Mochalin, S. O. Kucheyev and Y. Gogotsi, *Journal of the American Chemical Society*, 2006, 128, 11635-11642.

188. A. Hirsch and O. Vostrowsky, *Functional Molecular Nanostructures*, ed. A. D. Schlüter, Springer Berlin Heidelberg, 2005, vol. 245, ch. 5, pp. 193-237.

189. H. Kuzmany, A. Kukovecz, F. Simon, M. Holzweber, C. Kramberger and T. Pichler, *Synthetic Metals*, 2004, 141, 113-122.

190. L. Meng, C. Fu and Q. Lu, *Progress in Natural Science*, 2009, 19, 801-810.

191. C. Zhi, Y. Bando, C. Tang, S. Honda, K. Sato, H. Kuwahara and D. Golberg, *Angewandte Chemie International Edition*, 2005, 44, 7932-7935.

192. L. M. Ombaka, P. Ndungu and V. O. Nyamori, *Catalysis Today*, 2013, 217, 65-75.

193. C.-Y. Hu, Y.-J. Xu, S.-W. Duo, R.-F. Zhang and M.-S. Li, *Journal of the Chinese Chemical Society*, 2009, 56, 234-239.

194. P. R. Somani and M. Umeno, *Modern Research and Educational Topics in Microscopy*, 2007, 3, 634-642.

195. D. Geng, S. Yang, Y. Zhang, J. Yang, J. Liu, R. Li, T.-K. Sham, X. Sun, S. Ye and S. Knights, *Applied Surface Science*, 2011, 257, 9193-9198.

196. D. B. Williams and C. B. Carter, *The transmission electron microscope*, Springer, United State, 1996, vol. 2, pp. 3-17.

197. Z. Wang, *Journal of Physical Chemistry B*, 2000, 104, 1153-1175.

198. J. Geng, D. A. Jefferson and B. F. Johnson, *Chemical Communications*, 2004, 2442-2443.

199. J. F. Colomer, L. Henrard, P. Lambin and G. Van Tendeloo, *The European Physical Journal B - Condensed Matter and Complex Systems*, 2002, 27, 111-118.

200. http://binoculas.net/scanning-and-transmission-electron-microscope/, (accessed 4 June 2015).

201. J.-M. Bonard, K. A. Dean, B. F. Coll and C. Klinke, *Physical Review Letters*, 2002, 89, 197602.

202. R. Hirano, S. Iida, T. Amano, T. Terasawa, H. Watanabe, M. Hatakeyama, T. Murakami and K. Terao, *Journal of Micro/Nanolithography, MEMS, and MOEMS*, 2014, 13, 013009-013009.

203. Y.-H. Nien, *Carbon Nanotubes-Polymer Nanocomposites*, INTECH Open Access Publisher, Croatia, 2011, vol. 1, pp. 367-378.

204. W. Z. Li, S. S. Xie, L. X. Qian and B. H. Chang, *Science*, 1996, 274, 1701-1703.

205. D. Shindo and T. Oikawa, *Analytical Electron Microscopy for Materials Science*, Springer Japan, 2002, vol. 1, pp. 81-102.

206. T. A. Saleh, *Applied Surface Science*, 2013, 256, 298-304.

207. D. A. Skoog, F. J. Holler and S. R. Crouch, *Principles of Analytical Chemistry*, Thomson Brooks/Cole, Canada, 6th edn., 2007, vol. 1, pp. 840-868.

208. http://carbon.cudenver.edu/public/chemistry/classes/chem4538/raman.html, (accessed 28 August 2015).

209. G. D. R. Saito, M. S. Dresselhaus, *Physical Properties of Carbon Nanotubes*, Imperial College Press, London, 1999, vol. 10, pp. 190.

210. T. Y. K. Tanaka, and K. Fukui, *The Science and Technology of Carbon Nanotube*, ed. G. D. Riichiro Saito, Mildred S. Dresselhaus, Oxford: Elsevier, Armsterdam, 1999, vol. 6, pp. 51-62.

211. S. M. Bachilo, M. S. Strano, C. Kittrell, R. H. Hauge, R. E. Smalley and R. B. Weisman, *Science*, 2002, 298, 2361-2366.

212. A. Jorio, M. Pimenta, A. Souza Filho, R. Saito, G. Dresselhaus and M. Dresselhaus, *New Journal of Physics*, 2003, 5, 139.

213. T. B. a. F. Epron, *Materials Science and Technology*, 2005, 119, 105-118.

214. Y. Zhang, Y.-R. Zhen, O. Neumann, J. K. Day, P. Nordlander and N. J. Halas, *Nature Communications*, 2014, 5, 4424.

215. D. Bom, R. Andrews, D. Jacques, J. Anthony, B. Chen, M. S. Meier and J. P. Selegue, *Nano Letters*, 2002, 2, 615-619.

216. G. S. B. McKee and K. S. Vecchio, *Journal of Physical Chemistry B*, 2006, 110, 1179-1186.

217. http://nptel.ac.in/courses/103103026/module2/lec14/4.html, (accessed 10 June 2015).

218. U. Vohrer, I. Kolaric, M. Haque, S. Roth and U. Detlaff-Weglikowska, *Carbon*, 2004, 42, 1159-1164.

219. G. Ning, F. Wei, G. Luo and Y. Jin, *Carbon*, 2005, 43, 1439-1444.

220. C. Velasco-Santos, A. L. Martínez-Hernández, F. T. Fisher, R. Ruoff and V. M. Castaño, *Chemistry of Materials*, 2003, 15, 4470-4475.

221. G. Che, B. B. Lakshmi, E. R. Fisher and C. R. Martin, *Nature*, 1998, 393, 346-349.

222. Y. Qiao, C. M. Li, S.-J. Bao and Q.-L. Bao, *Journal of Power Sources*, 2007, 170, 79-84.

223. M. C. Bahome, L. L. Jewell, D. Hildebrandt, D. Glasser and N. J. Coville, *Applied Catalysis A: General*, 2005, 287, 60-67.

224. W. Zhang, Z. Zhang and Y. Zhang, *Nanoscale Research Letters*, 2011, 6, 1-22.

225. M. J. Biercuk, M. C. Llaguno, M. Radosavljevic, J. K. Hyun, A. T. Johnson and J. E. Fischer, *Applied Physics Letters*, 2002, 80, 2767-2769.

226. H.-M. Cheng, Q.-H. Yang and C. Liu, *Carbon*, 2001, 39, 1447-1454.

227. M. Hirscher and M. Becher, *Journal of Nanoscience and Nanotechnology*, 2003, 3, 3-17.

228. B. J. Landi, M. J. Ganter, C. D. Cress, R. A. DiLeo and R. P. Raffaelle, *Energy & Environmental Science*, 2009, 2, 638-654.

229. C. Niu, E. K. Sichel, R. Hoch, D. Moy and H. Tennent, *Applied Physics Letters*, 1997, 70, 1480-1482.

230. G. K. Mor, K. Shankar, M. Paulose, O. K. Varghese and C. A. Grimes, *Nano Letters*, 2006, 6, 215-218.

231. M. W. Rowell, M. A. Topinka, M. D. McGehee, H.-J. Prall, G. Dennler, N. S. Sariciftci, L. Hu and G. Gruner, *Applied Physics Letters*, 2006, 88, 233506.

232. L. Schlapbach and A. Zuttel, *Nature*, 2001, 414, 353-358.

233. C. Wang, M. Waje, X. Wang, J. M. Tang, R. C. Haddon and Yan, *Nano Letters*, 2004, 4, 345-348.

234. I. Kruusenberg, L. Matisen, Q. Shah, A. Kannan and K. Tammeveski, *International Journal of Hydrogen Energy*, 2012, 37, 4406-4412.

235. W. Li, C. Liang, W. Zhou, J. Qiu, Zhou, G. Sun and Q. Xin, *Journal of Physical Chemistry B*, 2003, 107, 6292-6299.

236. D. R. Kauffman, Y. Tang, P. D. Kichambare, J. F. Jackovitz and A. Star, *Energy & Fuels*, 2010, 24, 1877-1881.

237. M. G. Bellino, J. G. Sacanell, D. G. Lamas, A. G. Leyva and N. E. Walsöe de Reca, *Journal of the American Chemical Society*, 2007, 129, 3066-3067.

238. M. Hirscher and B. Panella, *Journal of Alloys and Compounds*, 2005, 404–406, 399-401.

239. M. Kaempgen, M. Lebert, M. Haluska, N. Nicoloso and S. Roth, *Advanced Materials*, 2008, 20, 616-620.

240. M. C. Bahome, L. L. Jewell, K. Padayachy, D. Hildebrandt, D. Glasser, A. K. Datye and N. J. Coville, *Applied Catalysis A: General*, 2007, 328, 243-251.

241. R. S. Oosthuizen and V. O. Nyamori, *Platinum Metals Review*, 2011, 55, 154-169.

242. K. Kostarelos, A. Bianco and M. Prato, *Nature Nanomtechnology*, 2009, 4, 627-633.

243. H. S. Oberoi, N. V. Nukolova, A. V. Kabanov and T. K. Bronich, *Advanced Drug Delivery Reviews*, 2013, 65, 1667-1685.

244. G. R. Bardajee, A. Pourjavadi and R. Soleyman, *Journal of Polymer Research*, 2011, 18, 337-346.

245. P. Pai, K. Nair, S. Jamade, R. Shah, V. Ekshinge and N. Jadhav, *Current Pharma Research Journal*, 2006, 1, 11-15.

246. J. Yao, M. Yang and Y. Duan, *Chemical Reviews*, 2014, 114, 6130-6178.

247. B. S. Harrison and A. Atala, *Biomaterials*, 2007, 28, 344-353.

248. A. Bianco and M. Prato, *Advanced Materials*, 2003, 15, 1765-1768.

249. C. A. Spindt, I. Brodie, L. Humphrey and E. R. Westerberg, *Journal of Applied Physics*, 1976, 47, 5248-5263.

250. Y. Saito and S. Uemura, *Carbon*, 2000, 38, 169-182.

251. K.-Y. Chun, H. S. Lee and C. J. Lee, *Carbon*, 2009, 47, 169-177.

252. D. Cathey, *Field Emission Displays*, 1995, 10, 131-136.

253. N. Soin, S. Sinha Roy, S. Roy, K. S. Hazra, D. S. Misra, T. H. Lim, C. J. Hetherington and J. A. McLaughlin, *Journal of Physical Chemistry C*, 2011, 115, 5366-5372.

254. W. J. Lee, J. M. Lee, S. T. Kochuveedu, T. H. Han, H. Y. Jeong, M. Park, J. M. Yun, J. Kwon, K. No, D. H. Kim and S. O. Kim, *American Chemical Society Nano*, 2012, 6, 935-943.

CHAPTER 3: EXPERIMENTAL

A detailed account of the methods employed in the synthesis of MWCNTs and their characterization techniques is herein presented. There are different methods used to synthesize MWCNTs such as laser ablation, arc-discharge and CVD. However, in this study the CVD method is used. The CVD method was preferred because of its simplicity, availability, selectivity and higher yields. The selectivity of the MWCNTs was controlled by synthetic parameters, *e.g.* catalyst type, carbon source and temperature. The MWCNTs were further purified using nitric acid and their characterizations were carried out using different characterization techniques.

3.1 Chemicals, gases, equipment and apparatus

The metallocenes used in all experiments were of analytical grade and hence used without further purification. Ferrocene (≥ 97%), nickelocene (≥ 97%), cobaltocene (≥ 97%), and ruthenocene (≥ 97%) were purchased from Sigma Aldrich LTD and supplied by Capital Labs suppliers. Sodium hydroxide (pellets, ≥ 97%) was purchased from Associated Chemical Enterprises (Pty) Ltd, South Africa. Toluene (≥ 99.5%) was purchased from BDH Chemicals Ltd, England. Acetonitrile (HPLC grade, 99.9%) and ethanol (98%) were purchased from Merck, Schuchardt, Germany. Nitric acid (55%) and sulphuric acid (98%) were purchased from Saarchem, Merck, South Africa. Double distilled water was supplied by BIby sterlin Ltd, England, Aqutron model A4000Dl. A gas mixture of 10% H_2 in Argon (v/v) (10% H_2:90% Ar) was purchased from Afrox Limited Gas Co., Durban, South Africa.

Samples were weighing on the Mettler AE 200 balance, Germany. Ultrasonic water bath treatment was performed on a digital ultrasonic heater supplied by Shalom Lab, South Africa. The injection pump employed was a New Era pump system Inc. and the Syringe Pump Model No. NE-300. Filtration was done in a Buchner filtration flask fitted with Whatman grade 4 filter paper.

3.2 General procedure

3.2.1 Cleaning glassware

All glassware used in the synthesis procedure were washed with soap and warm water, then further rinsed with acetone and dried in the oven. Quartz tubes and other glass apparatus used in the CVD method were cleaned by first scraping off the black carbonaceous deposits from CVD, followed by gentle scrubbing in soapy water. These were then rinsed with water in order to remove the soap, followed by rinsing with acetone until the solvent colour turned from orange to colourless. Any remaining black carbonaceous materials in quartz tube were removed by heating it at 800 °C for 30 minutes. After the black carbonaceous materials was removed the quartz tube was soaked in *aqua regia* (HCl:HNO_3 3:1 v/v) to dissolve accumulated iron and iron oxides. Thereafter, the tube was washed with water to completely remove the orange deposits. The injection-port and cold finger were occasionally soaked in sodium hydroxide and ethanol mixture (base bath), then washed with soapy water and rinsed with acetone.

3.2.2 Preparation of catalyst precursors

0.25 g (ferrocene, nickelocene, cobaltocene or ruthenocene) of a catalyst was weighed out and mixed with toluene or acetonitrile, as the carbon source, to make a solution of total mass, 10.0 g. This solution was sonicated for 10 minute in order to allow proper dissolution of the metallocene. It was then drawn into a disposable syringe attached to a SS 150 mm L non-boring 24 gauge bevelled-tip needle, inserted into the septum of the injector port and injected into the heated quartz tube at an injection pump rate of 0.8 mL min^{-1}.

3.2.3 CVD reactor set-up

The synthesis of the MWCNTs was accomplished by using a horizontal floating bed catalyst based on a similar design used in literature.[1] The setup used to grow the carbon nanotubes is similar to that shown in Figure 3.1. An Elite thermal systems Ltd. furnace was used, model TSH 12/50/610 fitted with an overtemperature controller (Eurotherm 2116) and a main zone furnace controller (Eurotherm 2416). The parameters used in the synthesis of CNTs are presented in Table 3.1 and were kept constant for all the runs.

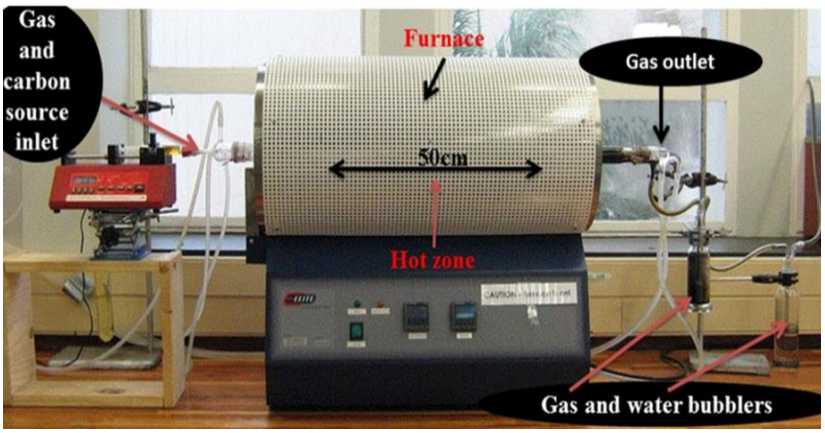

Figure 3.1: The CVD reactor used in this study

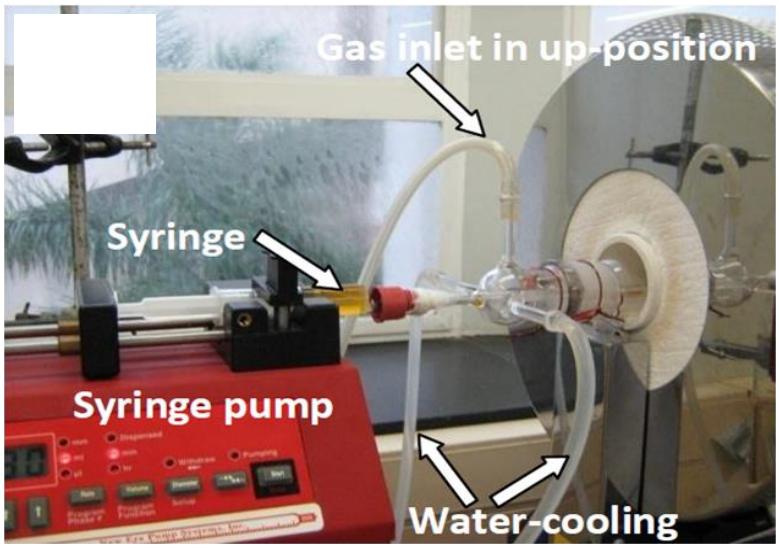

Figure 3.2: The components and arrangement of the injector port employed

Table 3.1: Parameters used in the synthesis of MWCNTs

Parameters	Types
Catalysts	Ferrocene, nickelocene, cobaltocene or ruthenocene
Carbon source	Toluene or acetonitrile
Reaction temperature	800, 850, 900, 950 or 1000 °C
Catalyst/carbon source	2.5 wt.%
Amount injected	10 mL
Injection rate	0.80 mL min^{-1}
Holding time	30 min
Gas	10% hydrogen in argon (v/v)
Temperature heat rate	10 °C min^{-1}
Gas flow rate	100 mL min^{-1}
Carrier gas pressure	80 kPa

A quartz tube reactor (80 cm in length and 2.8 cm internal diameter) was inserted horizontally into an electrical furnace with the outlet of the tube connected to a gas bubbler (Figure 3.1). At one end of the quartz reactor tube, a quartz water-cooled injection port (see Figure 3.2) was fitted, by using a ground glass joint, and at the other end a glass cold finger, was also fitted with a ground glass joint. Both ends were secured firmly onto the reactor tube by a series of hooks and elastic bands. This was done in order to ensure that if an increase in pressure was experienced in the reactor, the injection port and cold finger will not detach from the quartz tube and also to prevent gas leakage. The gas and water bubblers were similarly fitted with ground glass joints. The full setup of the furnace is shown in Figure 3.1.

3.2.4 Methods for the synthesis of MWCNTs

The temperatures inside the quartz tube were kept in the range of 800 - 1000 °C, under 10% hydrogen in argon (v/v). The carrier gas and reducing agent, was supplied into the system *via* silicon tubing at a rate of 100 mL min^{-1} at 80 kPa after the system had reached a temperature of 600 °C in order to remove oxygen, moisture and any other gas which might be present in the system. The carrier gas which contained the reducing agent (H_2 gas) was set at a constant flow rate and pressure was maintained for the duration of the synthesis. Waste gases exiting

the quartz reactor tube were allowed to pass through a water-trap and then vented to the exterior of the building.

The catalyst/carbon source solution was injected in the reactor by means of an injection pump. The furnace was maintained at the set maximum temperature (T_{max}) for the duration of injection. At the end of the reaction, the furnace was allowed to cool down and the gas source was switched off at about 250 °C. Thereafter, the furnace was allowed to cool to room temperature before the quartz components were dismantled. The carbonaceous products were scraped out of the quartz tube with a long stainless steel spatula. The products deposited in the hot zone (Figure 3.1) were collected and weighed. These products were obtained as shiny flakes (Figure 3.3 a) due to etching of the inner walls of the quartz tube or as black powder resembling soot (Figure 3.3 b).

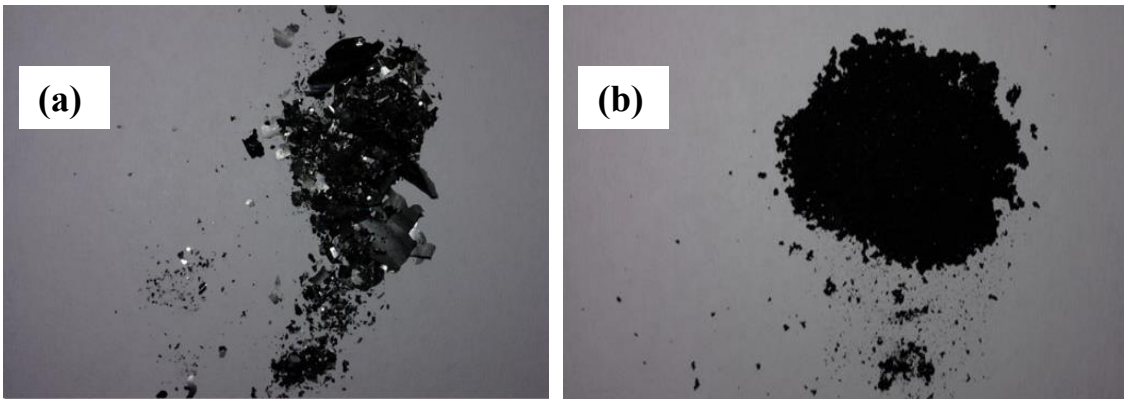

Figure 3.3: Photographs of (a) shiny flakes and (b) black carbonaceous powder obtained from ferrocene at a growth temperature of 900 and 800 °C, respectively

3.2.5 Purification of the MWCNTs

The MWCNTs that were synthesized usually have impurities in the form of amorphous carbon, other SCNMs and metal catalyst residues.[2,3] Therefore, purification of the synthesized MWCNTs was carried out as shown in Scheme 3.1. Amorphous carbon and SCNMs can be minimised by high heat temperature since they decompose at higher temperature (but less than 680 °C since higher temperature also cause MWCNTs to decompose). Acid treatment was used to remove the metal particles within the crude nanotube samples and it also assisted in opening their tips.[4] Three different methods were tested and compared.[5]

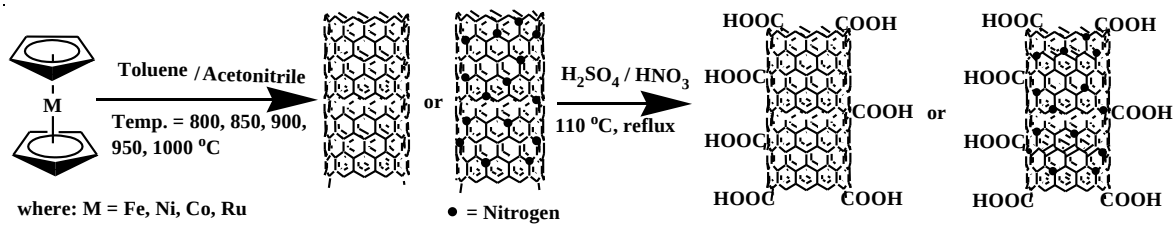

Scheme 3.1: Acid treated MWCNTs[6]

3.2.5.1 Method 1

MWCNTs (≈ 0.20 g) were grinded and calcinated in the CVD reactor for three hours at a temperature of 350 °C. After three hours the MWCNTs were transferred into a 150 mL round–bottom flask and 6 M nitric acid (15 mL) was added. This was done in order to expose the metal catalyst particles, thus making the purification more effective. The solution was then sonicated for 60 minute in order to disperse the CNTs. The mixture was further refluxed for 12 hours at a temperature of 110 °C in order to dissolve the metals. After 12 hours, the mixture was allowed to cool to room temperature and nitric acid was neutralized using sodium hydroxide. Then the mixture was sonicated for 40 minute. The purified MWCNTs were filtered and washed with distilled water until filtrate attained a pH of 7. The purified MWCNTs were then dried overnight in the oven at 130 °C.

3.2.5.2 Method 2

The same procedure as in method 1 was repeated but the mixture was refluxed for 24 hours instead of 12 hours.

3.2.5.3 Method 3

The same procedure as in method 1 was employed; however, the mixture was refluxed for 48 hours instead of 12 hours.

The verification of the purification process was determined by the use of TEM and TGA among other methods of characterization.

3.3 Characterization of the MWCNTs

This section describes the techniques, instruments and sample preparation used for MWCNTs characterization.

3.3.1 Transmission electron microscopy

The morphology of the MWCNTs was investigated by using transmission electron microscopy (TEM). A JEOL JEM model 1010 transmission electron microscope at 80 kV equipped with Megaview imaging system was used to obtain the TEM micrographs. Figure 3.4 depicts a photograph of the TEM instrument. TEM samples were prepared by firstly grinding using an agar mortar and pestle and the grounded sample was transferred into labelled vials. The ground sample was dissolved in 1 mL of 100% ethanol and allowed to sonicate for approximately 10 minutes. The sonication in ethanol allowed the MWCNTs to be evenly dispersed in order to obtain a representative sample that would be used for analysis.

A lacey or holey carbon-copper grid was dipped into the ethanolic dispersion. The ethanol was then allowed to evaporate by placing the grid near a lamp. The grid was then inserted into the specimen chamber of the TEM instrument. It was analysed under several magnifications. megaview digital camera was used to capture images and data, and also provide the magnification and scale bar. Image analysis involved measurements of external and internal diameters and lengths using the image J® software. The average diameters of the MWCNTs were quantified by measuring over 100 randomly chosen tubes. The same procedure was repeated for all samples. The average diameter of the tubes measured was calculated using equations 1 and 2:

$$100\ tubes \times 3\ measurements\ per\ tube\ = 300\ measurements \quad (1)$$

$$\frac{\sum All\ measurements}{300} = average\ diameter\ (nm)\ per\ sample \quad (2)$$

Figure 3.4: Photograph of JEOL JEM 1010 transmission electron microscope

3.3.2 High resolution transmission electron microscopy

The MWCNTs were also investigated by HRTEM. High magnification was performed with JEOL JEM 2100 (Figure 3.5), 200 kV and set at an accelerating voltage of 100 kV. HRTEM employed the ECSI 10 digital micrograph software. Sample preparation for HRTEM was done in a similar way as that of the TEM analysis (Section 3.3.1).

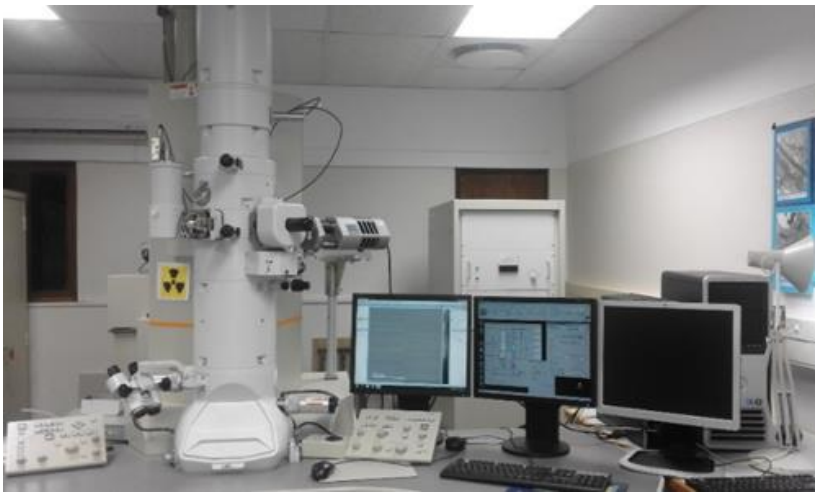

Figure 3.5: Photograph of JEOL JEM 2100 high resolution transmission electron microscope

3.3.3 Scanning electron microscopy

The morphology of the MWCNTs was investigated by use of SEM in order to determine the surface morphology. It was performed in a JEOL JSM 6100 model (Figure 3.6). An accelerating voltage of 10V was used. The working distance was kept between 4 and 6 mm with Probe current set at 3 p.A and aperture size was 30 µm. The aluminium stubs were used as sample holders. The aluminium stubs were coated with a piece of a sticky carbon tape. The sample was sprinkled on top of a carbon tape. Zeiss Smart SEM version 5.03.06 software was employed in the data acquisition and analysis. The JEOL JSM was used in conjunction with electron dispersive X-ray spectroscopy (EDX) during the imaging session.

Figure 3.6: Photograph of JEOL JSM 6100 scanning electron microscope

3.3.4 Electron dispersive X-ray spectroscopy

The EDX was used to determine the elemental composition of materials. EDX is good for analysis of both heavier elements such as iron and lighter element such as carbon. Bruker 1.8 software X-ray spectrometer attached to the JEOL JSM 6100 SEM instrument was used to generate EDX spectra and convert the data in spectra directly into tables of normalized weight percent for selected items. In the EDX analysis, 80 mm^2 X-max, Oxford instrument detector was used. The software employed was EDX Aztec. Samples were scanned at a rate between 5 to 10 kilo counts per second, with an accelerating voltage of 20 kV and working distance of 5-10 mm.

3.3.5 Raman spectroscopy

Raman spectrometer was used to investigate the crystallinity of the MWCNTs. A Delta Nu Advantage 532^{TM} Raman spectrometer (USA) with 1800b lines/mm grating was used to get the Raman spectra of the MWCNTs (Figure 3.7). The instrument was operated with NuSpec^{TM} software with excitation using a class 3b diode laser (Nd:YAG solid state crystal) operated at a wavelength of 532 nm. The laser was operated at 15 mW. The samples were ground to a very fine powder prior to analysis. It was placed in the sample holder and the focal length was centred at the irradiation centre at approximately 16.45 mm. The spectrometer was then covered with a black cloth before analysis. Data was collected by means of 2D CCD detector with an integration time of 60 seconds. An average of three spectra was acquired for MWCNTs and then background smoothing was done on the spectra. The spectra were interpreted using Origin software package.

Figure 3.7: Photograph of Delta Nu Advantage 532^{TM} Raman spectrometer

3.3.6 Thermogravimetric analysis

The analysis of the degradation of MWCNTs was investigated using a TA instrument Q series^{TM} Thermal Analyser DSC/TGA (Q600) instrument (Figure 3.8). A small homogenised sample (≈ 5 mg) was used. Samples were analysed as obtained without any sample preparation. A ramp temperature of 10 °C min^{-1} was used in all the samples. The samples were analysed in air flowing at 50 mL min^{-1} and heated from ambient temperature up to 1000 °C at a rate of 10 °C min^{-1}. TGA curves and first derivatives plots were generated with TA instruments universal analysis 2000 software. Origin software was used to re-plot the weight-loss curves for the determination of oxidative stability of MWCNTs (initiation and oxidation temperature).

Figure 3.8: Photograph of TA instrument Q series™ Thermal Analyser DSC/TGA (Q600) instrument used for thermogravimetric analysis

3.3.7 BET analysis

BET was used to determine the surface area, pore volume and size of the MWCNTs. Analysis of textural properties of the MWCNTs were performed at -196 °C on the Micromeritics Tri-star II 3020 version 1.03 instruments at 77 K in N_2 (supplied by Micromeritics, USA) as shown in Figure 3.9. Accurately weighed CNTs (0.1 g) were ground and then degassed at 90 °C for one hour and then at 160 °C for twelve hours using Micromeritics Flow before fitting them for analysis on the Micromeritics Tri-star II instrument. The pore volumes were obtained from the Barrett-Joyner-Halenda (BJH) model.

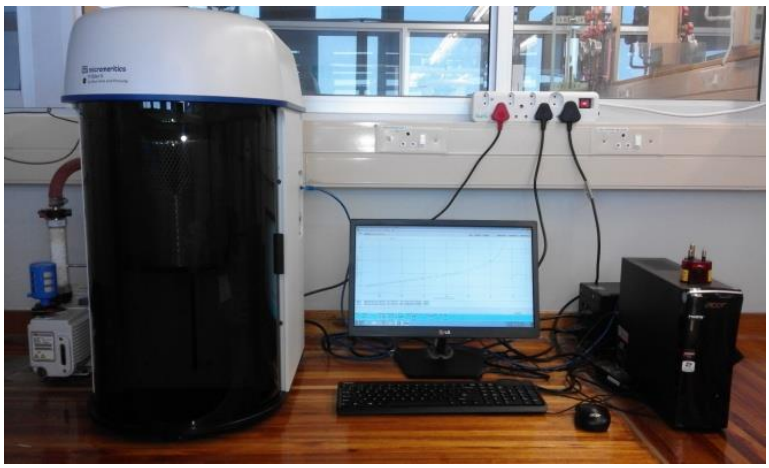

Figure 3.9: Photograph of Micromeritics Tri-star II instrument

3.3.8 Elemental analysis

Elemental analysis was used to investigate the relative composition of elements such as carbon and nitrogen present in the nitrogen-doped MWCNTs. The analysis was performed on a LECO CHNS-932 elemental analyser, standardised with acetanilide. Nitrogen-doped MWCNTs sample of approximately 5 mg was required and for each run the experiment was done in duplicate.

3.4 References

1. E. N. Nxumalo, V. O. Nyamori and N. J. Coville, *Journal of Organometallic Chemistry*, 2008, 693, 2942-2948.
2. Y.-Y. Fan, A. Kaufmann, A. Mukasyan and A. Varma, *Carbon*, 2006, 44, 2160-2170.
3. S. Porro, S. Musso, M. Vinante, L. Vanzetti, M. Anderle, F. Trotta and A. Tagliaferro, *Physica E*, 2007, 37, 58-61.
4. H. Hu, B. Zhao, M. E. Itkis and R. C. Haddon, *The Journal of Physical Chemistry B*, 2003, 107, 13838-13842.
5. H. Hu, B. Zhao, M. A. Hamon, K. Kamaras, M. E. Itkis and R. C. Haddon, *Journal of the American Chemical Society*, 2003, 125, 14893-14900.
6. Z. Dong, B. Yang, J. Jin, J. Li, H. Kang, X. Zhong, R. Li and J. Ma, *Nanoscale Research Letters*, 2009, 4, 335-340.

CHAPTER 4: RESULT AND DISCUSSION OF MWCNTs

This section presents results on the synthesis of multiwalled carbon nanotubes. The synthesis was carried out at five different growth temperatures for all the metallocenes. The materials were characterized by TEM, HRTEM, SEM, TGA, Raman spectroscopy and their texture investigated as discussed in Chapter 3. The results obtained were also compared to those of other authors who have previously used similar precursors.

4.1 Yield of SCNMs

The activity of metallocenes as catalysts in the synthesis of MWCNTs was tested. Toluene was used as carbon source and the reactions were done at 800, 850, 900, 950 or 1000 °C. Black, shiny, flaky powders that resemble soot were produced at all five growth temperatures, with the yield notably depending on the type of metallocene used. Varying the growth temperature was also found to have an effect on the yield of SCNMs. The five different temperatures (800, 850, 900, 950 and 1000 °C) showed that the yield increased with increase in growth temperature for all the metallocenes. The increase in yield with temperature was consistent with literature reports.[1,2] This could imply that relatively lower temperatures are not conducive for the carbon precursor dissociation and dissolution into the metallocene catalysts. Thus, increasing the reaction temperature favoured a faster supply of carbon and dissolution of carbon into the metallocene catalysts resulting in the formation of more SCNMs.

From Table 4.1, ferrocene seemed to produce the highest yields at all of the growth temperatures tested whilst ruthenocene had the lowest yield of SCNMs. In the case of ruthenocene, a number of possible factors were postulated for this low yields. Firstly, this could be caused by poor solubility of carbon in ruthenocene when compared with the other three metallocenes. Secondly, the much lower yield could also be attributed to some catalyst – toluene solution seeping through to the other end of the reactor tube, unreacted, hence not available to form MWCNTs at the hot stage. Some of the SCNMs may have been left on the rough inner-wall of the quartz tube during harvesting even after a through recovery procedure. It was observed that as the metal size decreases (Ru > Ni > Co > Fe) the yield increases (Table 4.1). The highest yield of 1532.1 mg was obtained when ferrocene was used as a catalyst at a growth temperature of 1000 °C.

Table 4.1: Yields of SCNMs obtained from the pyrolysis of metallocenes (2.5 wt.%) in a solution of toluene

Temperature/ °C	SCNMs[a] /mg	SCNMs[b] /mg	SCNMs[c] /mg	SCNMs[d] /mg
1000	1532.1	1343.9	1412.1	1278.3
950	826.8	823.8	825.3	545.1
900	665.6	652.9	538.0	499.4
850	495.0	325.8	420.4	213.4
800	362.1	224.7	157.8	137.2

Superscript represent the catalyst used; [a] ferocene, [b] nickelocene, [c] cobaltocene, [d] ruthenocene

4.2 Purification of as-synthesised shaped carbon nanomaterials (SCNMs)

Samples of as-synthesized MWCNTs usually come with other impurities such as amorphous carbon, carbon spheres and transition metal nanoparticles which are introduced as catalysts during synthesis (Figure 4.1 a).[3-5] The SCNMs were purified using methods which involved refluxing with an acid solution for different number of hours. The acid treatment was chosen because it has been reported to cause minimal damage, open the ends of the MWCNTs and enable removal of metal nanoparticles impurities.[6-8] Additionally, acid purification also introduces oxygen-containing groups on the surface of MWCNTs.[9]

The MWCNTs were firstly ground and then calcined in the oven for three hours at a temperature of 350 °C to remove amorphous carbon and then refluxed using 6M nitric acid in three different time periods designated as; method 1 (Section 3.2.5.1), method 2 (Section 3.2.5.2) and method 3 (Section 3.2.5.3). The refluxing times were varied in order to investigate the effectiveness of the purification method and also to find the best method for the purification of the MWCNTs. In this work, the acid treatment did not affect the outer- and inner-diameters of the MWCNTs. Some authors have reported that a mixture of concentrated H_2SO_4 and HNO_3 does not produce defects in MWCNTs.[10,11] The results obtained in this study, using same mixture showed a similar trend. During refluxing, the reaction mixture turned yellow, indicating that residual metal nanoparticles were removed from the MWCNTs.[12]

For optimization of the time dependent methods, ferrocene catalysed MWCNTs were investigated and the optimum method was chosen based on TEM and TGA results. The optimum method was further used for the purification of MWCNTs obtained from other metallocenes. Purified MWCNTs were expected to contain minimal or no amorphous carbon as observed in the TEM images and the TGA thermograms. The materials that were synthesized from ferrocene at a growth temperature of 800 °C were used to compare these purification methods. This was chosen because ferrocene as a catalyst has been widely used in the synthesis of CNTs at 800 °C.[13,14]

MWCNTs were dispersed by sonication in ethanol and a lacey or holey carbon-copper grid was dipped in the ethanolic dispersion. The grid was dried in order for ethanol to evaporate and then it was inserted into the TEM instrument for analysis. The TEM images for method 1 and method 2 which involved refluxing of MWCNTs for 12 and 24 hours, respectively, showed that the removal of metal nanoparticles was effective and the length of the MWCNTs were not cut into small pieces (Figure 4.1 b and c). However, the results obtained for method 3, which involved refluxing for 36 hours resulted in breakage of the MWCNTs to shorter length as observed from the TEM analysis (Figure 4.1 d). This was attributed to the longer hours of refluxing in a harsh acidic environment. The MWCNTs appeared cleaner indicating that large quantities of metal nanoparticles were removed.

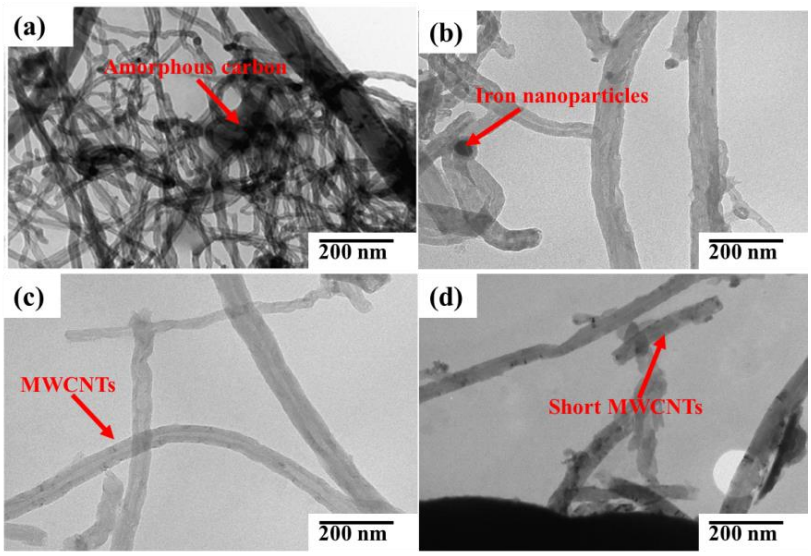

Figure 4.1: TEM images of SCNMs (a) as-synthesized, (b) MWCNTs purified from method 1, (c) MWCNTs purified from method 2 and (d) MWCNTs purified from method 3

The amount recovered during purification was also investigated, by comparing the mass of MWCNTs before purification and after purification. In each experiment, a mass of 120 mg was weighed out for purification and the masses recovered for method 1, method 2 and method 3 were 96.0, 84.4 and 78.0 mg, respectively. Thus, it was found that the highest amount recovered was achieved in method 1, with method 3 giving the lowest recovery. In the case of method 3, the destruction was caused by the long hours of refluxing. After purification, the materials were found to be more crystalline as shown by the Raman studies (Table 4.2). It was observed that as the refluxing time increased, the crystallinity of the MWCNTs also increased. Purification of MWCNTs with acids result in addition of carboxylate groups on the tube walls. Hence, longer hours of reflux may result in more carboxylate groups being attached onto the MWCNT walls. This causes a decrease the in I_D/I_G ratio. Therefore, the lower I_D/I_G ratio, in method 3 could be attributed to the destruction of the walls of the CNTs by acid functionalization/carboxylation.[15]

Table 4.2: Results obtained from different purification methods

	Mass purified/mg	**Mass recovered/mg**	**Purified yield/%**	**I_D/I_G ratio**
as-synthesized	-	-	-	0.99
method 1	120	96.0	80	0.78
method 2	120	84.4	72	0.72
method 3	120	78.0	65	0.63

In order to further assess the effectiveness of the three purification methods, the samples were further subjected to thermogravimetric analysis. It was used to investigate the thermal stability of the MWCNTs and also the amount of metal content present after purification. Figure 4.2 shows the thermograms of the purified materials obtained and compared with that of the as-synthesized materials. Methods 1 and 3 produced less thermally stable MWCNTs than method 2. The decomposition temperatures for SCNMs which are purified using methods 1, 2 and 3 were 390, 520, and 410 °C, respectively. The residual iron content for the SCNMs obtained from methods 1, 2 and 3 were 0.5, 0.1 and 0%, respectively. The iron content decreased when the refluxing hours during purification was increased. From the thermograms, it was observed that method 3, which had the longest reflux hours, was able to reduce the iron content from 20 to 0%. As the condition became harsher (longer reflux hours and higher temperatures) the

stability of the MWCNTs decreased (method 3). The harsh conditions tend to produce more defects on the MWCNTs and shorten the tubes which lowered the thermal stability. The thermograms showed that there is a weight loss around 180 to 400 °C from as-synthesized and method 3 (Figure 4.2 – region marked *). This was caused by the presence of amorphous carbon materials.

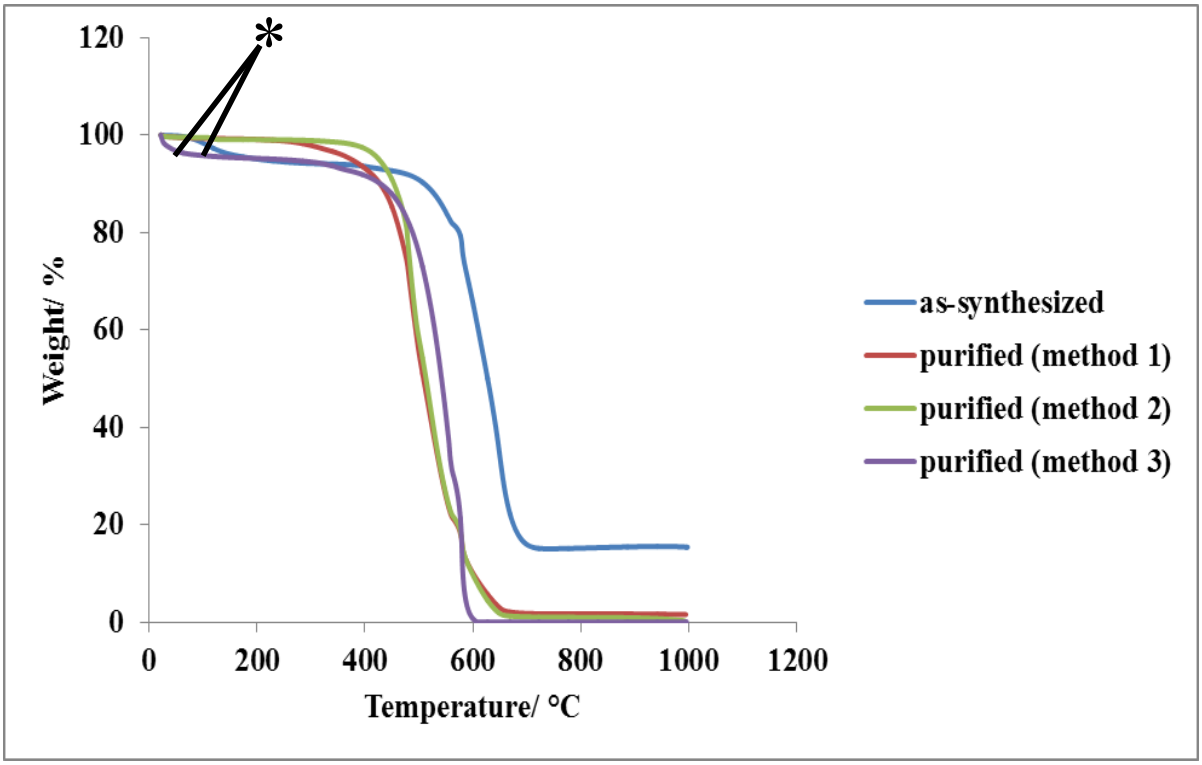

Figure 4.2: TGA thermograms of samples obtained from ferrocene catalysed MWCNTs synthesis at a growth temperature of 800 °C purified by the three purification methods *vs.* the as-synthesized

From Table 4.1 and Figures 4.1- 4.2, it was decided that the best purification method is method 2, since it maintained the size of the MWCNTs with high crystallinity, low content of metal nanoparticles and better thermal stability were obtained. It was then further applied in the purification of other SCNMs which were synthesized from other metallocenes.

4.3 Effect of growth temperature

4.3.1 SCNMs distribution

TEM analysis was used to investigate the quality, type, size and distribution of the various SCNMs produced in the different synthesis reactions temperatures. All the reactions at the various growth temperatures investigated produced MWCNTs. This concurs with the earlier report of a similar process which involved the pyrolysis of a mixture containing benzene and an organometallic precursor (ferrocene, cobaltocene or nickelocene).[16] It had been also reported that in the absence of metallocenes or the catalyst, the pyrolysis only gave rise to nanospheres. However, when ferrocene was used, large quantities of MWCNTs were obtained.[16]

In our finding, various structural morphologies of the SCNMs were observed from the TEM images. The TEM images showed that the use of different metallocenes produced different SCNMs such as, MWCNTs, carbon nanospheres, carbon nanofibers and amorphous carbon. These results are in agreement with the findings of Nxumalo *et al*.[17] who reported formation of similar products on pyrolysis of ferrocenylaniline in different proportions by using toluene as a carbon source. The distribution of these materials varied with growth temperature and metallocenes used. Apart from growth temperature and the kind of metallocene used, the distribution of SCNMs also depended on the reaction temperature, gas flow rate, reaction time and pressure.[18] A summary of the results obtained from different metallocenes used as catalysts precursors are presented in Table 4.3.

In these results, higher growth temperature favoured the formation of carbon spheres in large proportions. For example, large amount of carbon sphere (90%) were obtained from MWCNTs grown from ruthenocene at 1000 °C. It was observed that lowering the growth temperature to 800 or 850 °C yielded more amorphous carbon. It was also noted that a growth temperature of 850 °C had the largest amounts of MWCNTs when compared to other temperatures used. Ferrocene as a catalyst gave highest yield of MWCNTs, in all of the growth temperatures, whilst ruthenocene provided the least yield (Table 4.3).

Table 4.3: SCNMs distribution

Temperature/°C	Ferrocene	Nickelocene	Cobaltocene	Ruthenocene
1000	40(Ts), 60(Cs)	30(Ts), 50(Cs), 10(CNF)	35(Ts), 65(Cs)	10(Ts), 90(Cs)
950	60(Ts), 40(Cs)	50(Ts), 50(Cs)	45(Ts), 55(Cs)	30(Ts), 70(Cs)
900	65(Ts), 35(Cs)	60(Ts), 40(Cs)	65(Ts), 35(Cs)	35(Ts), 65(Cs)
850	85(Ts), 13(Cs), 2(Am)	80(Ts), 15(Cs), 5(Am)	70(Ts), 26(Cs), 4(Am)	62(Ts), 38(Cs), 8(Am)
800	50(Ts), 46(Cs), 4 (Am)	55(Ts), 39(Cs), 6 (Am)	60(Ts), 32(Cs), 8(Am)	40(Ts), 50(Cs), 10(Am)

*Ts - tubes, Cs - carbon spheres, CNF – carbon nanofiber, Am – amorphous carbon

A considerably larger amount of spheres (fused) were produced at 1000 °C compared to 800, 850 or 900 °C (Table 4.3). MWCNTs synthesized at all growth temperatures had iron nanoparticle encapsulated in them (Figure 4.3 a-e). This is consistent with earlier reports whereby organometallic complexes have been used in the synthesis of MWCNTs.[19] It is from these iron nanoparticles that MWCNTs grow, therefore it is not surprising to find them encapsulated within the tubes. MWCNTs grown at 800 °C have similar morphology to that grown at 850, 900 and 1000 °C while those grown at 950 °C had some bamboo compartments (Figure 4.3 d). The bamboo compartments could have been caused by the nitric acid which was used during purification and likely to added nitrogen in the MWCNT walls.

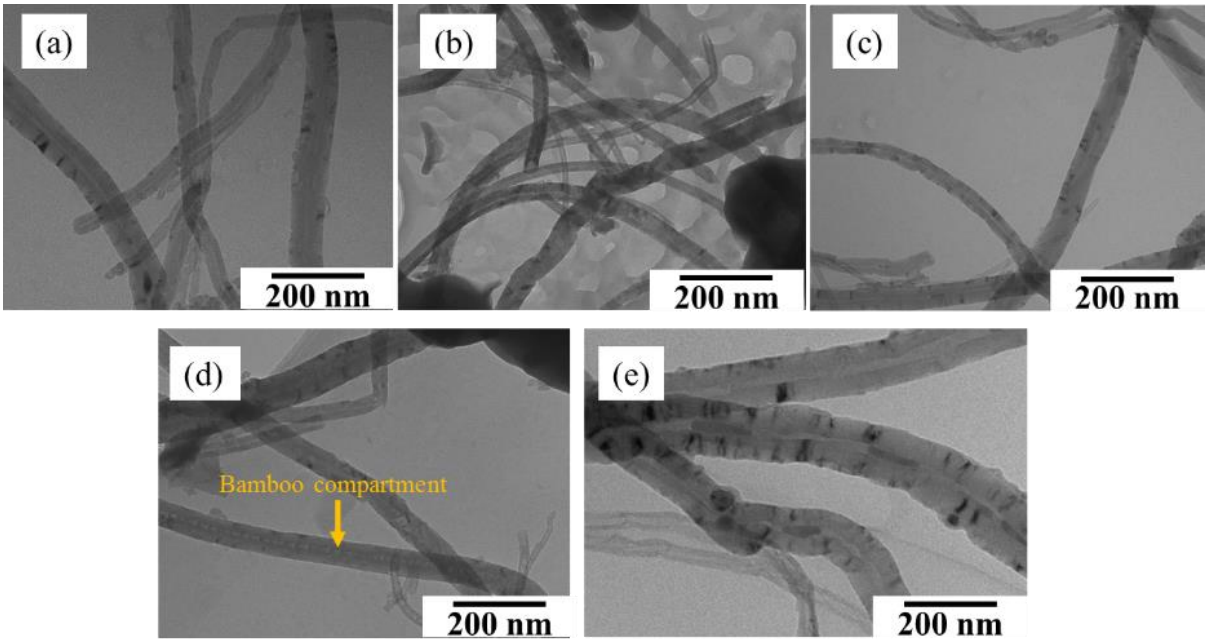

Figure 4.3: TEM images of MWCNTs synthesized from ferrocene at different growth temperatures (a) 800, (b) 850, (c) 900, (d) 950 and (e) 1000 °C

The use of nickelocene as a catalyst at higher temperature resulted in the mixture of MWCNT, carbon sphere and carbon nanofiber structures. The MWCNTs grown at 800 °C were also found to show rough surface and curved shape as shown in Figure 4.4 a. Again unexpected bamboo compartments were observed at a growth temperature of 900 °C (Figure 4.4 c). At a growth temperature of 950 °C, a large number of sub-bundle structures were observed, in which the MWCNTs appeared well oriented and tightly packed (Figure 4.4 d). Similar sub-bundle structures were reported by Wang *et al.*[20] The formation of carbon nanofibers together with MWCNTs and nanospheres was observed at a growth temperature of 1000 °C (Figure 4.4 e).

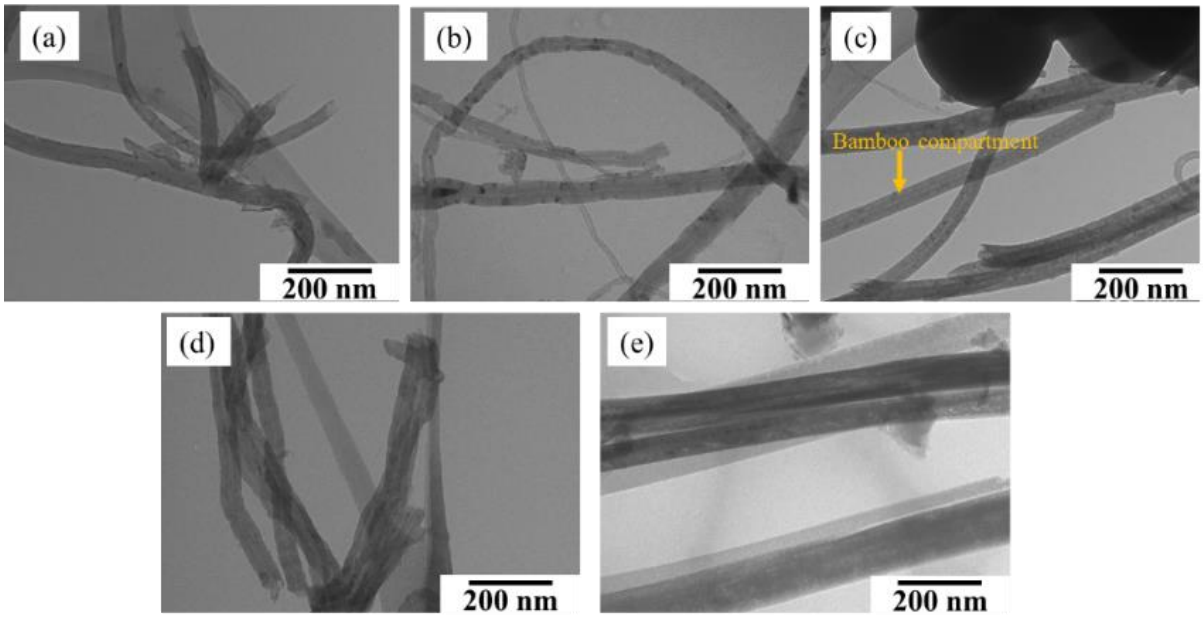

Figure 4.4: TEM images of MWCNTs synthesized from nickelocene at different growth temperatures (a) 800, (b) 850, (c) 900, (d) 950 and (e) 1000 °C

Similar to the MWCNTs synthesized from ferrocene, the MWCNTs from cobaltocene also contains cobalt nanoparticles (Figure 4.5 a-e). Onion-like structure with encapsulated cobalt particles were obtained at a growth temperature of 800 °C. Similar onion-like structures were reported by Sen *et al*.[16] when metallocene was used as a catalyst and benzene as a carbon source. Helical coil MWCNTs were obtained at a growth temperature of 950 °C (Figure 4.5 d). Helicity of the tubes was caused by the distribution of carbon ring defect in the carbon ring networks. However, a majority of the nanotubes had a curly shape. For all the growth temperatures it was observed that these MWCNTs contained less metal content

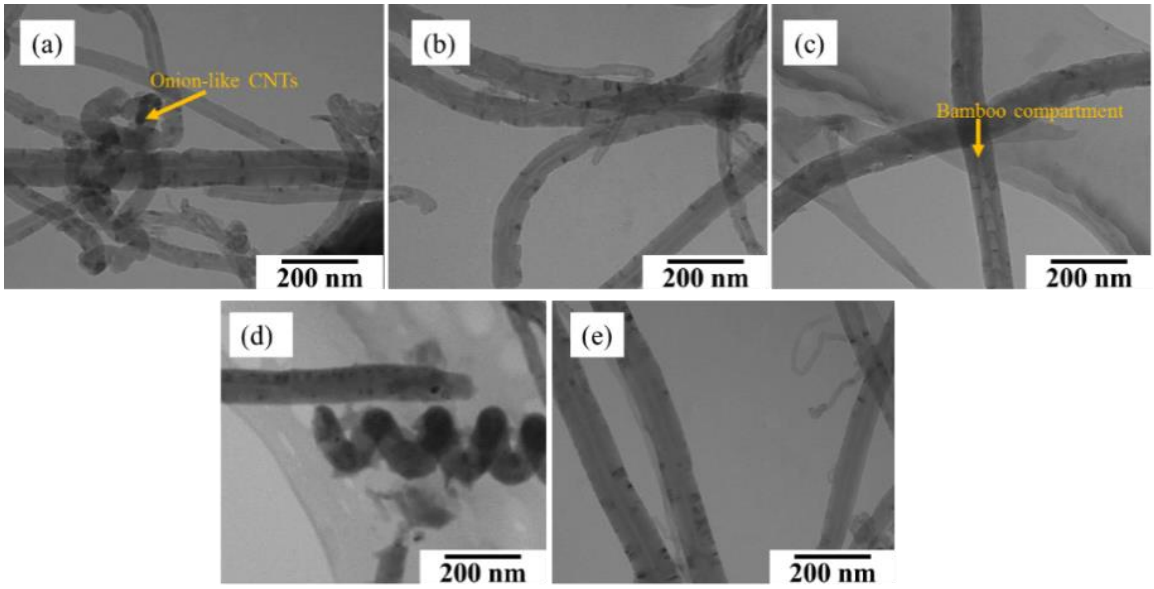

Figure 4.5: TEM images of MWCNTs synthesized from cobaltocene at different growth temperatures (a) 800, (b) 850, (c) 900, (d) 950 and (e) 1000 °C

The SCNMs which were synthesized from ruthenocene had large amounts of carbon spheres and small amounts of MWCNTs at all growth temperatures (Table 4.3 and Figure 4.6). However, the growth temperature of 1000 °C was found to produced higher amount of carbon spheres than tubes. The large amount of MWCNTs was observed at 900 °C and these CNTs had rough surfaces (Figure 4.6 c).

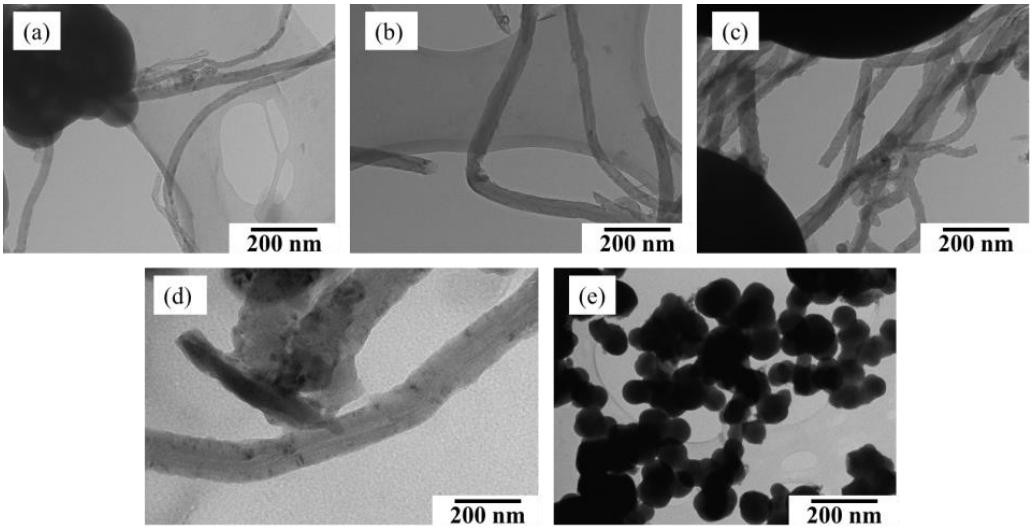

Figure 4.6: TEM images of MWCNTs synthesized from ruthenocene at different growth temperatures (a) 800, (b) 850, (c) 900, (d) 950 and (e) 1000 °C

4.3.2 Elemental analysis

In order to determine elemental composition, the MWCNTs were further characterized using EDX. The samples were scanned on different areas for analysis (Figure 4.7). Different percentages of elements are presented in Table 4.4. MWCNTs were found to contain different elements such as carbon, oxygen and the corresponding metal, *i.e.* iron, nickel, cobalt or ruthenium (depending on the catalyst used). It was observed that the MWCNTs had carbon contents greater than 91%. All the MWCNTs had high amounts of carbon. The MWCNTs obtained from ferrocene, nickelocene, cobaltocene and ruthenocene respectively had percentage of 95, 92, 94 and 94% (Table 4.4) of carbon content. The highest carbon content was obtained from MWCNTs grown from ferrocene. MWCNTs had different metal content. The metal content in these MWCNTs came from the metallocene catalysts used in the synthesis. The metal content was low which suggest, that they were not incorporated into the structures of the MWCNTs, most of the metal nanoparticles were carried away through to the exhaust system and also removed during purification.

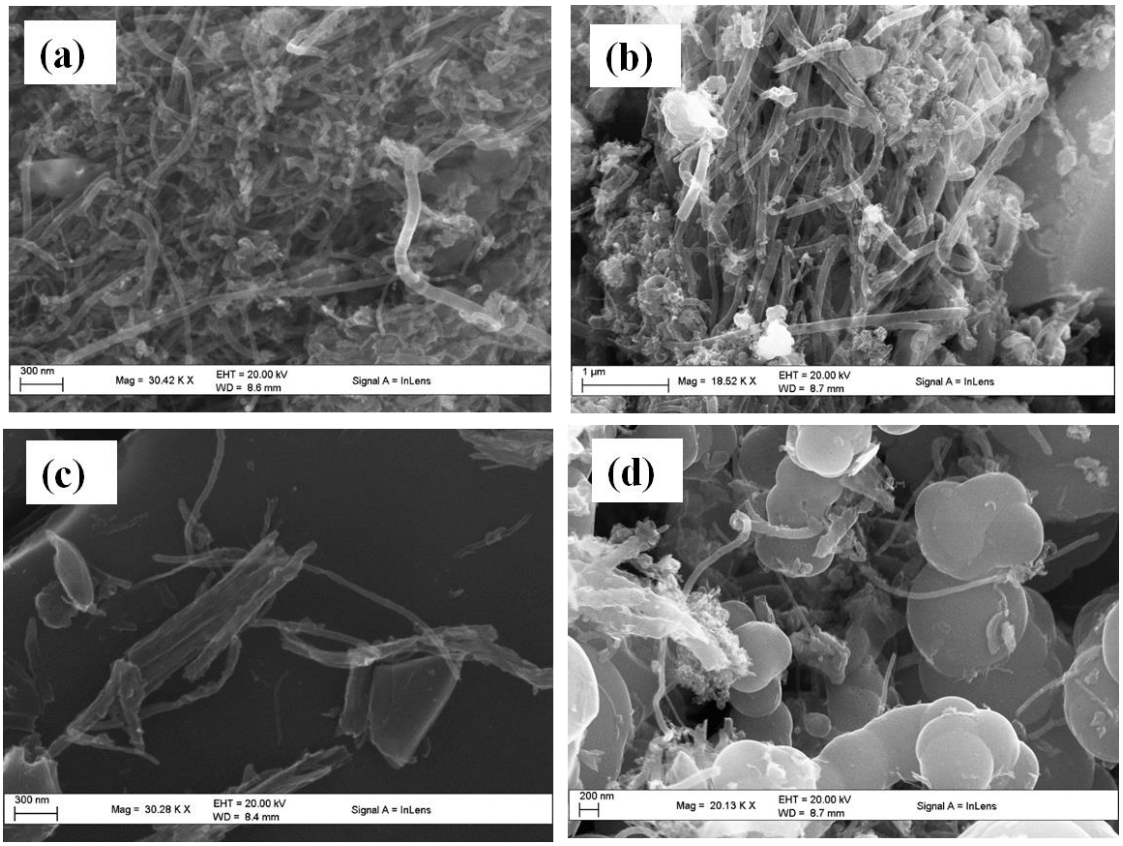

Figure 4.7: SEM images of MWCNTs synthesized at 850 °C from (a) ferrocene, (b) nickelocene, (c) cobaltocene and (d) ruthenocene as catalysts

Table 4.4: Elemental composition of MWCNTs synthesized at 850 °C

Element	Content/%			
	Ferrocene	**Nickelocene**	**Cobaltocene**	**Ruthenocene**
C	95	92	94	94
O	4.48	8.02	6.15	5.64
Metal	0.06	0.02	0.15	0.60

4.3.3 A**verage inner- and outer-diameters**

It was observed that the inner- and outer-diameters of the MWCNTs increased with growth temperatures (Figure 4.8 and 4.9**)**. The outer-diameters of the tubes ranged from 48 to 80 nm. However, other researchers have shown that the diameter of MWCNTs ranges from 15 to 200 nm.[21,22] The smallest average outer-diameter (48 nm) was produced at 800 °C when ruthenocene was used as a catalyst for synthesis of MWCNTs. The maximum average outer-diameter was obtained at a growth temperature of 1000 °C with nickelocene as catalyst (80 nm). Ruthenocene as a catalyst seems to favour the formation of tubes with smaller inner-and outer-diameters; the smallest average inner-diameter (8 nm) was observed at 1000 °C (Figure 4.9).

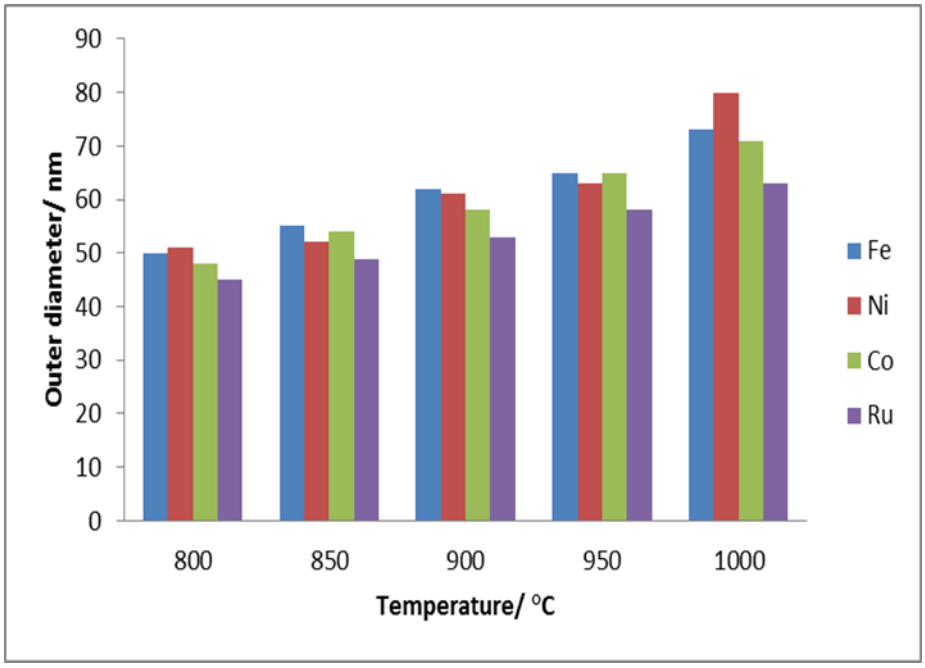

Figure 4.8: Outer-diameters of the MWCNTs synthesized from different metallocenes at different growth temperatures

It is believed that at higher temperature there are more frequent collisions of metal nanoparticles (NPs) and these results in the NPs getting bigger and bigger. The MWCNTs grown from these now larger iron nanoparticles have relatively larger diameters.[23,24] Also, at high temperatures catalyst particles on the substrate surface coagulate into larger islands. At lower temperatures the islands are smaller due to lower activation energies and thus their surface mobility is hampered. It can therefore be argued that higher reaction temperature lead to the growth of larger catalyst nanoparticles and subsequently produce nanotubes with larger outer-diameters.[25]

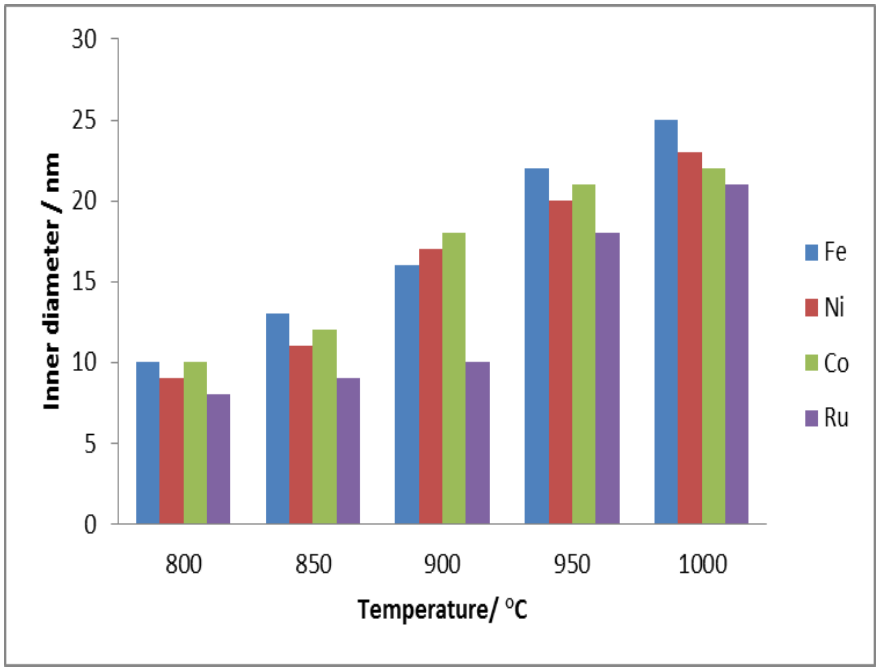

Figure 4.9: Inner-diameters of the MWCNTs synthesized from different metallocenes at different growth temperatures

4.3.4 Crystallinity of MWCNTs

Raman spectroscopy is an excellent tool for investigating the graphitic nature of carbon materials. Raman spectra of the MWCNTs generally show two characteristic peaks: G-band at ~ 1590 cm^{-1} originating from the Raman active E_{2g} mode and D-band at about 1350 cm^{-1} which is normally explained as a disorder-induced feature due to a finite particle size effect. This disorder is normally quantified using the I_D/I_G ratio, which essentially represents the extent of disorder in the graphitic carbon. Thus, as the ratio approaches 0 the MWCNTs will have a more ordered structure. Materials are termed disordered if they have an I_D/I_G ratio which is equal to or above 1, then they are classified as graphitic. For ease of comparison, the results from the Raman experiments are shown in Table 4.5.[26]

Table 4.5 shows characteristic bands of MWCNTs, the D- and G-bands at approximately 1350 and 1580 cm^{-1}, respectively. Literature associates the D band with disorder (sp^3 carbons) and the G-band is associated with the crystalline graphite structures (sp^2 carbons) of carbon nanotubes.[27] It was observed that the growth temperature has no effect in graphitic nature or crystallinity of the MWCNTs. However, the catalyst used had an effect on the nature of MWCNTs. The MWCNTs synthesized from cobaltocene were found to be more crystalline and the less crystalline were obtained from nickelocene and ruthenocene. The MWCNTs from

cobaltocene had I_D/I_G ratios of 0.59, 0.53, 0.44, 0.37 and 0.68 for 800, 850, 900, 950 and 1000 °C growth temperatures, respectively. Comparatively more crystalline MWCNTs were obtained from ferrocene and ruthenocene at a growth temperature of 800 °C which had the lowest I_D/I_G ratio of 0.23 and 0.52, respectively, while the MWCNTs grown from nickelocene and cobaltocene were more crystalline at a growth temperature of 950 °C (with I_D/I_G of 0.37 and 0.52, respectively).

Table 4.5: Raman spectroscopy analysis of MWCNTs

Catalyst	Temperature/°C	D-band/cm^{-1}	G-band/cm^{-1}	I_D/I_G
Ferrocene	1000	1358	1588	0.35
	950	1360	1579	0.77
	900	1368	1593	0.62
	850	1360	1590	0.99
	800	1356	1590	0.23
Nickelocene	1000	1376	1618	0.96
	950	1359	1647	0.40
	900	1380	1586	0.98
	850	1372	1591	0.76
	800	1367	1603	0.65
Cobaltocene	1000	1362	1588	0.68
	950	1367	1558	0.37
	900	1350	1576	0.44
	850	1368	1602	0.53
	800	1372	1574	0.59
Ruthenocene	1000	1342	1586	0.88
	950	1354	1563	0.65
	900	1356	1581	0.63
	850	1340	1583	0.99
	800	1345	1560	0.52

4.3.5 Thermal stability of MWCNTs

TGA experiment provided information on the thermal stability and purity of the MWCNTs. Thermograms of the weight percentage as a function of decomposition temperature for various synthesis temperatures are presented in the Appendix section (Figures A5-A8). All the results were obtained under the same conditions as described in Chapter 3. For every sample analysis, the TGA analysis was done from ambient temperatures to 1000 °C. The materials were heated in air at a rate of 10 °C min^{-1} and the profiles showed that all the samples were stable up to 500 °C. The presence of water was denoted by a loss in weight below 200 °C whereas amorphous carbon on the other hand decomposed between 200 and 400 °C.[28] Thereafter, the decomposition temperatures observed between 450 and 700 °C were characteristic of MWCNTs.[29,30] The slopes of the decompositions also shed light on the materials formed, a steep sharp curve indicated decomposition of a pure material, and a gentle, smooth curve showed a mixture.

The thermal stability of the carbon nanostructures grown from ferrocene, nickelocene, cobaltocene and ruthenocene (2.5 wt.%) are compared in Table 4.6. The thermal stability of the different metallocenes decreased in the order ferrocene > cobaltocene > nickelocene > ruthenocene. For example, the MWCNTs which were synthesized from a growth temperature of 800 °C from ferrocene, cobaltocene, nickelocene and ruthenocene have a decomposition temperature of 602, 531, 520 and 377 °C, respectively. This was also evident in the results of other growth temperatures. The stability of the MWCNTs varies with the growth temperature. Most stable MWCNTs (grown from cobaltocene) were obtained at a temperature of 950 °C with a decomposition temperature of 649 °C. This agrees with the lower I_D/I_G value (suggesting more crystalline material) which is observed in the Raman studies (Table 4.5). The SCNMs grown from ruthenocene were found to be less stable (with a decomposition temperature of 377 °C) than those of other metallocene and this was attributed to ruthenocene being less superaromatic than the other metallocenes.[31]

Table 4.6: Decomposition temperature of MWCNTs

Metallocene	Temperature/°C	Decomposition temperature/°C	Residual metal content/%
Ferrocene	1000	520	0
	950	509	4.1
	900	518	1.5
	850	503	0.2
	800	602	6.0
Nickelocene	1000	525	3.0
	950	600	6.2
	900	568	9.4
	850	580	0
	800	520	8.5
Cobaltocene	1000	520	1.5
	950	649	0
	900	570	0
	850	569	2.1
	800	531	0.5
Ruthenocene	1000	448	0
	950	447	5.3
	900	547	7.5
	850	525	10
	800	377	2.3

An increase in thermal stability was observed with rise in growth temperature for MWCNTs synthesized from cobaltocene. The decomposition temperature of the MWCNTs grown from a growth temperature of 800 to 950 °C increased with the increase in growth temperature but decreased at higher growth temperature of 1000 °C. A similar trend was observed for MWCNTs grown from ruthenocene. The MWCNTs grown from cobaltocene at a growth temperature of 800, 850, 900, 950 °C had decomposition temperatures of 520, 649, 570, 569 °C respectively and at higher growth temperature of 1000 °C was 531 °C. However, this was

not observed for MWCNTs synthesized from ferrocene and nickelocene. MWCNTs grown from ferrocene at growth temperatures of 800, 850, 900, 950 and 1000 °C had decomposition temperatures of 520, 509, 518, 503 and 602 °C, respectively, while for those from nickelocene were 525, 600, 568, 580 and 520 °C. Hence, their decomposition temperature did not show significant dependence on growth temperature.

The gradients of the weight loss profile for decomposition temperatures of the five growth temperatures are all similar, which suggests a similar degree of product distribution of the MWCNTs synthesized from cobaltocene (Figure 4.10 a). The sharper thermogram gradients combined and the narrower decomposition temperature ranges observed from the thermograms of cobaltocene, indicated that these growth temperatures produced a smaller range of SCNMs structure types, and hence likely to be purer samples. Lower decomposition temperatures were observed for the MWCNTs synthesized from ruthenocene, at 800, 850, 900, 950 and 1000 °C which decomposed at 377, 525, 547, 447 and 448 °C, respectively (Table 4.7). This was an indication of levels of impurities in these products. The weight loss (Figure 4.10 b) for these ruthenocene samples at $T < 200$ °C is attributed to the loss of moisture from the materials.

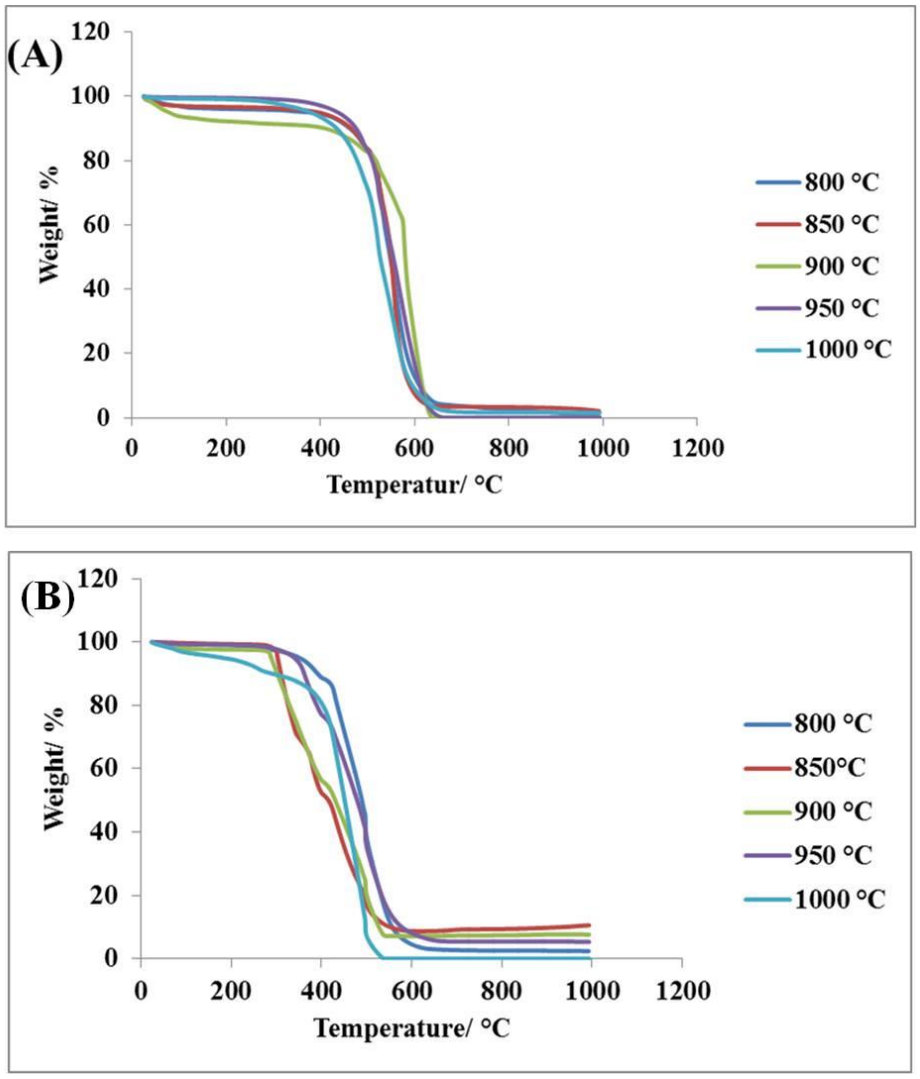

Figure 4.10: Thermogravimetric analysis of MWCNTs synthesized from (A) cobaltocene and (B) ruthenocene

The residual weight (5–10%) observed in the TGA profiles is ascribed to metal oxide (*e.g.* FeO_x) residues formed in air from the catalysts. The residual metal content for all of the catalysts used showed that at higher growth temperature more residual metal quantity were produced compared to the lower growth temperatures. For example, at a growth temperature of 1000 °C, MWCNTs from ferrocene, nickelocene, cobaltocene and ruthenocene had a residual metal of 0, 3.0, 1.5 and 0% respectively. The high residual metal oxide content may be caused by the metal nanoparticles encapsulated inside the MWCNTs. The highest residual metal content was obtained at a growth temperature of 800 °C, for ferrocene and nickelocene were 6.0 and 8.5% respectively, while for cobaltocene and ruthenocene were 2.1 and 10%, respectively, at 850 °C. Cobaltocene produced MWCNTs with lower residual metal

nanoparticle as compared to other metallocenes. This shows that cobaltocene had a higher solubility in toluene.

4.3.6 Textual studies of MWCNTs

BET method was used to determine surface area of MWCNTs. Textural properties and specific surface area information obtained from nitrogen sorption measurements at 77 K are presented in Table 4.7. External surface of MWCNTs generally ranges from 50 to 1315 m^2 g^{-1}.[32] However, the surface areas for as-synthesized MWCNTs range from 10 to 500 m^2 g^{-1}. Activation or chemical treatments of MWCNTs that are employed during purification and processing can result in opening the capped ends of the nanotube ends.[33] This allows access for nitrogen molecules to be adsorb on the of inside the nanotube and thus the measured surface area of a MWCNT is no longer an external surface area issue only but also include the surface area inside the nanotubes. It has been reported that an increase in surface area is experienced when MWCNTs are chemical treated.[34]

In this work, the MWCNTs from ferrocene at a growth temperature of 800 °C had a surface area of 7.3456 m^2 g^{-1} before acid treatment, however, after purification the surface was 280.2447 m^2 g^{-1}. The results showed that the surface area of the MWCNTs increased after acid treatment. This was expected since the impurities such as, amorphous carbon and residual metal were eliminated while introducing various functional groups and de-bundling the individual MWCNTs. Increase in surface area shows that the heating and acid treatment was capable of enlarging the surface of as-synthesized MWCNTs by creating defects like small hole defect on the surface.[32]

Table 4.7: BET surface area and pore volume of MWCNTs

Metallocene	Temperature/°C	Surface area/m^2 g^{-1}	Pore volume/cm^3 g^{-1}	Pore size/nm
Ferrocene	1000	12.2694	0.145292	36.1661
	950	17.6146	0.060343	14.5208
	900	45.0058	0.043892	4.5210
	850	66.0057	0.307644	22.0801
	800	280.2447	0.947583	15.5320
Nickelocene	1000	6.9195	0.033906	26.9102
	950	12.0487	0.046317	23.0897
	900	26.2148	0.280173	35.7432
	850	34.6506	0.086762	14.2765
	800	55.0847	0.118128	11.7647
Cobaltocene	1000	3.7536	0.011735	33.3908
	950	15.4568	0.019764	7.8601
	900	19.1734	0.036001	7.0731
	850	23.3605	0.025594	44.1675
	800	34.9837	0.094468	14.9717
Ruthenocene	1000	3.8329	0.013124	9.8298
	950	6.4938	0.020764	11.3235
	900	13.9445	0.091358	28.8840
	850	18.6512	0.105162	25.3510
	800	39.2307	0.035473	4.6817

The BET results showed that the MWCNTs from higher growth temperatures had lower surface areas as compared to those from lower growth temperatures. It had been speculated that rise in growth temperature speeds up the pyrolysis and deposition of toluene, thus rapid deposition of amorphous carbon heavily blocked the micropores on the surface of MWCNTs at higher temperatures. Additionally, higher temperatures encouraged the formation of carbon spheres which have larger surface areas, thus lowering the overall surface area of the sample. These results correlate with the TEM images which showed that at higher growth temperatures, higher

amounts of carbon nanospheres were formed (Figure 4.3 b). As stated before, that MWCNTs have larger surface area, their surface area is affected by nanofiber or tube diameter and agglomeration. It was observed that the higher the growth temperature, the more pronounced the formation of non-tubular carbon like nanofibers, and correspondingly a decrease in surface areas. This was observed from SCNMs synthesized from nickelocene at 1000 °C (Table 4.7)

For all the MWCNTs synthesized, the highest surface area was obtained at 800 °C. The MWCNTs from ferrocene generally had comparatively higher surface areas. The highest surface (280.2447 m^2 g^{-1}) was observed at 800°C from ferrocene while, lowest surface area (3.7536 m^2 g^{-1}) was obtained from MWCNTs which were synthesized from cobaltocene at 1000 °C. However, the BET specific surface area of MWCNTs synthesized from ruthenocene was much lower than that of ferrocene. MWCNTs prepared from ferrocene at 800 °C had the best adsorption ability (pore volume - 0.947583 cm^3 g^{-1}), while the adsorption ability of the CNTs synthesized from cobaltocene at 1000 °C (0.011735 cm^3 g^{-1}) was the lowest.

The pore volume and size of the MWCNTs are not affected by the growth temperature. Small pores are due to inner channels of MWCNTs while large pores are as a result of entanglement of MWCNTs. The highest pore size was obtained from the MWCNTs prepared from cobaltocene at 850 °C. High contribution of small pores supports the earlier observation from TEM analysis because these samples were found to contain high amounts of tubes with open ends. The MWCNTs which were synthesized from ferrocene at 900 °C had a lower pore size of 4.5210 nm. The low pore size distribution may be caused by the higher presence of functional groups on the surface of modified MWCNTs.

The amount of adsorbed nitrogen at relative pressure was also investigated using adsorption isotherm. It is known that there are five adsorption isotherms being Type I, Type II Type III Type IV and Type V. Appendix (Figure A9 - 12) shows nitrogen adsorption isotherms of CNTs grown from different growth temperatures. The adsorption isotherms (Figure A10 – 12) represent Type IV isotherm along with a define hysteresis loop which is associated with capillary condensation that involved in the mesoporous material.[35] However, MWCNTs synthesized from ferrocene have Type III because they lack a hysteresis loop and this indicates that they have weak adsorbate-adsorbent interaction.

4.4 References

1. M. H. Khedr, K. S. Abdel Halim and N. K. Soliman, *Applied Surface Science*, 2008, 255, 2375-2381.
2. W. K. Maser, A. M. Benito and M. T. Martínez, *Carbon*, 2002, 40, 1685-1695.
3. T. Ebbesen and P. Ajayan, *Nature*, 1992, 358, 220-222.
4. M. Fuhrer, *Science*, 2000, 288, 494.
5. A. Thess, R. Lee, P. Nikolaev, H. Dai, P. Petit, J. Robert, C. Xu, Y. H. Lee, S. G. Kim and A. G. Rinzler, *Science*, 1996, 273, 483-487.
6. Z. Shi, Y. Lian, X. Zhou, Z. Gu, Y. Zhang, S. Iijima, Q. Gong, H. Li and S.-L. Zhang, *Chemical Communications*, 2000, 461-462.
7. K. Tohji, H. Takahashi, Y. Shinoda, N. Shimizu, B. Jeyadevan, I. Matsuoka, Y. Saito, A. Kasuya, S. Ito and Y. Nishina, *The Journal of Physical Chemistry B*, 1997, 101, 1974-1978.
8. B. Liu, T. Wågberg, E. Olsson, R. Yang, H. Li, S. Zhang, H. Yang, G. Zou and B. Sundqvist, *Chemical Physics Letters*, 2000, 320, 365-372.
9. K. A. Worsley, I. Kalinina, E. Bekyarova and R. C. Haddon, *Journal of the American Chemical Society*, 2009, 131, 18153-18158.
10. E. Farkas, M. Elizabeth Anderson, Z. Chen and A. G. Rinzler, *Chemical Physics Letters*, 2002, 363, 111-116.
11. L. Stobinski, B. Lesiak, L. Kövér, J. Tóth, S. Biniak, G. Trykowski and J. Judek, *Journal of Alloys and Compounds*, 2010, 501, 77-84.
12. M. Pumera, *Langmuir*, 2007, 23, 6453-6458.
13. R. Sen, A. Govindaraj and C. N. R. Rao, *Chemical Physics Letters*, 1997, 267, 276-280.
14. M. S. Mohlala, X. Liu, M. J. Witcomb and N. J. Coville, *Applied Organometallics Chemistry*, 2007, 21, 275-280.
15. V. Datsyuk, V. Kalyva, M. Papagelis, K. Parthenios, J. Tasis, D. Siokou, A. Kallitsis and I. Galiotis, *Carbon*. 2008, 46, 833-840

16. D. C. Lee, F. V. Mikulec and B. A. Korgel, *Journal of American Society*, 2004, 126, 4951-4957.

17. E. N. Nxumalo, V. O. Nyamori and N. J. Coville, *Journal of Organometallic Chemistry*, 2008, 693, 2942-2948.

18. A. A. Koós, F. Dillon, E. A. Obraztsova, A. Crossley and N. Grobert, *Carbon*, 2010, 48, 3033-3041.

19. J. D. Harris, R. P. Raffaelle, T. Gennett, B. J. Landi and A. F. Hepp, *Materials Science and Engineering: B*, 2005, 116, 369-374.

20. Y. Wang, M. Li, Y. Gu, X. Zhang, S. Wang, Q. Li and Z. Zhang, *Nanoscale*, 2015, 7, 3060-3066.

21. A. Cao, L. Ci, D. Li, B. Wei, C. Xu, J. Liang and D. Wu, *Chemical Physics Letters*, 2001, 335, 150-154.

22. N. Grobert, M. Mayne, M. Terrones, J. Sloan, R. Dunin-Borkowski, R. Kamalakaran, T. Seeger, H. Terrones, M. Rühle and D. Walton, *Chemical Communications*, 2001, 471-472.

23. C. P. Deck and K. Vecchio, *Carbon*, 2005, 43, 2608-2617.

24. D. Pradhan and M. Sharon, *Materials Science and Engineering: B*, 2002, 96, 24-28.

25. M. Kumar and Y. Ando, *Carbon*, 2005, 43, 533-540.

26. G. D. R. Saito, M. S. Dresselhaus, *Physical Properties of Carbon Nanotubes*, Imperial College Press, London, 1999, vol. 10, pp. 190.

27. S. M. Bachilo, M. S. Strano, C. Kittrell, R. H. Hauge, R. E. Smalley and R. B. Weisman, *Science*, 2002, 298, 2361-2366.

28. H. Li, N. Zhao, C. He, C. Shi, X. Du and J. Li, *Materials Science and Engineering: A*, 2008, 473, 355-359.

29. D. Porwal, K. Mukhopadhyay, K. Ram and G. Mathur, *Thermochimica Acta*, 2007, 463, 53-59.

30. P. Piedigrosso, Z. Konya, J.-F. Colomer, A. Fonseca, G. Van Tendeloo and J. B. Nagy, *Physical Chemistry Chemical Physics*, 2000, 2, 163-170.

31. A. N. Nesmeyanov, A. A. Lubovich and S. P. Gubin, *Bulletin of the Academy of Sciences of the USSR, Division of chemical science*, 1972, 21, 1761-1764.

32. A. Peigney, C. Laurent, E. Flahaut, R. R. Bacsa and A. Rousset, *Carbon*, 2001, 39, 507-514.

33. E. Frackowiak, S. Delpeux, K. Jurewicz, K. Szostak, D. Cazorla-Amoros and F. Béguin, *Chemical Physics Letters*, 2002, 361, 35-41.

34. E. Raymundo-Piñero, P. Azaïs, T. Cacciaguerra, D. Cazorla-Amorós, A. Linares-Solano and F. Béguin, *Carbon*, 2005, 43, 786-795.

35. B. Naik, C. H. Manoratne, A. Chandrashekhar, A. Iyer, V. S. Prasad and N. N. Ghosh, *Journal of Experimental Nanoscience*, 2013, 8, 462-479.

CHAPTER 5: RESULT AND DISCUSSION OF N-MWCNTs

This chapter summarizes the results obtained during the synthesis of N-MWCNTs. The effects of varying parameters, such as catalyst and temperature, on the N-MWCNTs and other SCNMs are presented. The measure of these effects was based on N-MWCNTs produced, the size and yield, and also the nitrogen content incorporated into the tubes.

5.1 SCNMs, yields and distribution

N-MWCNTs were synthesized from a solution of ferrocene, nickelocene, cobaltocene or ruthenocene, in acetonitrile at different growth temperatures, *i.e.* 800, 850, 900, 950 or 1000 °C. Ferrocene was used as a catalyst in order to provide reference data as it has been widely investigated.[1-4] In this work, it was observed that at lower growth temperature (800 °C), lower effective carbon decomposition rate was achieved compared to higher growth temperature (1000 °C). Thus, a faster carbon decomposition rate provided higher yields of carbonaceous materials as compared to the lower growth temperature. Consequently, the yield of carbonaceous material, with all the catalysts used, showed an increase as the growth temperatures was increased. Cobaltocene as a catalyst gave a higher yield in comparison to other catalysts used (Table 5.1). All the growth temperatures tested for ruthenocene produced lower yields of carbonaceous materials. This may be caused by lower solubility of the ruthenocene in acetonitrile.

All investigated growth temperatures had different morphological profiles of SCNMs. The three main SCNMs obtained were: N-MWCNTs, carbon spheres and amorphous carbon. A growth temperature of 800 °C gave high amounts of the amorphous carbon. However, as the growth temperature was raised the amount of amorphous carbon decreased. Also, it was observed that as the growth temperatures increased, percentage yield of tubes decreased while the percentage of carbon spheres increased. The higher percentage of carbon spheres at higher growth temperature was caused by the agglomeration of catalyst nanoparticles into larger particles, thus not suitable for N-MWCNTs formation.[5] High amount of well-structured N-MWCNTs were observed at 850 °C (Table 5.1) and for instance, ferrocene, nickelocene, cobaltocene and ruthenocene gave 85, 80, 75 and 65%, respectively. From these results it was concluded that when ferrocene is used as catalyst, high amounts of N-MWCNTs are obtained compared to the other three catalysts investigated.

Table 5.1: Distribution of SCNMs synthesized from different metallocenes at the varying temperatures

Metallocenes	Temperature/ °C	Yield /mg	Distribution/%
Ferrocene	1000	533.7	50 (CSs), 50 (Ts)
	950	414.9	40 (CSs), 60 (Ts)
	900	320.9	30 (CSs), 70 (Ts)
	850	295.4	15 (Am), 85 (Ts)
	800	221.3	50 (Am), 50 (Ts)
Nickelocene	1000	415.0	60 (CSs), 35 (Ts)
	950	381.7	55 (CSs), 45 (Ts)
	900	229.0	50 (CSs), 50 (Ts)
	850	182.0	20 (Am), 80 (Ts)
	800	127.1	40 (Am), 60 (Ts)
Cobaltocene	1000	760.9	70 (CSs), 30 (Ts)
	950	644.1	60 (CSs), 40 (Ts)
	900	397.0	45 (CSs), 55 (Ts)
	850	352.2	25 (Am), 75 (Ts)
	800	277.8	60 (Am), 40 (Ts)
Ruthenocene	1000	490.3	65 (CS), 35 (Ts)
	950	336.7	50 (CS), 50 (Ts)
	900	263.1	45 (CS), 55 (Ts)
	850	134.1	35 (Am), 65 (Ts)
	800	84.1	55 (Am), 45 (Ts)

*CSs – carbon spheres, Ts – tubes, Am – amorphous carbon

TEM analyses showed different variation of micro-structures of C-N nanotubes which were synthesized at different growth temperatures. In Figures 5.1 to 5.4, the TEM micrographs showed that the nitrogen-doping effect where by the tubes structure showed formation of bamboo-like compartments. This was also observed in the N-MWCNTs structures which were separated by compartments similar to those reported by Nxumalo *et al.*[6] However, the presence of these bamboo compartments in the tubes does not necessary indicate nitrogen incorporation since the bamboo compartment structure have been discovered in Y-junction MWCNTs which lack nitrogen.[1]

In Figure 5.1 d and e, the TEM images showed kinked morphology in the N-MWCNTs produced at higher growth temperatures (950 and 1000 °C). Kinked morphology in the N-MWCNTs was caused by the development of pentagonal and heptagonal structure into the graphene layers.[7] Pentagonal and heptagonal structures are induced by pyridinic and pyrrolic nitrogen-doping.

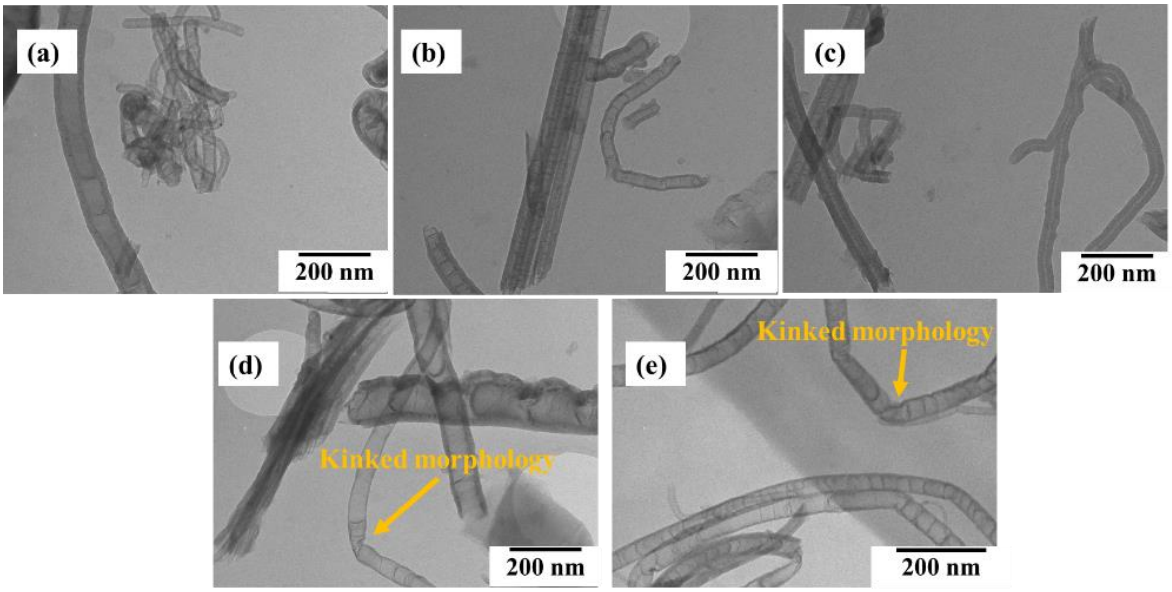

Figure 5.1: TEM images of the N-MWCNTs synthesized from ferrocene at different growth temperatures (a) 800, (b) 850, (c) 900, (d) 950 and (e) 1000 °C

When nickelocene catalyst was used at a temperature of 800 °C, a mixture of nanotubes and amorphous carbon were obtained. The formation of spheres increased with growth temperature while the amount of MWCNTs decreased (Ts: CSs, 35:60). This implied that for nickelocene,

a lower growth temperatures are favoured the N-MWCNTs production while relatively higher temperature favoured carbon spheres production. The SEM images (Appendix – Figure B1) and TEM image in Figure 5.2 b reveal that at a growth temperature of 850 °C, very aligned N-MWCNTs were obtained.

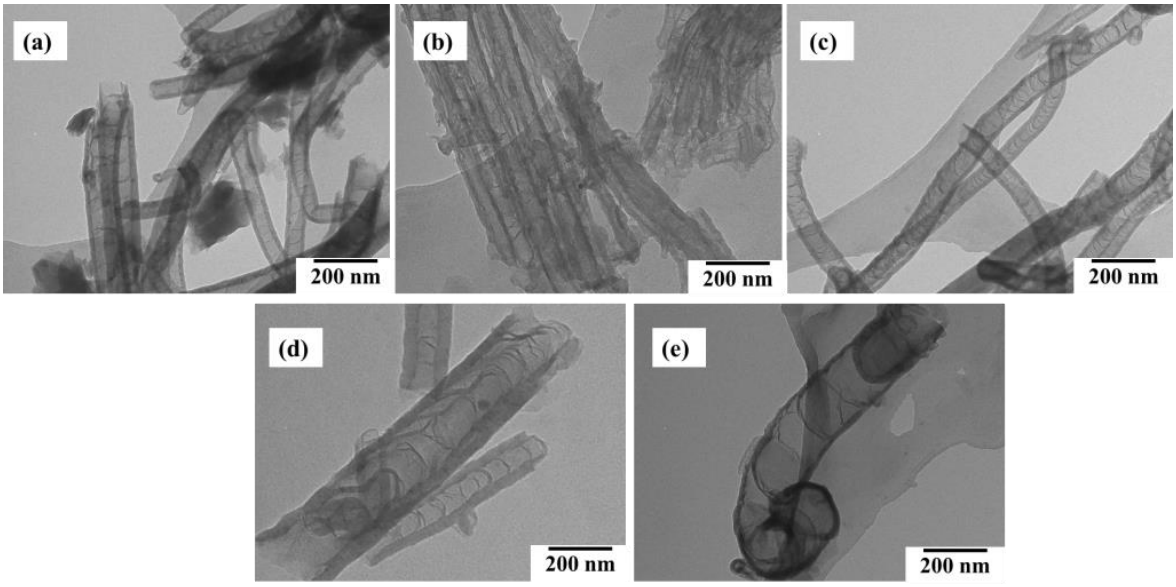

Figure 5.2: TEM images of the N-MWCNTs synthesized from nickelocene at different growth temperatures (a) 800, (b) 850, (c) 900, (d) 950 and (e) 1000 °C

Spaghetti-like MWCNTs were observed at a growth temperature of 800 to 900 °C when cobaltocene was used as the catalyst (Figure 5.3). Most of N-MWCNTs grown at lower temperature (800 and 850 °C) had curled compartment layers with regular and uniform separation while the higher temperature of 1000 °C had random and irregular separation. This was also seen in the SEM image (Appendix – Figure B1). At 1000 °C, small amount of N-MWCNTs were observed under carbon nanospheres.

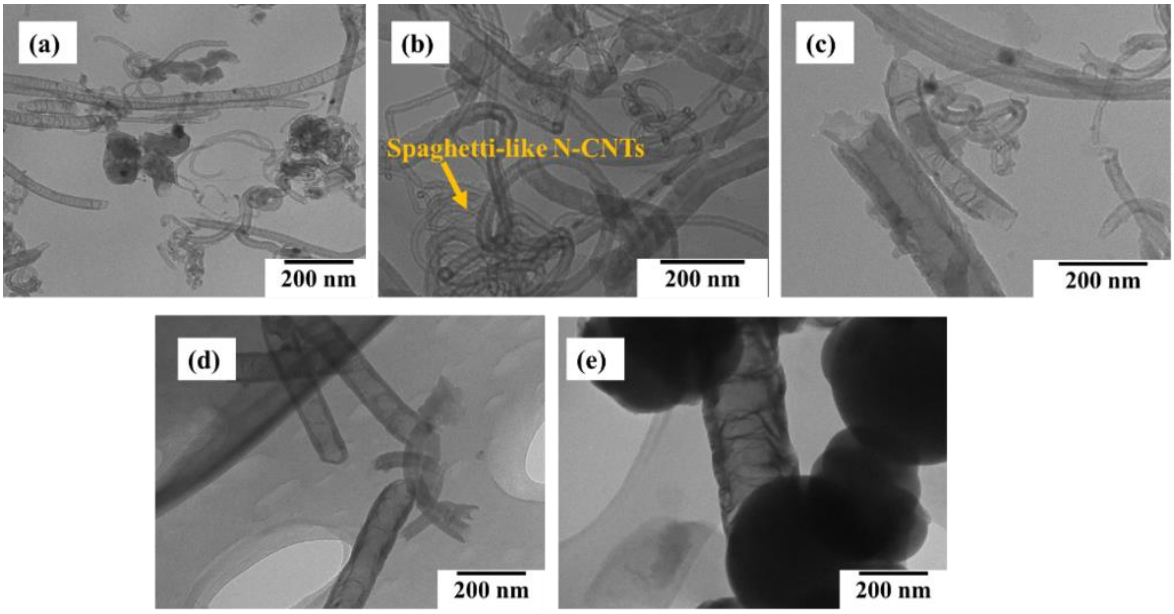

Figure 5.3: TEM images of the N-MWCNTs synthesized from cobaltocene at different growth temperatures (a) 800, (b) 850, (c) 900, (d) 950 and (e) 1000 °C

When ruthenocene was used as a catalyst, helical N-MWCNTs were obtained at growth temperatures of 800 and 900 °C (Figure 5.4 a and c). All the N-MWCNTs were open at the end with hemi-spherical caps as shown in Figure 5.4 b. At 850 °C, NMWCNTs with open ends were observed (Figure 5.4 b). The open ends are caused by acid treatment.[8] The residual metal particles were observed within the walls of the N-MWCNTs (Figure 5.4 d). This indicated N-MWCNTs were mostly grown by the tip-growth mechanism.[9] Tip-growth mechanism occurs when the residual metal nanoparticle resides at the top of the MWCNTs.

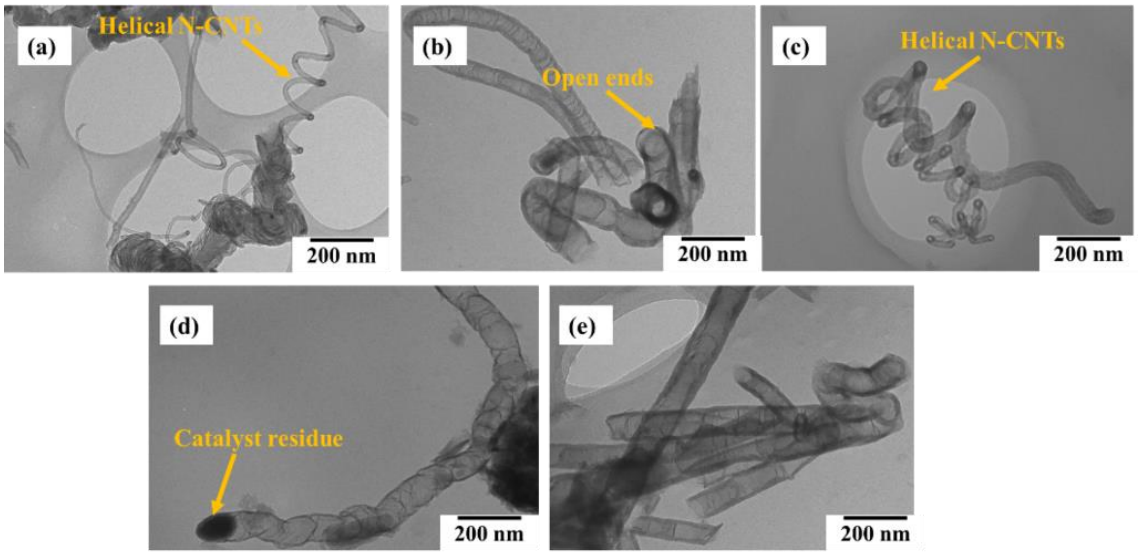

Figure 5.4: TEM images of the N-MWCNTs synthesized from ruthenocene at different growth temperatures (a) 800, (b) 850, (c) 900, (d) 950 and (e) 1000 °C

5.2 Elemental analysis

EDX analysis was used to investigate the elemental composition of SCNMs grown at 850 °C. The growth temperature at 850 °C was chosen for this analysis because of high amount of MWCNT obtained in this temperature. Different amounts of elements are shown in Table 5.2. The materials were found to contain carbon, oxygen, nitrogen and different metals, *i.e.* iron, nickel, cobalt or ruthenium (depending on the catalyst used). The highest metal nanoparticles were obtained from SCNMs grown from ferrocene (3.22%).

The presence of nitrogen in the SCNMs serves as indication that nitrogen was incorporated into the CNTs walls. The amount of nitrogen was 3.42, 5.23, 5.00 and 0% in the SCNMs from ferrocene, nickelocene, cobaltocene and ruthenocene, respectively (Table 5.2). The greater nitrogen content was in SCNMs obtained from catalyst nickelocene containing 5.23%. However, SCNMs that were grown from ruthenocene were found to lack nitrogen content. This was not conclusive since the EDX analysis may not have been good enough in picking up nitrogen in sample, as it only analysed certain areas on the sample instead of the bulk materials. To eliminate this uncertainty, the samples were then further analysed using elemental analysis in order to confirm the actual nitrogen content. This is further discussed in Section 5.3 and results are tabulated in Table 5.2

Table 5.2: Elemental composition of N-MWCNTs synthesized from different metallocenes at 850 °C using EDX

Element	Content/%			
	Ferrocene	**Nickelocene**	**Cobaltocene**	**Ruthenocene**
C	91.20	89.37	84.20	88.34
O	2.13	5.07	9.03	10.40
N	3.45	5.23	5.00	0
Metal	3.22	0.34	1.77	1.26

5.3 Effect of growth temperature

5.3.1 Bamboo compartments distance and nitrogen content of N-MWCNTs

The size of bamboo compartments (length) were measured from the TEM images of different samples and are presented in Table 5.3. The compartment distance indicates the level of nitrogen in the MWCNTs. An increase in nitrogen percentage caused a decrease in compartment distance.[6,10] This was observed from N-MWCNTs synthesized from a growth temperature of 850 °C for all of the metallocene catalysts used.

N-MWCNTs synthesized from nickelocene were observed to have the shortest distance of bamboo compartments (15.6 nm) and therefore, contained highest percentage of nitrogen (18.207%). The bamboo compartment distance of the N-MWCNTs was found to increase with the increase in growth temperatures from 850 to 900 °C. However, from a growth of 950 to 1000 °C a drop of nitrogen percentage was seen. An increase in temperature with nitrogen content was also reported by Jang *et al.*[10,11] A growth temperature of 1000 °C was found to produce MWCNTs with longer bamboo compartment having a length of 36.0, 30.5, 30.3 and 49.2 nm when synthesized using ferrocene, nickelocene, cobaltocene and ruthenocene catalysts, respectively. However, from a growth temperature of 800 to 850 °C, a decrease in bamboo compartment distance was observed. This trend was observed in all of the metallocene catalyst used.

Table 5.3: Elemental analysis of the N-MWCNTs synthesized from different metallocenes at different growth temperatures

Metallocenes	Temperature/°C	Bamboo compartment distance/nm	Nitrogen content/%
Ferrocene	1000	36.0	7.665
	950	38.5	6.566
	900	35.7	7.530
	850	30.1	8.619
	800	49.4	1.590
Nickelocene	1000	30.5	5.122
	950	25.1	7.394
	900	20.3	13.630
	850	15.6	18.207
	800	18.8	14.411
Cobaltocene	1000	30.3	5.906
	950	28.6	7.710
	900	25.9	12.742
	850	20.8	11.881
	800	35.2	1.160
Ruthenocene	1000	49.2	5.215
	950	45.5	5.792
	900	43.6	5.894
	850	40.0	6.521
	800	50.3	3.367

The elemental analysis of carbon, hydrogen and nitrogen (CHN) was performed in order to investigate the relationship between nitrogen-doping and growth temperature. The percentage of nitrogen content in the MWCNTs for all samples increased with increase in growth temperature from 800 to 850 °C. However, from growth temperatures of 900 to 1000 °C, the percentage content of nitrogen decreased. Tang *et al.*[12] reported that as the growth temperature increase from 800 to 900 °C, the level of nitrogen-doping decreased by half. The decrease in

nitrogen contents maybe caused by escape of some of the high energy elemental nitrogen or radicals which were not fully incorporated within the graphene structure through the exhaust system. This was clearly seen from the water trap which demonstrated vigorous bubbling.

Highly doped N-MWCNTs formed had shorter bamboo compartments because more nitrogen atoms were incorporated. The length of the bamboo compartments indicates the extent of nitrogen doping. At 1000 °C, the bamboo compartments were relatively longer in size when compared to those of the lower growth temperature of 850 °C. As the growth temperature increased, the N-content decreased, this resulted in the increased compartment separation.[13,14] Comparable observations were made by Keru *et al*.[15] who also reported an increase in nitrogen content in MWCNTs with decrease in growth temperature.

MWCNTs grown from ferrocene at 850 °C were much more aligned and contained higher level of nitrogen-doping than those from other growth temperatures. Koo´s *et al.*[16] reported comparable results. The highest nitrogen content was obtained at a growth temperature of 850 °C for all metallocenes; 18.20, 11.88, 8.61 and 6.52% for nickelocene, cobaltocene, ferrocene and ruthenocene, respectively (Figure 5.5). Their elemental analyses at 850 °C, correlates with the TEM images from Figure 5.1 b, 5.2 b, 5.3 b and 5.4 b as shown by their shorter bamboo compartments. The N-MWCNTs which were synthesized from ruthenocene catalyst contained longest bamboo compartment distances at all the growth temperatures used when compared to other metallocenes.

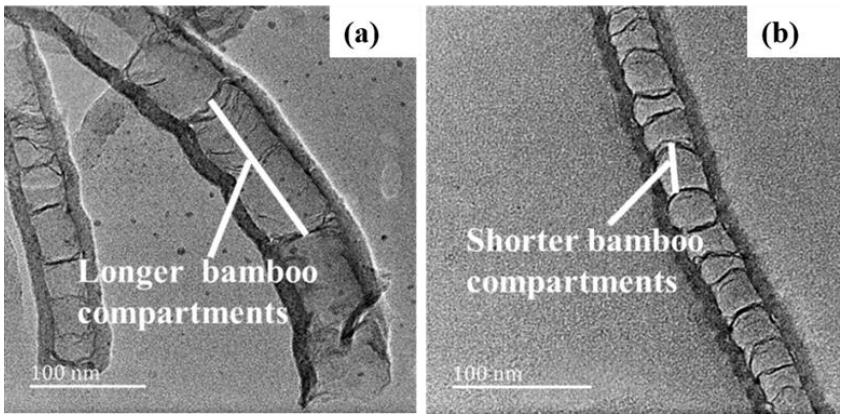

Figure 5.5: HRTEM images of N-MWCNTs grown at 850 °C from (a) ruthenocene and (b) nickelocene which indicate the distances of bamboo compartments

5.3.2 Average inner- and outer-diameters of N-MWCNTs

The outer- and inner-diameters of the N-MWCNTs were investigated using TEM images and the results are summarized in Figures 5.6 and 5.7. From all of the catalysts used it was observed that the growth temperature had a huge impact on the outer- and inner-diameters of the N-MWCNTs formed. The outer- and inner-diameters of the N-MWCNTs increased with growth temperatures. However, other reports indicated that higher temperature results in thinner and longer CNTs while lower temperature yielded thicker and shorter CNTs.[17,18] The difference of these results with the reported trend could be attributed not only to the different methods used during synthesis, but also by the kind of catalyst and carbon source used. In addition, the use of acetonitrile (as carbon source) formed MWCNTs with bigger inner-diameters and smaller wall thicknesses. The increased internal diameter and reduced wall thickness could be due to the level of nitrogen doping.

The N-MWCNTs from different metallocenes had different averages of outer- and inner-diameter, ranging from 40 to 78 nm for outer-diameter and from 30 to 72 nm for inner-diameter. This suggests that as the growth temperature increase, more sintering of the metallocene catalysts occur, which results to larger-sized N-MWCNTs being formed. Similar observation of lager diameters of N-MWCNTs have been made using other different precursors.[19,20] N-MWCNTs grown from nickelocene exhibited a larger outer-diameter (52 nm) at a growth temperature of 800 °C. However, the OD of N-MWCNTs synthesized from ferrocene increased ranging from 63 nm at 850 °C to 79 nm at 1000 °C. These N-MWCNTs had largest ODs. The smallest ODs were recorded for N-MWCNTs grown from ruthenocene; 51, 53, 56 and 62 nm at 850, 900, 950 and 1000 °C, respectively.

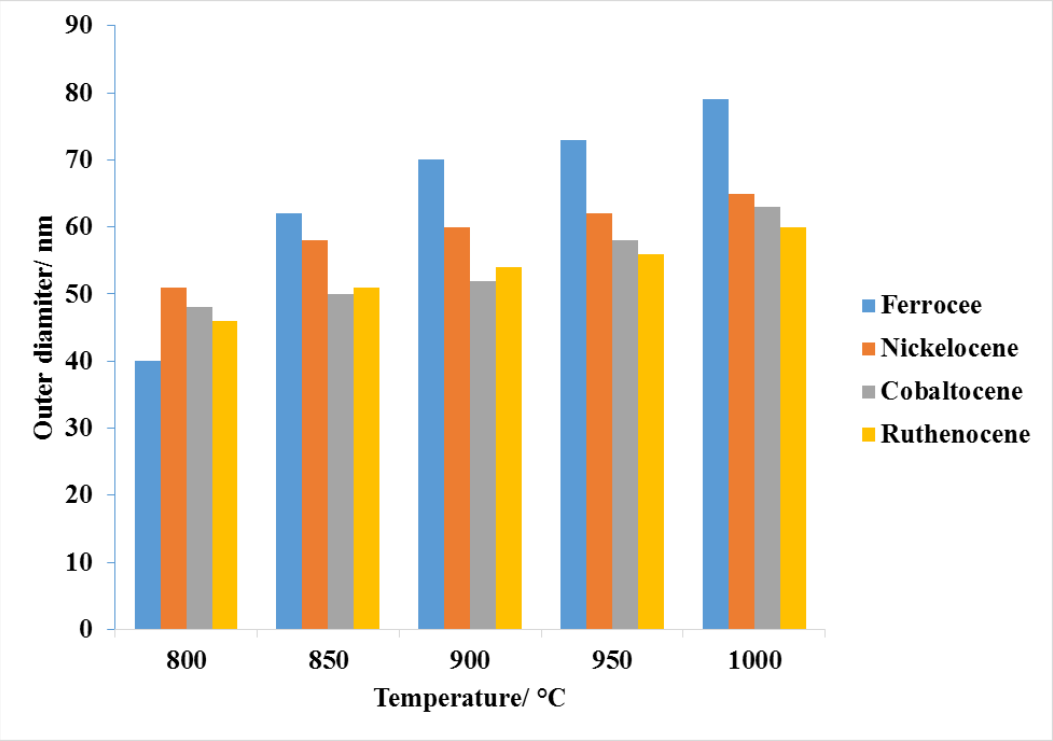

Figure 5.6: Outer-diameter of the N-MWCNTs synthesized from different metallocenes at different growth temperatures

A similar trend was observed for inner-diameters (IDs) of N-MWCNTs. The IDs increased with the increase in growth temperatures of N-MWCNTs. The N incorporated in the MWCNTs caused larger IDs compared to undoped MWCNTs reported in Chapter 4 (Figure 4.8). Similar observations were noted when aniline/ferrocene was used in the synthesis of N-CNTs.[21] It had been reported that N-MWCNTs with high nitrogen content have smaller IDs.[22] This was observed in the N-MWCNTs grown from nickelocene and cobaltocene. However, N-MWCNTs from ferrocene had larger inner-diameter as compared to other catalysts. This also correlates with the nitrogen content of these N-MWCNTs because they had lower nitrogen doping level. For example, N-MWCNTs grown from 850 °C had 8.619% of nitrogen content and an inner-diameter of 58 nm.

For all of the N-MWCNTs grown from different catalysts, it was observed that the N-MWCNTs grown at growth temperature of 850 °C had the smallest inner wall thickness. These findings were similar with those of Ionescu *et al.*[23] who reported that there was an increase in inner-diameter of N-MWCNTs and decrease in wall thickness with increased nitrogen doping.

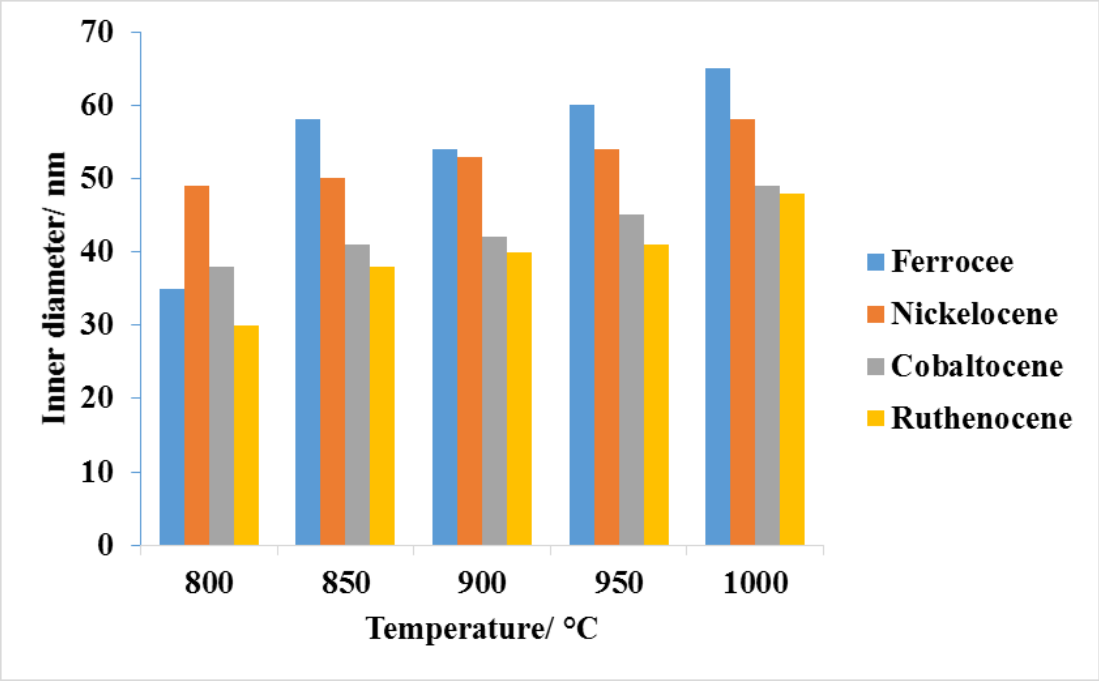

Figure 5.7: Inner-diameter of N-MWCNTs synthesized from different metallocenes at different growth temperatures

5.3.3 Crystallinity of N-MWCNTs

The quality of N-MWCNTs was investigated by using Raman spectroscopy based on I_D/I_G ratio. A higher I_D/I_G ratio implied that there is higher degree of disorder, while a low I_D/I_G ratio implied that the materials are more graphitic and correspondingly higher crystallinity of N-MWCNTs.[21] The intensity ratio (I_D/I_G) also plays an important role in estimating the defect concentration of nitrogen content in the MWCNTs.[24,25] The intensity ratio of D- to G-band is affected by the number of defects which arise from incorporation of nitrogen. Therefore, as the concentration of nitrogen atoms increase, the D-bands becomes more intense and broader peaks are observed.[26]

In the research done by Nxumalo *et al.*[21], which involved the synthesis of CNTs and N-CNTs using ferrocene/toluene and ferrocenylaniline/toluene, it was observed that N-CNTs were more disordered than the CNTs grown from ferrocene/toluene. Therefore, similar results were obtained in this work, even though Nxumalo *et al.* had made use of organometallic catalysts as the nitrogen source, while in this study, acetonitrile[27]was used as both carbon and nitrogen source.

It was observed that as the growth temperature increased from 800 to 850 °C, the level of nitrogen-doping increased which implies a higher level of disorder in N-MWCNTs. This was observed in all N-MWCNTs synthesized from different metallocenes (Table 5.4). For instance, N-MWCNTs from ferrocene, grown at 800 and 850 °C had an I_D/I_G ratio of 1.20 and 1.32, respectively. The higher level of disorder from Raman spectroscopy, also agrees with the results obtained from TEM images (Figure 5.1 – 5.4) and elemental analysis (Table 5.3). This similar substantial increase of I_D/I_G ratio was also observed by Droppa *et al.*[28] in his findings on the incorporation of nitrogen in carbon nanotubes.

As the growth temperatures increase from 900 to 1000 °C, lower the level of disorder was observed. For example, N-MWCNTs from ferrocene had an I_D/I_G ratio of 1.17, 1.09 and 1.07 at a growth temperature of 900, 950 and 1000 °C, respectively. This could be caused by reduction of amorphous products as well as, drop in level of nitrogen-doping (Table 5.3). This shows that N-MWCNTs become more crystalline as the growth temperatures increases. This was observed for all metallocenes investigated. Table 5.4 shows a shift in the D-band and G-band from 1389 to 1340 cm^{-1} and 1611 to 1550 cm^{-1}, when the growth temperature increase from 800 to 1000 °C, respectively. Similar shifting trend was also observed by Yadav *et al.*[10] when growth temperature was increased from 850 to 950 °C.

Table 5.4: Raman analysis of N-MWCNTs

Metallocenes	Temperature/°C	D-band/cm^{-1}	G-band/cm^{-1}	I_D/I_G
Ferrocene	1000	1365	1561	1.07
	950	1377	1564	1.09
	900	1379	1565	1.17
	850	1383	1579	1.32
	800	1379	1573	1.20
Nickelocene	1000	1349	1565	0.99
	950	1359	1580	1.04
	900	1373	1611	1.28
	850	1379	1609	1.65
	800	1373	1605	1.40
Cobaltocene	1000	1363	1569	1.02
	950	1378	1570	1.06
	900	1381	1574	1.08
	850	1389	1595	1.24
	800	1389	1587	1.11
Ruthenocene	1000	1336	1550	1.12
	950	1340	1550	1.21
	900	1368	1553	1.43
	850	1372	1553	1.51
	800	1350	1552	1.37

The Raman analysis of N-MWCNTs, revealed that the I_D/I_G ratio was high at a growth temperature of 850 °C for ferrocene, nickelocene, cobaltocene and ruthenocene: *i.e.* 1.32, 1.65, 1.24 and 1.51, respectively. These results are consistent with elemental analysis, where N-MWCNTs from nickelocene displayed significantly higher amounts of structural defect as compared to the other N-MWCNTs. However, the N-MWCNTs synthesized from ruthenocene were found to be more disordered (I_D/I_G ratio - 1.51), even with low level of nitrogen-doping. This may be caused by the poor solubility of ruthenocene in acetonitrile before their synthesis and also it may be caused by the high amounts of amorphous products present in these N-

MWCNTs products. N-MWCNTs grown from ferrocene and cobaltocene had lower I_D/I_G ratio as compared to those of nickelocene and ruthenocene. It can be speculated that the metallocenes which contains larger metal sizes produces higher disorders. The lowest I_D/I_G ratio was obtained from N-MWCNTs synthesized from ferrocene, nickelocene, cobaltocene and ruthenocene at 1000 °C, *i.e.* 1.07, 0.99, 1.02 and 1.12, respectively.

5.3.4 Thermal stability of N-MWCNTs

The thermal stabilities of SCNMs were evaluated by thermogravimetric analysis under an air flow rate of 30 mL min^{-1} and constant heating of 10 °C min^{-1}. Appendix (Figure B26-29) shows TGA thermograms and their corresponding derivative curves for the N-MWCNTs synthesized from 800 to 1000 °C. The presence of nitrogen in the MWCNTs was indicated by the change in their decomposition temperatures[21] from the TGA analysis. N-MWCNTs were found to be less stable than their undoped counterparts and this was attributed to the structural disorder introduced by the presence of nitrogen into the carbon lattices.[29,30] These results are in accordance with those reported by Nxumalo *et al*.[21] The decomposition of N-MWCNTs corresponds with the lattice defects. Higher decomposition temperatures have lower defects due to lower nitrogen incorporation in the MWCNTs. The increase in thermal stability as the growth temperatures increased was thus observed. The TGA decomposition temperatures of the synthesized materials are listed in Table 5.5.

From Table 5.5 it can be concluded that the N-MWCNTs with more nitrogen incorporated and grown at lower growth temperatures are less thermally stable. For instance, N-MWCNTs synthesized from a growth temperature of 850 °C, using ferrocene, nickelocene, cobaltocene and ruthenocene had lower decomposition temperatures of 416, 400, 514 and 380 °C, respectively. The possible reason for this could be due to high content of impure materials besides high nitrogen content, compared to those that were synthesized from higher growth temperatures. The nitrogen doping in this work produced less thermally stable, less graphitic and more disordered MWCNTs. The elemental analysis in Table 5.3 showed that N-MWCNTs synthesized from ruthenocene had lowest nitrogen-doping level, however, their Raman analysis indicated higher degree of disorder giving reason why they showed lower thermal stabilities in the TGA analysis. This indicate that not only nitrogen content in MWCNTs contribute to thermal stabilities but also presence of other forms of carbon in the sample.

Generally, for all metallocenes investigated, it was observed that N-MWCNTs synthesized at a temperature of 850 °C showed lowest thermal stabilities and were found to have the highest levels of nitrogen-doped. This inverse relationship between the thermal stability and N concentrations in N-MWCNTs found in this work is in agreement with what is reported in literature.[31,32]

Table 5.5: Decomposition temperatures of N-MWCNTs

Metallocene	Temperature/°C	Decomposition temperature/°C	Residual metal content/%
Ferrocene	1000	598	2
	950	561	5
	900	522	5.5
	850	416	2
	800	446	10
Nickelocene	1000	609	3
	950	535	1
	900	501	2
	850	400	4
	800	484	10
Cobaltocene	1000	602	6
	950	569	3
	900	563	4.5
	850	514	2
	800	523	2.5
Ruthenocene	1000	534	1
	950	449	3
	900	440	3
	850	380	1
	800	400	4

The N-MWCNTs grown from cobaltocene and ferrocene were found to be more thermally stable indicated by their higher decomposition temperatures which ranged from 500 to 620 °C. However, they contain lower nitrogen content as compared to N-MWCNTs grown from nickelocene. The N-MWCNTs which were synthesized from a growth temperature of 1000 °C from ferrocene, cobaltocene, nickelocene and ruthenocene have a decomposition temperature of 598, 609, 602 and 534 °C, respectively. The stability of the N-MWCNTs therefore, depended on the growth temperature. Most stable N-MWCNTs (grown from nickelocene)

were obtained at a temperature of 1000 °C with a decomposition temperature of 609 °C whereas those from ruthenocene were found to be least stable with a decomposition temperature of 380 °C.

The residual weights of the investigated samples ranged from 1 to 10 wt.%. There was no clear trend in the residual metal contents of N-MWCNTs and thus independent of the growth temperatures for most metallocenes. However, for N-MWCNTs grown from ruthenocene, the residual metal contents decreased with increase in growth temperatures. The mean residual weights between 5 to 10 wt.%, is normally ascribed to the metal oxide residues formed during the oxidation of the residual catalysts. The highest residual metal content in this work was obtained for N-MWCNTs synthesized from ferrocene and nickelocene (10 wt.%) at a growth temperature of 800 °C. Ruthenocene as a catalyst, in this work produced lowest residual metal contents at growth temperatures; 800, 850, 900, 950 and 1000 °C which were 4, 1, 3, 3 and 1 wt.%, respectively.

The highest residual metal content was obtained at a growth temperature of 800 °C, for ferrocene, nickelocene and ruthenocene being 10, 10 and 4 wt.%, respectively. Cobaltocene on the other hand, the highest metal content of 6 wt.% was obtained at 1000 °C. The lowest residual metal content was obtained from ferrocene and ruthenocene at 1000 and 850 °C were 2 and 1 wt.%, respectively. Also, for cobaltocene (2 wt.%), was observed at a growth temperature of 850 °C and nickelocene (1 wt.%) at 950 °C.

5.3.5 Textual morphology of N-MWCNTs

The surface area, pore volume and pore size of the N-MWCNTs are shown in Table 5.6. As the growth temperature increased the surface area and the pore volume decreased. However, the pore size of the N-MWCNTs showed that they are independent of the growth temperature because their size varied non-linearly. Higher temperature gave low surface areas because of significantly larger percentage of spheres which lowered the overall surface areas of these materials. These results correlate with the TEM image and Table 5.1 which showed that at higher growth temperature there were high amounts of carbon nanospheres.

All metallocenes investigated gave products with higher surface areas at a temperature of 800 °C. The N-MWCNTs from ferrocene were found to have highest surface area at all growth temperatures. The highest (79.34 $m^2 g^{-1}$) surface area was observed at 850 °C from ferrocene and the lowest surface area was obtained for N-MWCNTs which were synthesized by use of cobaltocene at a temperature of 1000 °C (1.79 $m^2 g^{-1}$). N-MWCNTs prepared from ferrocene at 850 °C had the best adsorptive ability (pore volume – 0.403552 $cm^3 g^{-1}$), while the adsorption ability of the N-MWCNTs synthesized using cobaltocene at 1000 °C (0.008940 $cm^3 g^{-1}$) was the least. There was no clear correlation between the surface area and the level of nitrogen in these MWCNTs.[21]

Table 5.6: BET analysis of N-MWCNTs

Metallocene	Temperature/°C	Surface area/m^2 g^{-1}	Pore Volume/cm^3 g^{-1}	Pore size/nm
Ferrocene	1000	13.5623	0.082034	29.8355
	950	19.9382	0.105751	23.1771
	900	39.6166	0.210284	22.8971
	850	79.3403	0.403552	24.1556
	800	46.8805	0.271490	23.6588
Nickelocene	1000	3.8447	0.016453	20.1153
	950	18.6512	0.105162	25.3510
	900	19.2347	0.069782	17.0795
	850	24.4370	0.52668	11.8216
	800	46.0432	0.245566	22.6914
Cobaltocene	1000	1.7927	0.008940	45.5730
	950	3.3263	0.012015	33.2794
	900	21.1077	0.116755	23.3178
	850	55.8089	0.234028	19.4269
	800	34.6506	0.086762	14.2765
Ruthenocene	1000	3.8329	0.013124	9.8298
	950	6.4939	0.020764	11.3235
	900	14.7967	0.035254	10.8439
	850	21.1077	0.116755	23.3178
	800	32.4737	0.088358	12.1531

The BET results showed that the N-MWCNTs obtained from higher growth temperatures had lower surface area as compared to those from lower growth temperatures. It was speculated that raising the growth temperature speeds up the pyrolysis and deposition of acetonitrile. This rapid deposition of carbon heavily blocked the micropores on the surface of N-MWCNTs at higher temperature, thereby dramatically decreasing the adsorptive surface. Additionally, higher temperatures gave low surface areas because of higher percentages of carbon spheres which lowered the overall surface area of materials.

The highest surface areas were obtained at a growth temperature of 800 °C for N-MWCNTs grown from nickelocene and ruthenocene while for ferrocene and cobaltocene was obtained at 850 °C. The N-MWCNTs from ferrocene were found to show higher surface area at all the growth temperatures. The highest surface area (79.3403 m^2 g^{-1}) was observed at 850 °C from ferrocene and the lowest surface area was obtained from N-MWCNTs which were synthesized from cobaltocene at a temperature of 1000 °C. However, the BET specific surface areas of N-MWCNTs synthesized from ruthenocene was much lower than that of ferrocene. N-MWCNTs prepared from nickelocene at 850 °C had the best adsorption ability (pore volume; 0.52668 cm^3 g^{-1}), while the adsorption ability of the N-MWCNTs synthesized from cobaltocene at 1000 °C (0.008940 cm^3 g^{-1}) was the lowest.

The pore volume and size of the N-MWCNTs were affected by the growth temperatures. Normally, small pores are due to inner channels of N-MWCNTs while large pores are as a result of entanglement of N-MWCNTs. The highest pore size was obtained from the N-MWCNTs prepared from cobaltocene at 850 °C. The observed high surface area for these N-MWCNTs could be largely contributed by the small pores because the TEM images showed these samples to contain majorly open ended tubes (Figure 5.4 b). The synthesized N-MWCNTs had varied lowest pore sizes at different growth temperatures. For instance, cobaltocene, nickelocene, ferrocene and ruthenocene at 800, 850, 900 and 1000 °C had 14.28, 11.82, 22.89, and 9.83 nm pore size, respectively. However, at the same synthesis temperature there was no observable trend. The low pore size distribution of the metallocenes based MWCNTs may be caused by the higher presence of functional groups onto the surface of modified MWCNTs.

Nitrogen adsorption isotherms of N-MWCNTs grown from different growth temperatures are shown in the Appendix (Figures B30-33). The adsorption isotherms in Figures B30, B31 and B33 represent the result of N-MWCNTs grown from ferrocene, nickelocene and ruthenocene, respectively. They are Type IV isotherms with small and almost ill-defined hysteresis loops while Figure B31 consist of a defined hysteresis loop. The isotherms show high adsorption at relative pressures (P/P_0) up to 1.0, which indicate the formation of large mesopores and micropores. It is interesting to note that the N-MWCNTs grown from nickelocene, cobaltocene and ruthenocene at 800 °C had larger relative pressure ranges (0.5-1.0 nm). However, for

NMWCNTs synthesized from ferrocene, a larger relative pressure was obtained at a growth temperature of 850 °C.

5.4 References

1. R. Yadav, D. Singh, T. Shripathi and O. N. Srivastava, *Journal of Nanopartle Ressearch*, 2008, 10, 1349-1354.
2. J. Liu, R. Czerw and D. L. Carroll, *Journal of Materials Research*, 2005, 20, 538-543.
3. M. Terrones, H. Terrones, N. Grobert, W. K. Hsu, Y. Q. Zhu, J. P. Hare, H. W. Kroto, D. R. M. Walton, P. Kohler-Redlich, M. Rühle, J. P. Zhang and A. K. Cheetham, *Applied Physics Letters*, 1999, 75, 3932-3934.
4. M. Terrones, R. Kamalakaran, T. Seeger and M. Ruhle, *Chemical Communications*, 2000, 2335-2336.
5. M. Kumar and Y. Ando, *Journal of Nanoscience and Nanotechnology*, 2010, 10, 3739-3758.
6. E. N. Nxumalo and N. J. Coville, *Materials*, 2010, 3, 2141.
7. L. Liu, F. Liu and J. Zhao, *Nano Research*, 2014, 7, 626-657.
8. N. Karousis, N. Tagmatarchis and D. Tasis, *Chemical Reviews*, 2010, 110, 5366-5397.
9. A. Gohier, C. P. Ewels, T. M. Minea and M. A. Djouadi, *Carbon*, 2008, 46, 1331-1338.
10. R. Yadav, P. Dobal, T. Shripathi, R. S. Katiyar and O. N. Srivastava, *Nanoscale Research Letters*, 2009, 4, 197-203.
11. J. W. Jang, C. E. Lee, S. C. Lyu, T. J. Lee and C. J. Lee, *Applied Physics Letters*, 2004, 84, 2877-2879.
12. C. Tang, Y. Bando, D. Golberg and F. Xu, *Carbon*, 2004, 42, 2625-2633.
13. E. N. Nxumalo, Doctoral Dissertation, Faculty of Science, University of the Witwatersrand, Johannesburg, 2011, 63-73.
14. Z. Li, E. Dervishi, Y. Xu, V. Saini, M. Mahmood, O. D. Oshin, A. R. Biris and A. S. Biris, *Catalysis Letters*, 2009, 131, 356-363.
15. G. Keru, P. G. Ndungu and V. O. Nyamori, *Journal of Nanomaterials*, 2013, 2013, 1-7.
16. A. A. Koós, M. Dowling, K. Jurkschat, A. Crossley and N. Grobert, *Carbon*, 2009, 47, 30-37.

17. T. Dikonimos Makris, L. Giorgi, R. Giorgi, N. Lisi and E. Salernitano, *Diamond and Related Materials*, 2005, 14, 815-819.

18. L. Piao, Y. Li, J. Chen, L. Chang and J. Y. S. Lin, *Catalysis Today*, 2002, 74, 145-155.

19. R. Kurt, C. Klinke, J.-M. Bonard, K. Kern and A. Karimi, *Carbon*, 2001, 39, 2163-2172.

20. Y. T. Lee, N. S. Kim, S. Y. Bae, J. Park, S.-C. Yu, H. Ryu and H. J. Lee, *The Journal of Physical Chemistry B*, 2003, 107, 12958-12963.

21. E. N. Nxumalo, V. O. Nyamori and N. J. Coville, *Journal of Organometallic Chemistry*, 2008, 693, 2942-2948.

22. X. Y. Tao, X. B. Zhang, F. Y. Sun, J. P. Cheng, F. Liu and Z. Q. Luo, *Diamond and Related Materials*, 2007, 16, 425-430.

23. M. I. Ionescu, Y. Zhang, R. Li, H. Abou-Rachid and X. Sun, *Applied Surface Science*, 2012, 258, 4563-4568.

24. E. Liang, P. Ding, H. Zhang, X. Guo and Z. Du, *Diamond and Related Materials*, 2004, 13, 69-73.

25. L. Bulusheva, A. Okotrub, I. Kinloch, I. Asanov, A. Kurenya, A. Kudashov, X. Chen and H. Song, *Physica Status Solidi B*, 2008, 245, 1971-1974.

26. T. Maiyalagan and B. Viswanathan, *Materials Chemistry and Physics*, 2005, 93, 291-295.

27. R. Che, L.-M. Peng, Q. Chen, X. Duan and Z. Gu, *Applied Physics Letters*, 2003, 82, 3319-3321.

28. R. Droppa, P. Hammer, A. Carvalho, M. Dos Santos and F. Alvarez, *Journal of Non-Crystalline Solids*, 2002, 299, 874-879.

29. R. Kurt and A. Karimi, *Journal of Chemical Physics*, 2001, 2, 388-392.

30. X. Ma and E. Wang, *Applied Physics Letters*, 2001, 78, 978.

31. S. Choi, K. H. Park, S. Lee and K. H. Koh, *Journal of Applied Physics*, 2002, 92, 4007-4011.

32. S. Maldonado, S. Morin and K. J. Stevenson, *Carbon*, 2006, 44, 1429-1437.

CHAPTER 6: CONCLUSION AND FUTURE STUDIES

The purpose of this study was to investigate the effect of metallocene catalysts and carbon sources on the synthesis of MWCNTs and determine suitable conditions (temperature) for the growth of MWCNTs. This chapter therefore provides overall conclusions of and it highlights future studies on the synthesis of MWCNTs and their applications.

6.1 Conclusion

The discovery of SCNMs especially, MWCNTs has attracted a lot of interest in nanotechnology because of their unique physical, chemical, mechanical and electrical properties. Due to the aforementioned properties, SCNMs have been investigated and found to be potentially applicable in a wide range of fields. The challenge is to synthesize MWCNTs economically in large quantities. Modern methods like arc discharge, laser ablation have disadvantages of producing low yield and short MWCNTs. Laser ablation technique is expensive due to use of lasers and high power consumptions. However, CVD is capable of producing pure MWCNTs in high yields and it is easy to scale up the production. MWCNTs from CVD technique are known to poses high surface areas and low density, which enhance their adsorption properties.

MWCNTs and other SCNMs were successfully synthesized by the CVD method. They were further successfully functionalized by refluxing with concentrated nitric acid. The acid treatment process was found to reduce agglomeration, remove amorphous carbon and residual metal content in MWCNTs. Treatment with nitric acid was also observed to open tube ends. The best method for the purification of the MWCNTs was Method 2 which involved refluxing for 24 hours. This method produced purer MWCNTs as compared to other methods which caused damage to the MWCNTs.

The SCNMs produced were successfully characterized using various standard instrumental techniques, *viz*: transmission electron microscopy, high resolution transmission electron microscopy, scanning electron microscopy, electron dispersive X-ray spectroscopy, Raman spectroscopy, thermogravimetric analysis, Brunauer-Emmet-Teller surface area and porosity analysis and elemental analysis.

The SCNMs were produced in highest yield in the temperature range, 800 to 1000°C. Increasing growth temperature was shown to have a positive increase in inner- and outer-diameters of MWCNTs with a high quality at a growth temperature of 850 °C. The inner-diameter of MWCNTs increased from 8 to 26 nm while the outer-diameter, from 48 to 80 nm. This was in agreement with TEM, TGA and BET analyses that showed that the samples at a growth temperature ranging from 800 to 900 °C were purer in terms of structural/morphological distribution, especially in the middle of this temperature range; 850 °C. The thermal stabilities of these MWCNTs were also observed to vary *pseudo*-linearly with the growth temperatures. The best growth temperature for synthesis of MWCNTs chosen was 850 °C. At this temperature, higher yields of MWCNTs were recovered, the MWCNTs were longer, had larger surface areas, better thermal stability and high crystallinity. In this study cobaltocene was more effective than the metallocene catalysts in the synthesis of MWCNTs with respect to the crystallinity of the MWCNTs and low content of residual metal catalysts.

The N-MWCNTs were synthesized by ‘‘in situ’’-doping method using acetonitrile as a carbon source and growth temperature ranging from 800 to 1000 °C. Various morphological profiles of the N-MWCNTs, amorphous carbon and carbon spheres were obtained at different growth temperatures. The formation of carbon spheres and amorphous carbon depended on the growth temperature. The highest growth temperature (1000 °C) formed more carbon spheres while the lowest growth temperature (800 °C) favoured the formation of amorphous carbon. In this study, high quality and aligned N-MWCNTs were obtained in good yields at a growth temperature of 850 °C.

All the N-MWCNTs that were synthesized are bamboo-shaped. The size of the bamboo compartments decreased with increase in growth temperature because of the nitrogen content in the N-MWCNTs. Small bamboo compartments indicate that more nitrogen was incorporated into the MWCNTs framework. The highest nitrogen-doping level was obtained at a growth temperature of 850 °C for all metallocene catalysts used. Different metallocenes produced different percentages of nitrogen-doping content. In this regard, nickelocene gave the highest nitrogen–doping (18.21%). The inner- and outer-diameters of N-MWCNTs were similarly observed to increase with increase in growth temperatures.

The thermal stability and crystallinity of the N-MWCNTs are independent of the growth temperature, but varied inversely with the percentage of nitrogen content in the N-MWCNTs. N-MWCNTs with high percentages of nitrogen content are less thermally stable and more disordered. Thus, those that had lower nitrogen content were more thermally stable and more crystalline. It was also observed that N-MWCNTs synthesised at a lower growth temperature had higher surface area as compared to those that were synthesized at higher growth temperatures. The lower surface area was attributed to the large amount of carbon spheres formed at higher growth temperatures in addition to their low nitrogen content. In general, the growth temperatures were found to affect the yield, type of SCNMs formed, and level of nitrogen doping.

The carbon sources (toluene and acetonitrile) studied had fundamental effect on the morphology of MWCNTs. Toluene provided more pristine MWCNTs with fewer defects, hence, more structured while acetonitrile mainly formed N-MWCNTs. These N-MWCTs showed higher defect levels and less crystallinity. MWCNTs grown from toluene had smaller inner-diameter while those that are grown from acetonitrile had larger inner-diameters. MWCNTs had inner-diameters ranging from 8 to 26 nm whereas that for N-MWCNTs ranged from 30 to 65 nm. MWCNTs formed from a solution of toluene were more thermally stable (high decomposition temperature) as compared with those which were synthesized from acetonitrile (low decomposition temperature)

6.2 Future studies

There are many investigations that can be further carried out based on findings from this research, of particular interest are:

- Investigating the effect of using metallocenes (especially nickelocene, cobaltocene and ruthenocene) and 4-nitroaniline or 4-methylaniline in the synthesis of aryl derivatives of metallocenes.
- Application of aryl derivatives (synthesized above) in the synthesis of MWCNTs and also investigate the effect of the heteroatoms (N and O) from the aryl derivatives on MWCNTs.
- From literature, it has been demonstrated that growth temperature is not the only factor that affects crystallinity but also the type of catalyst and its concentration are also

capable of determining the crystallinity of the MWCNTs, therefore since a catalyst concentration of 2.5 wt.% has been investigated in this work, a higher catalyst concentration (5, 10 or 15 wt.%) can be further investigated.

- Investigate the effect of variation of the reaction conditions such as gas flow rate on the types and yields of the N-MWCNTs.
- Determine the effect of varying the carbon and nitrogen source concentration (toluene or acetonitrile) and also investigate the mechanism of formation and shape of the compartment of the N-MWCNTs.
- Investigate the effect of using pyridine as a carbon and nitrogen source for the synthesis of N-MWCNTs.
- Investigate the effect of doping MWCNTs with boron (triphenylborane) or sulphur (thiophene) using similar metallocenes and varying the dopant concentration (1.0, 2.5 and 5.0 wt.%).
- Synthesis N-MWCNTs or B-MWCNTs/polymer composites using direct solution mixing and oxidative *in situ* polymerization.
- Application of N-MWCNTs or B-MWCNTs/polymer composites in organic solar cells as excitation dissociation sites and transfer of charge carriers (investigate the effectiveness of the polymer wrapped on the walls of the CNTs and the results on the use of nanocomposite in the active layer of organic solar cells).
- Investigate the effect of using bimetallic catalysts (*e.g.* ferrocene-nickelocene, ferrocene-cobaltocene or ferrocene-ruthenocene) in the synthesis of MWCNTs.

In general, discounting the mentioned possibilities that could be investigated, there are lot of other investigation that would be interesting to explore in the future.

APPENDICES

Appendix A (MWCNTs)

EDX

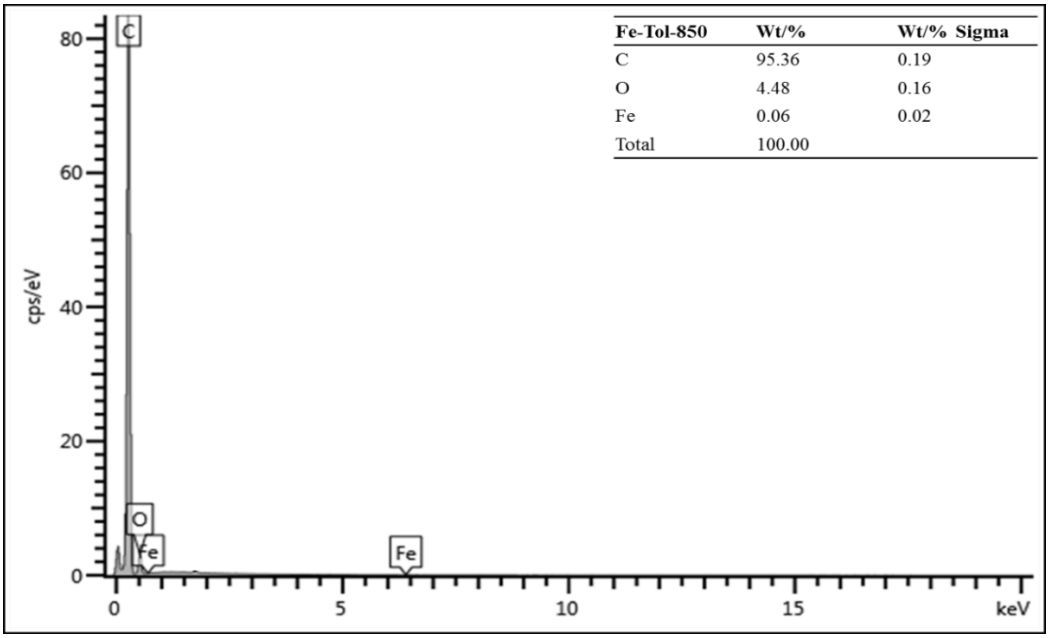

Fe-Tol-850	Wt/%	Wt/% Sigma
C	95.36	0.19
O	4.48	0.16
Fe	0.06	0.02
Total	100.00	

Figure A1: Elemental composition present in MWCNTs synthesized from ferrocene at a growth temperature of 850 °C

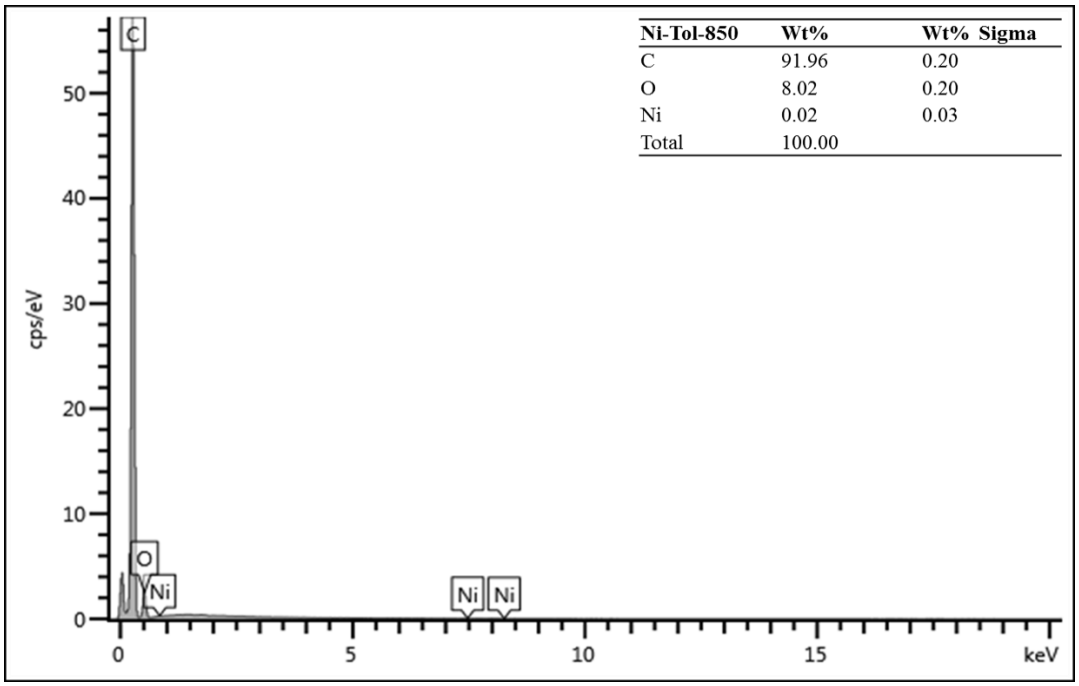

Ni-Tol-850	Wt%	Wt% Sigma
C	91.96	0.20
O	8.02	0.20
Ni	0.02	0.03
Total	100.00	

Figure A2: Elemental composition present in MWCNTs synthesized from nickelocene at a growth temperature 850 °C

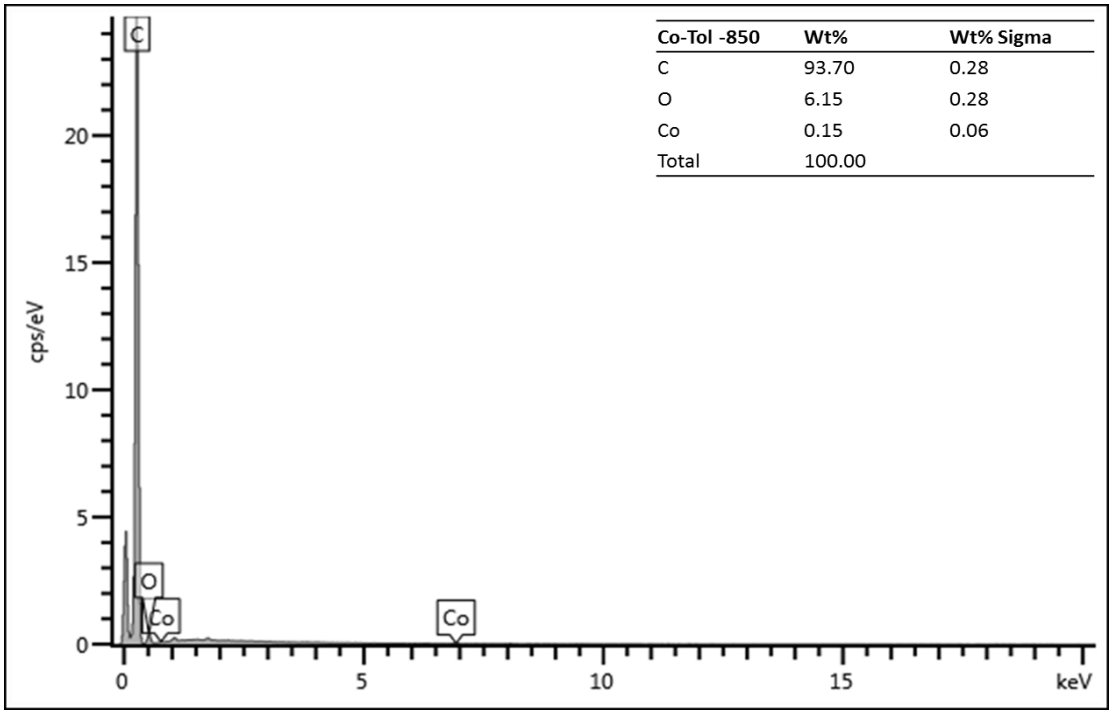

Co-Tol -850	Wt%	Wt% Sigma
C	93.70	0.28
O	6.15	0.28
Co	0.15	0.06
Total	100.00	

Figure A3: Elemental composition present in MWCNTs synthesized from cobaltocene at a growth temperature of 850 °C

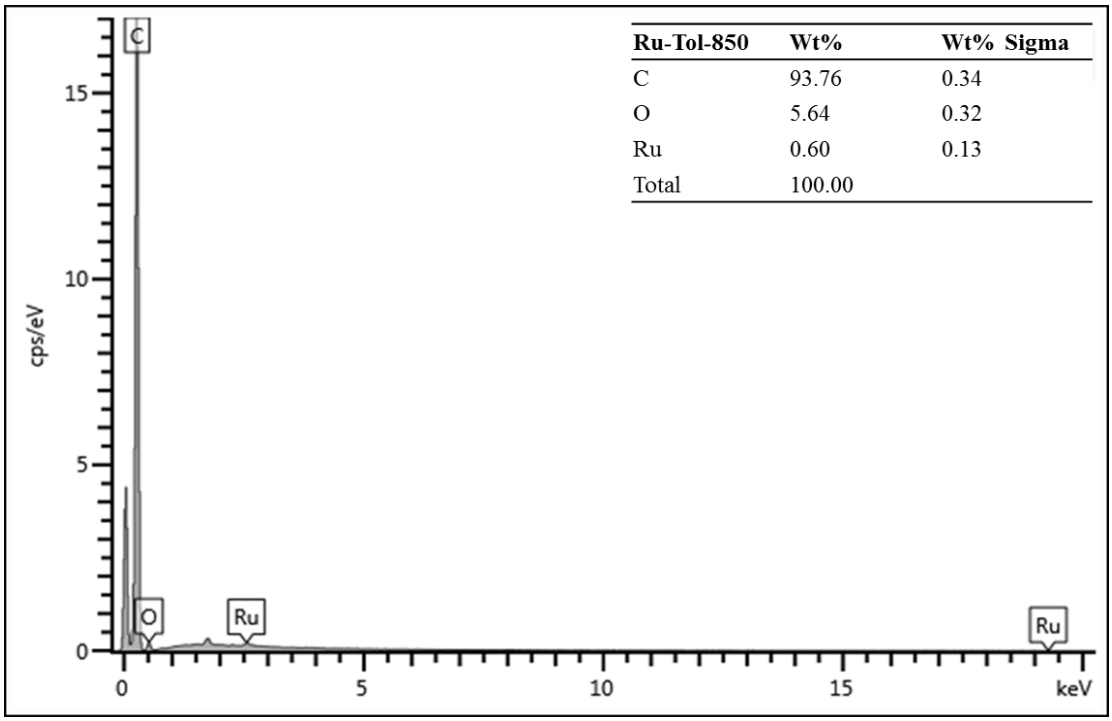

Ru-Tol-850	Wt%	Wt% Sigma
C	93.76	0.34
O	5.64	0.32
Ru	0.60	0.13
Total	100.00	

Figure A4: Elemental composition present in MWCNTs synthesized from ruthenocene at a growth temperature of 850 °C

TGA

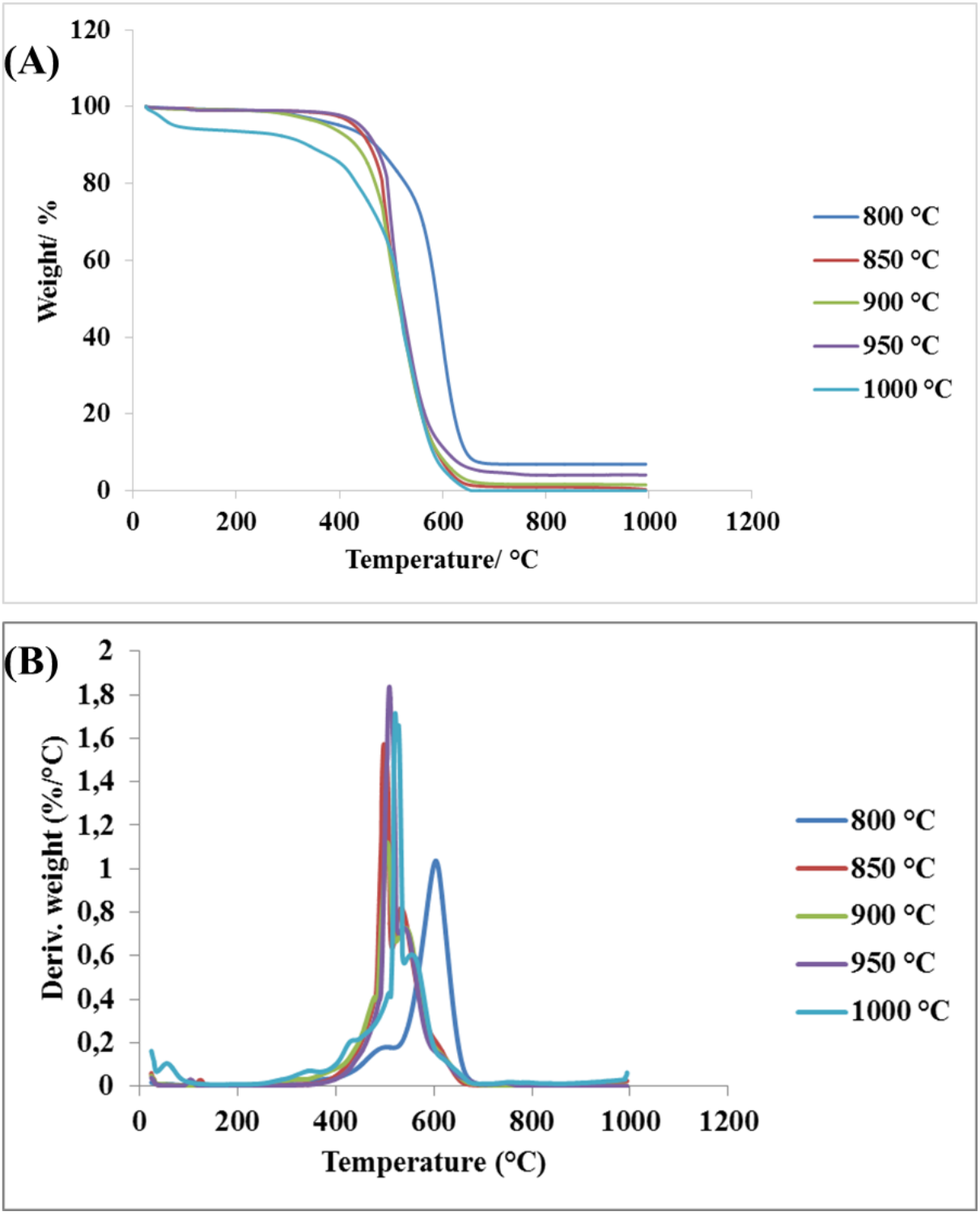

Figure A5: Thermogravimetric analysis of MWCNTs synthesized from ferrocene (A) showing amount of residue on the purified samples and (B) their derivatives % weight loss

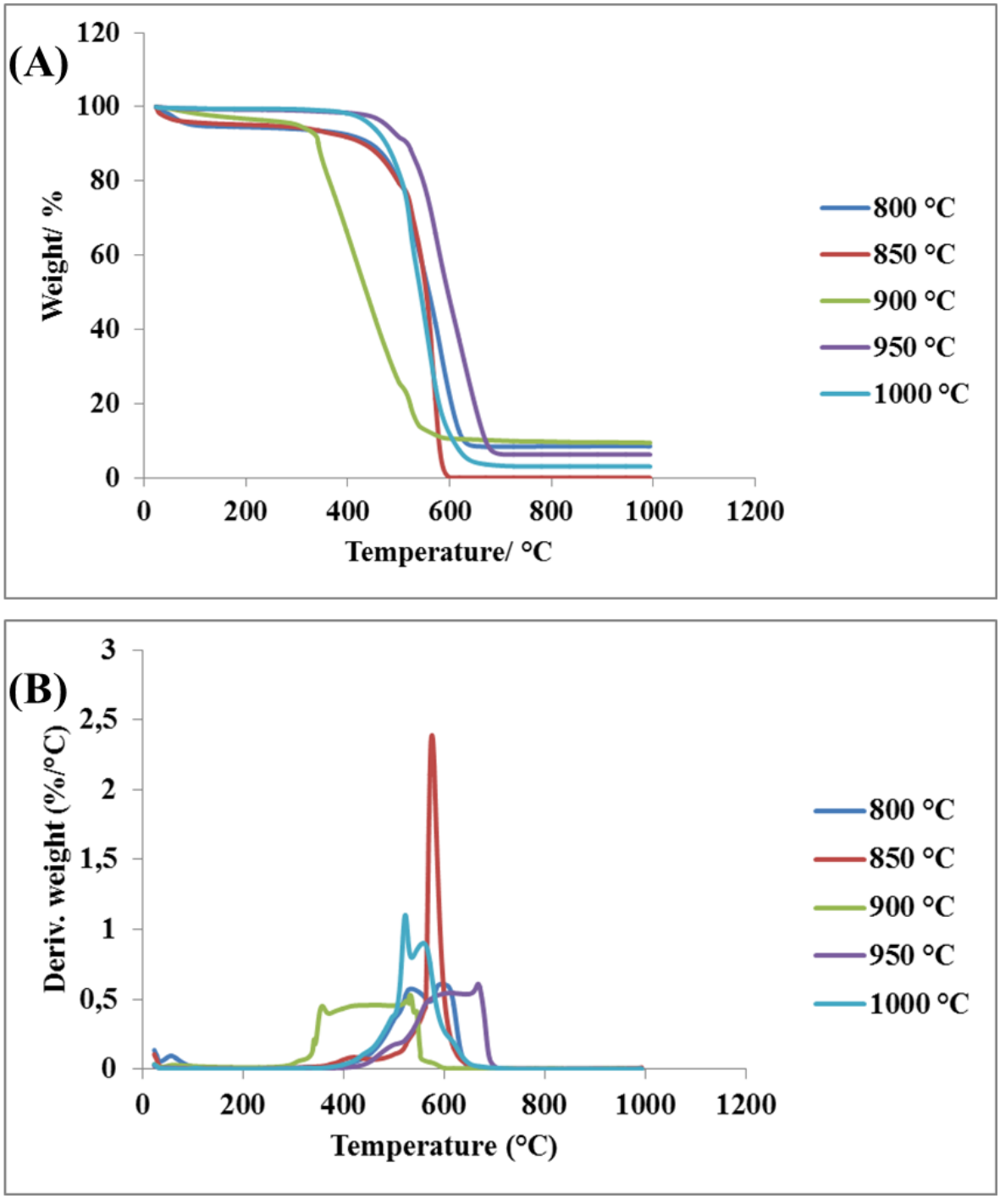

Figure A6: Thermogravimetric analysis of MWCNTs synthesized from nickelocene (A) showing amount of residue remaining on the purified samples and (B) their derivatives % weight loss

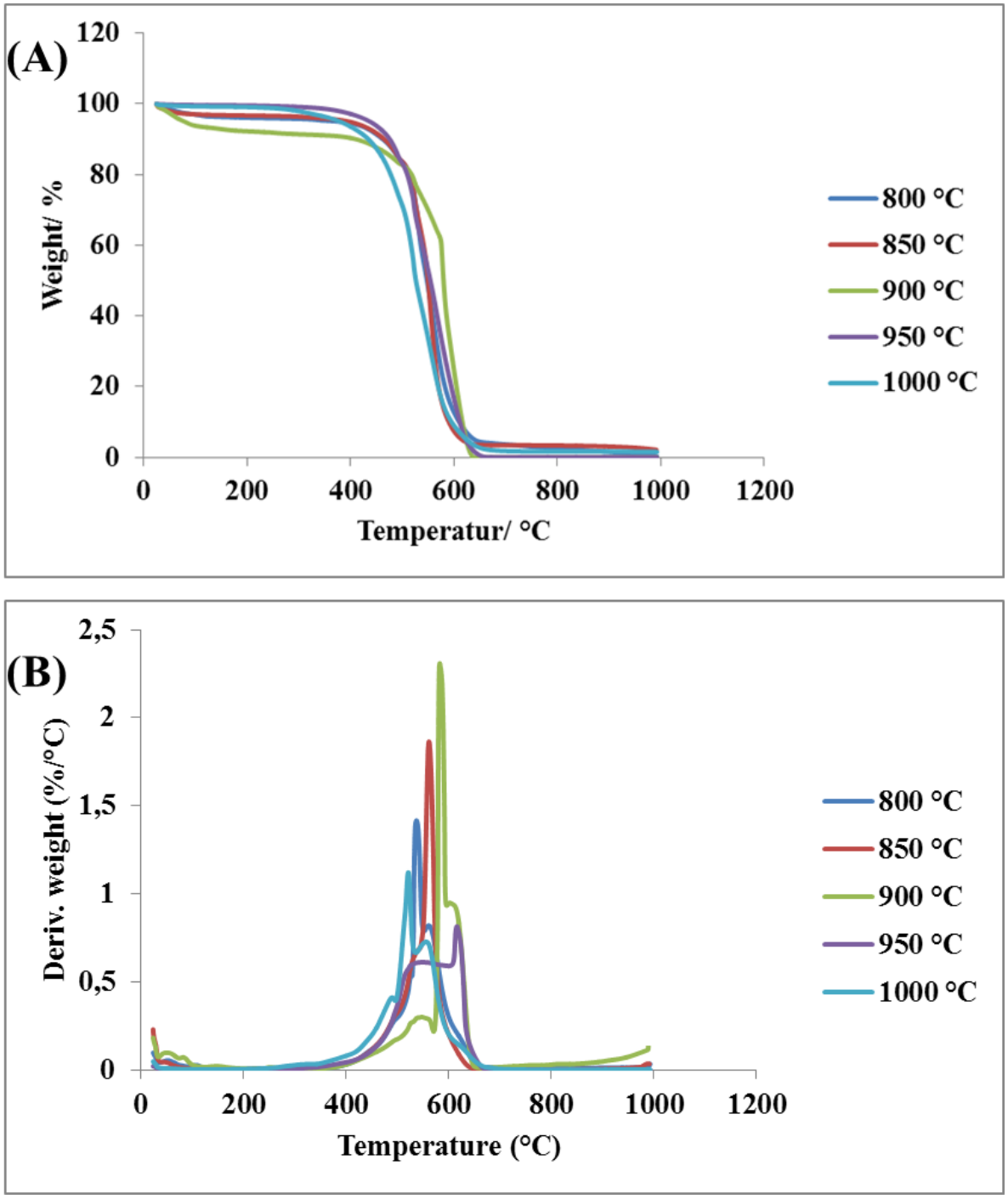

Figure A7: Thermogravimetric analysis of MWCNTs synthesized from cobaltocene (A) showing amount of residue remaining on the purified samples and (B) their derivatives % weight loss

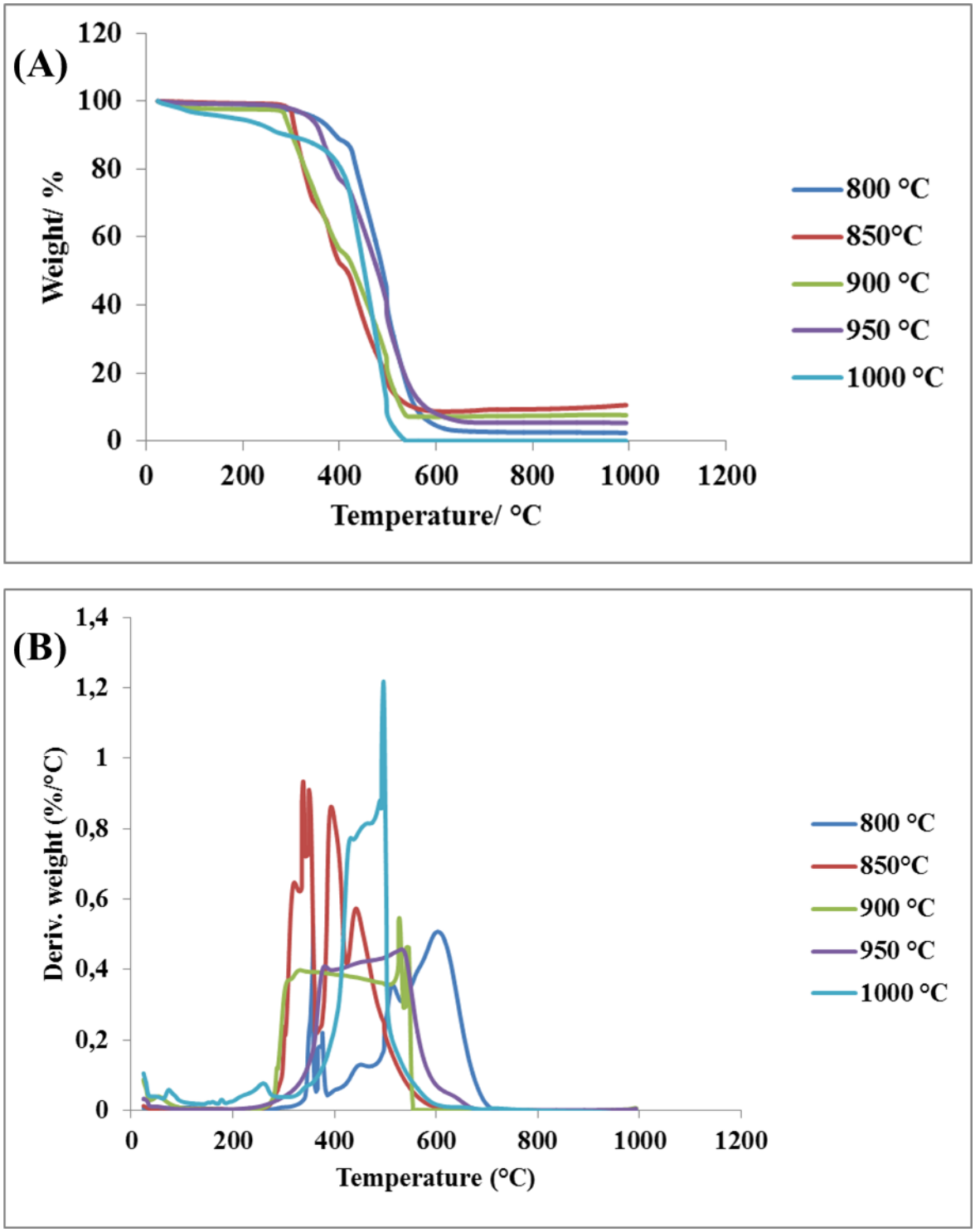

Figure A8: Thermogravimetric analysis of MWCNTs synthesized from ruthenocene (A) showing amount of residue remaining on the purified samples and (B) their derivatives % weight loss

BET analysis

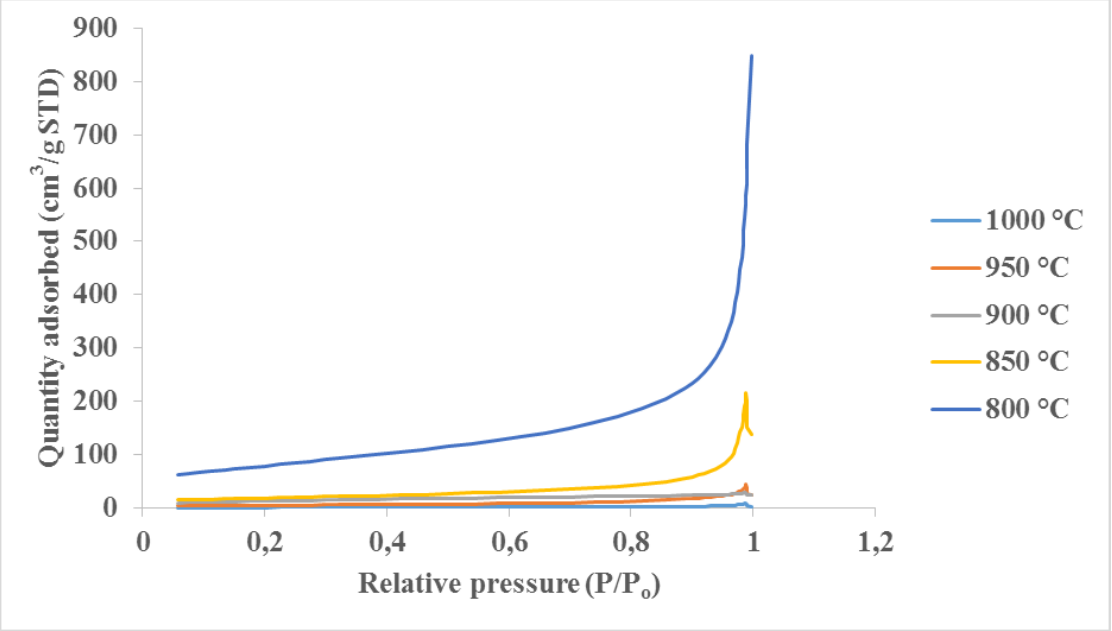

Figure A9: Representative N_2 adsorption isotherms of MWCNTs synthesized from ferrocene at different growth temperatures

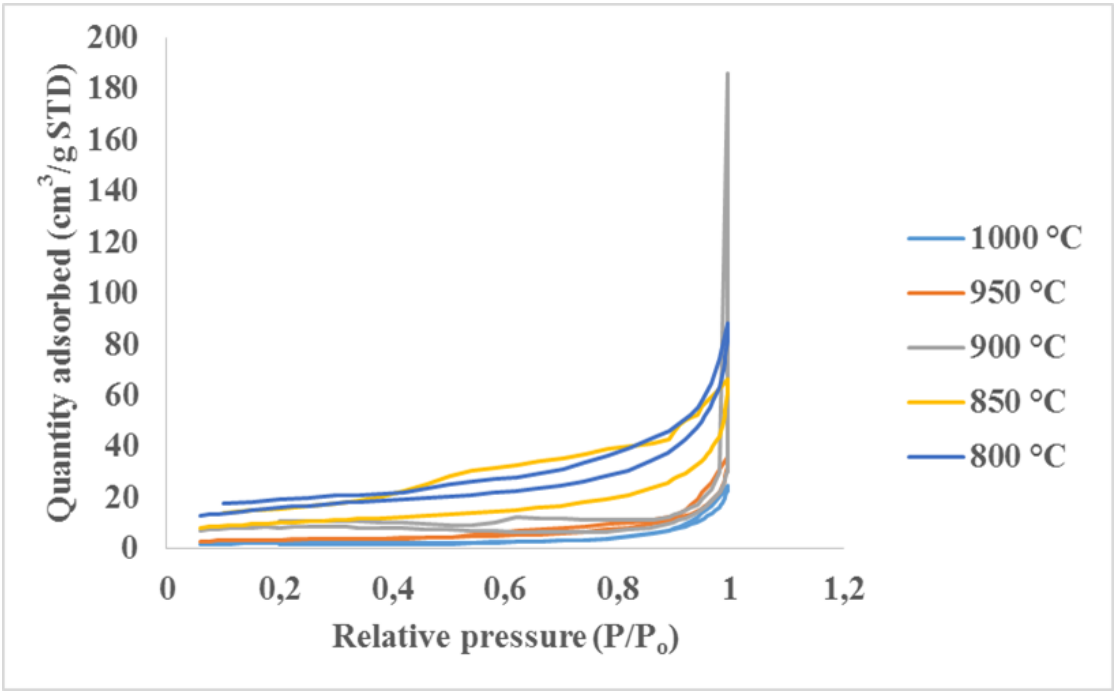

Figure A10: Representative N_2 adsorption isotherms of MWCNTs synthesized from nickelocene at different growth temperatures

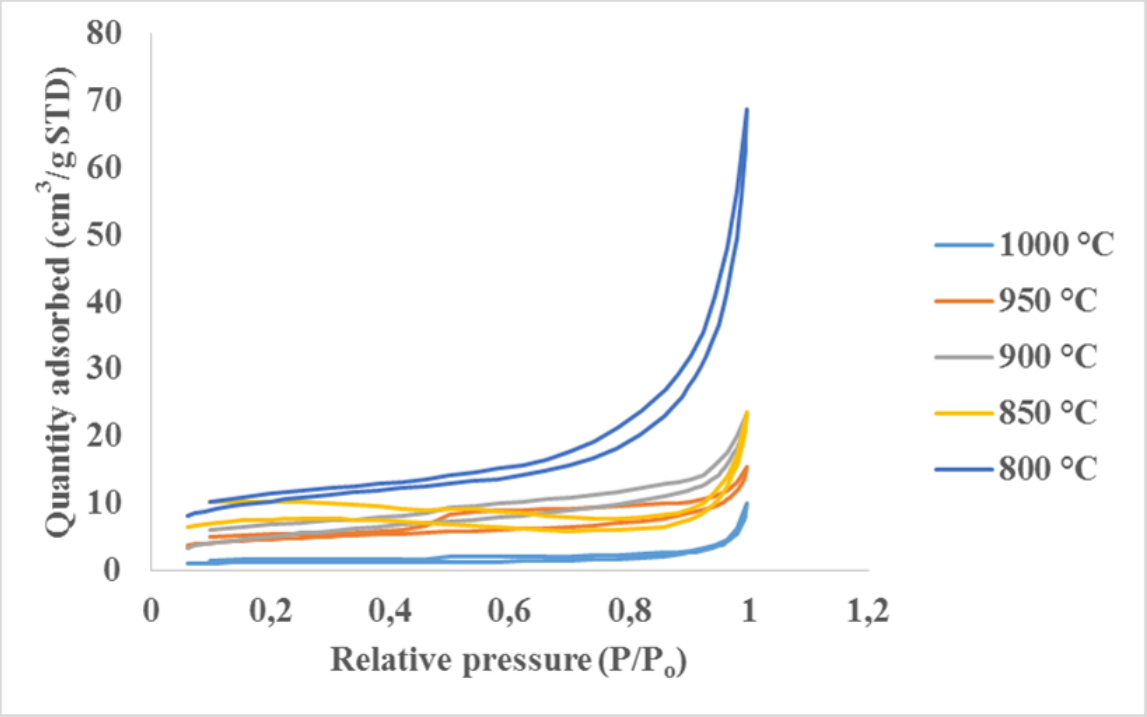

Figure A11: Representative N_2 adsorption isotherms of MWCNTs synthesized from cobaltocene at different growth temperatures

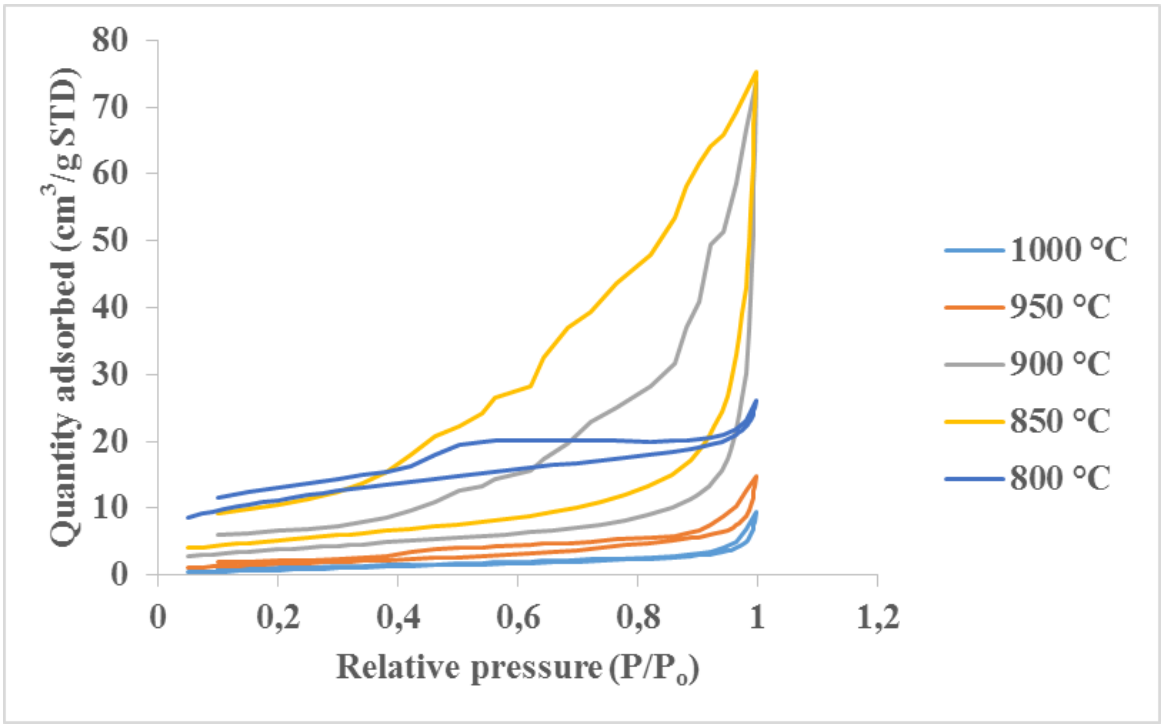

Figure A12: Representative N_2 adsorption isotherms of MWCNTs synthesized from ruthenocene at different growth temperatures

Appendix B (N-MWCNTs)

SEM images

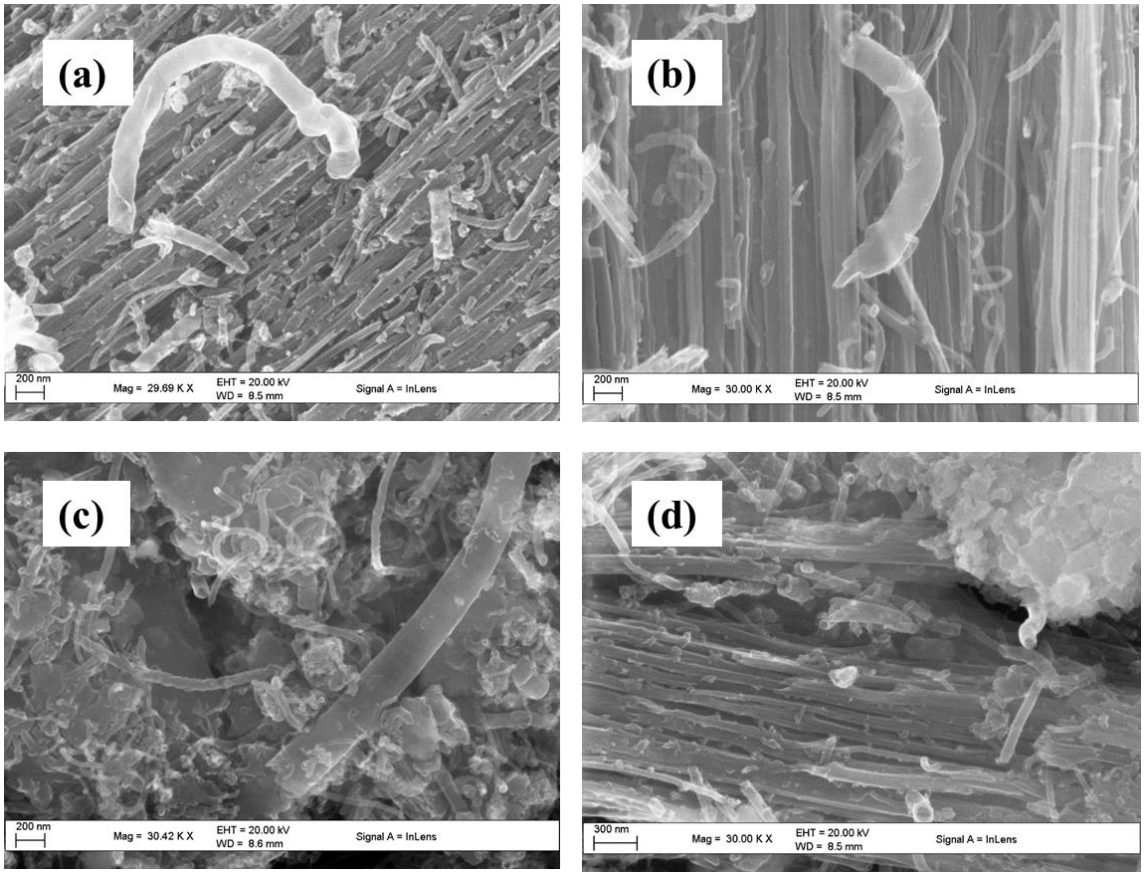

Figure B1: SEM images of N-MWCNTs synthesized at a growth temperature of 850 C from different metallocenes (a) ferrocene, (b) nickelocene, (c) cobaltocene and (d) ruthenocene

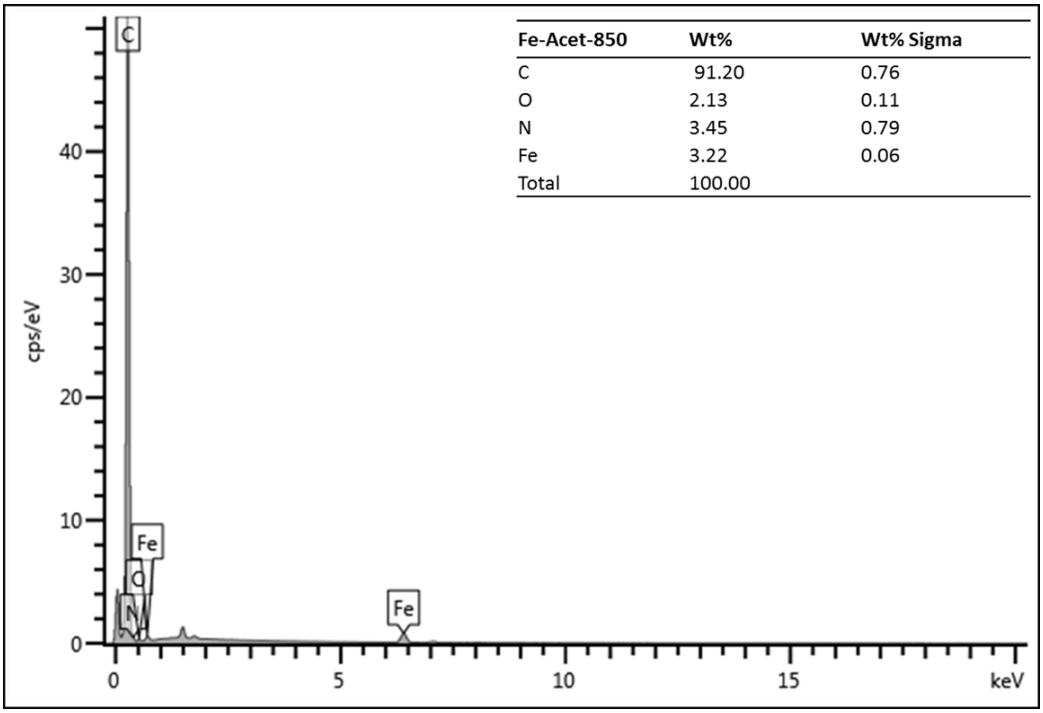

Fe-Acet-850	Wt%	Wt% Sigma
C	91.20	0.76
O	2.13	0.11
N	3.45	0.79
Fe	3.22	0.06
Total	100.00	

Figure B2: Elemental composition present in N-MWCNTs synthesized from ferrocene at a growth temperature of 850 °C

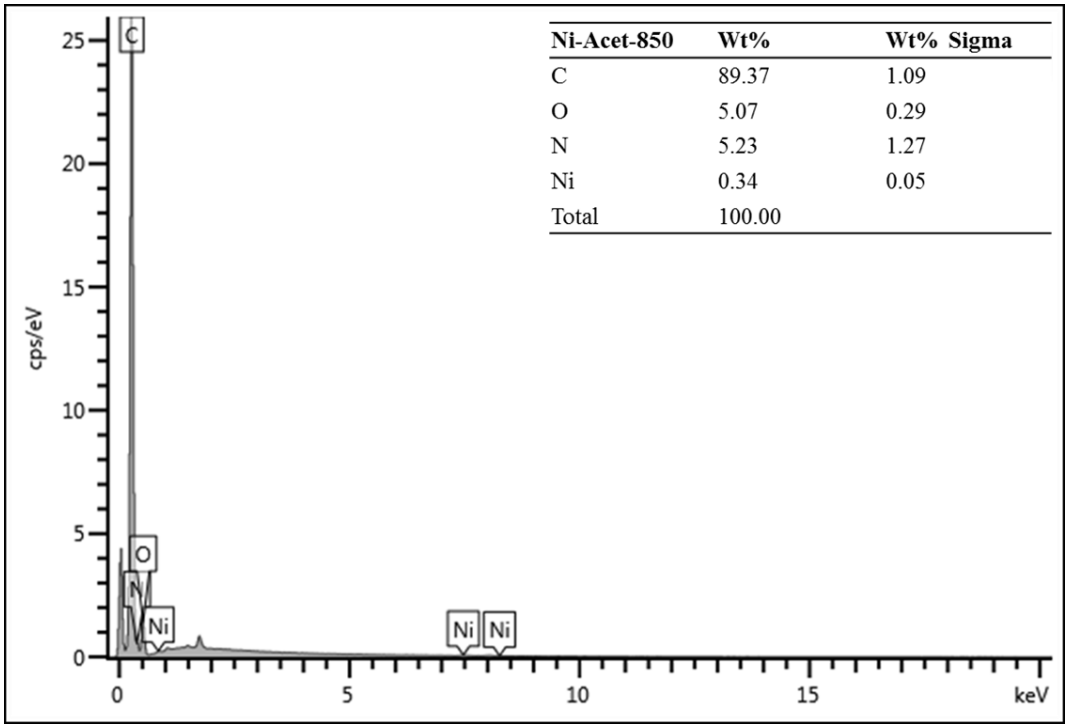

Ni-Acet-850	Wt%	Wt% Sigma
C	89.37	1.09
O	5.07	0.29
N	5.23	1.27
Ni	0.34	0.05
Total	100.00	

Figure B3: Elemental composition present in N-MWCNTs synthesized from nickelocene at a growth temperature of 850 °C

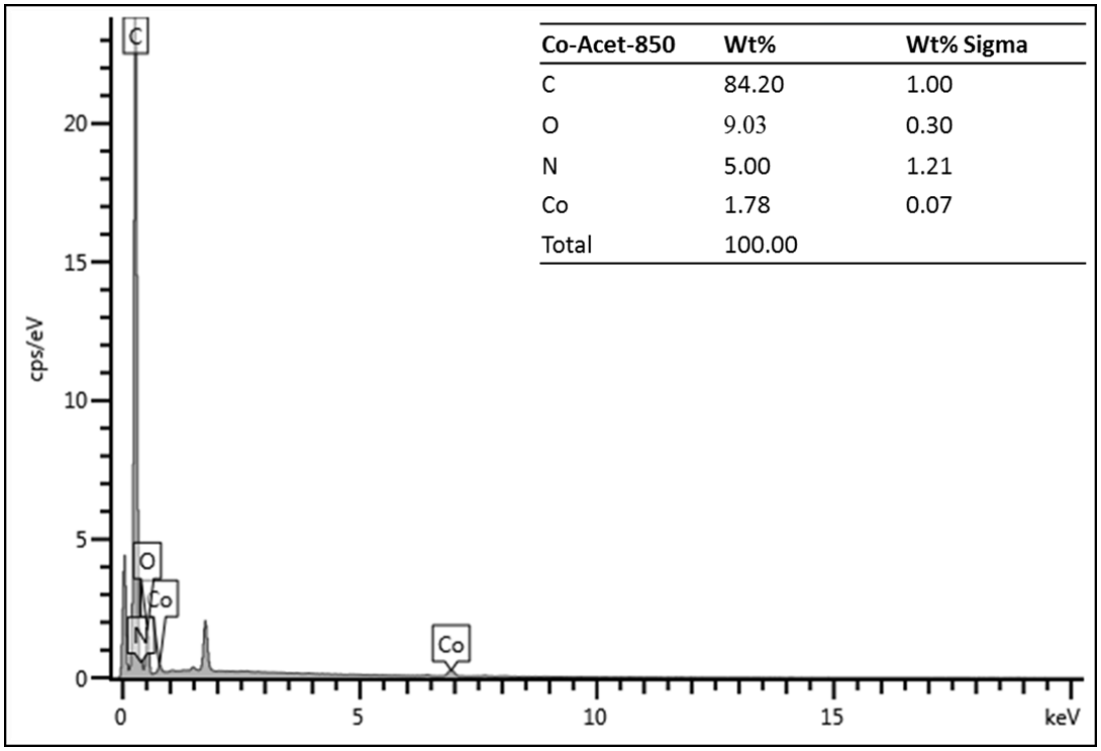

Co-Acet-850	Wt%	Wt% Sigma
C	84.20	1.00
O	9.03	0.30
N	5.00	1.21
Co	1.78	0.07
Total	100.00	

Figure B4: Elemental composition present in N-MWCNTs synthesized from cobaltocene at a growth temperature of 850 °C

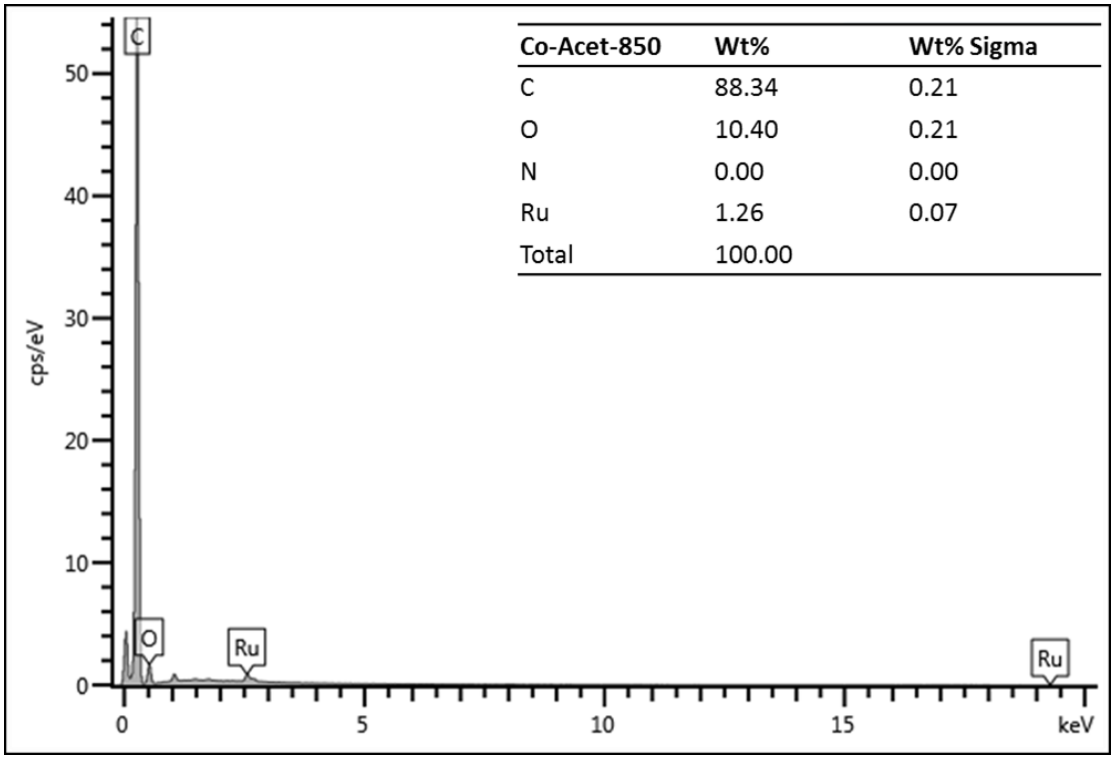

Co-Acet-850	Wt%	Wt% Sigma
C	88.34	0.21
O	10.40	0.21
N	0.00	0.00
Ru	1.26	0.07
Total	100.00	

Figure B5: Elemental composition present in N-MWCNTs synthesized from ruthenocene at a growth temperature of 850 °C

Elemental analysis

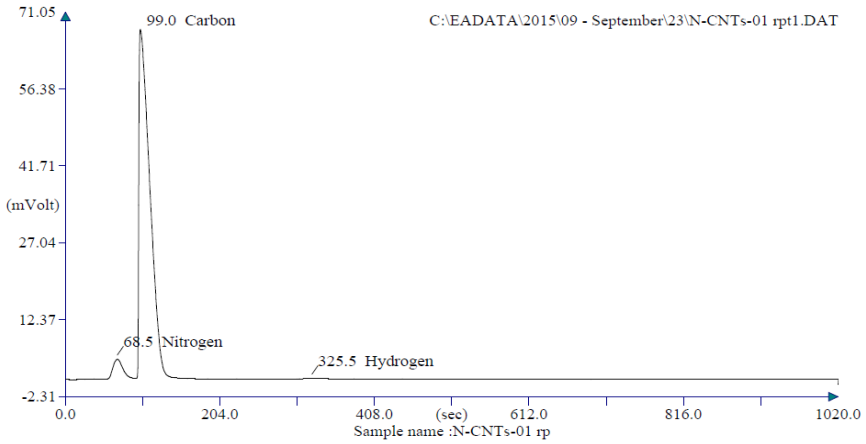

Retention Time (min)	Element Name	Element %
1.142	Nitrogen	7.665
1.650	Carbon	59.552
5.425	Hydrogen	0.191
		67.408

Figure B6: CHNS spectrum of N-MWCNTs synthesized from ferrocene at a growth temperature of 1000 °C

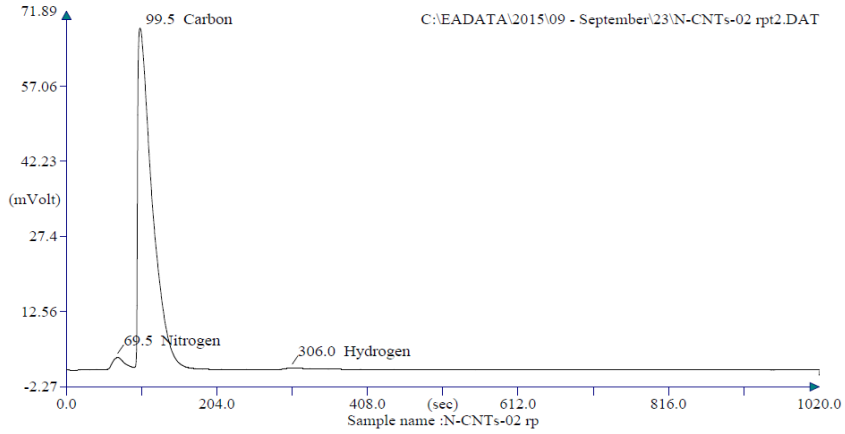

Retention Time (min)	Element Name	Element %
1.158	Nitrogen	6.566
1.658	Carbon	87.026
5.100	Hydrogen	0.400
		93.992

Figure B7: CHNS spectrum of N-MWCNTs synthesized from ferrocene at a growth temperature of 950 °C

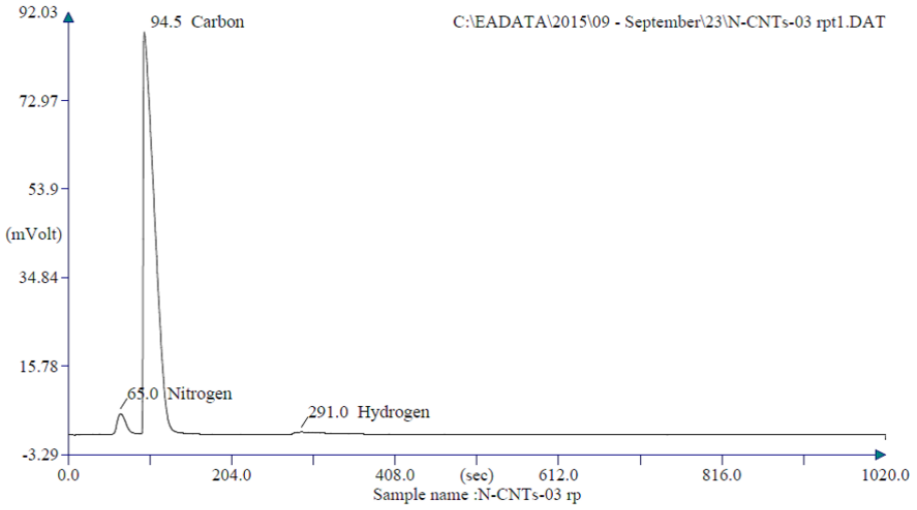

Retention Time (min)	Element Name	Element %
1.083	Nitrogen	7.530
1.575	Carbon	74.857
4.850	Hydrogen	0.643
		83.030

Figure B8: CHNS spectrum of N-MWCNTs synthesized from ferrocene at a growth temperature of 900 °C

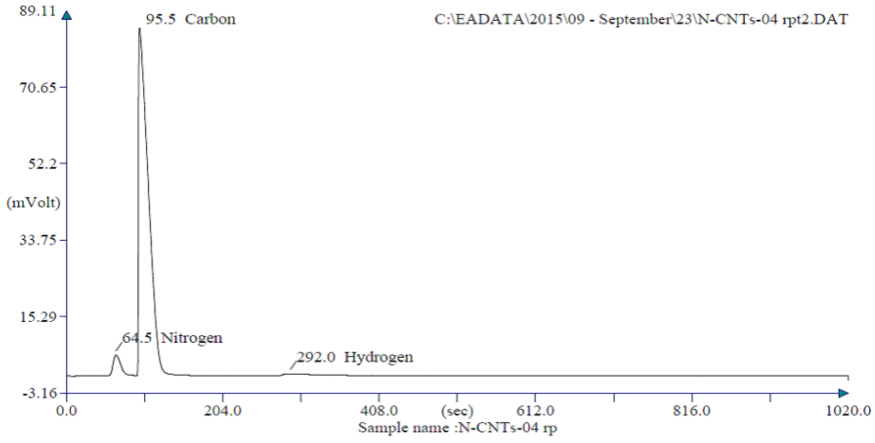

Retention Time (min)	Element Name	Element %
1.075	Nitrogen	8.619
1.592	Carbon	74.230
4.867	Hydrogen	0.642
		83.491

Figure B9: CHNS spectrum of N-MWCNTs synthesized from ferrocene at a growth temperature of 850 °C

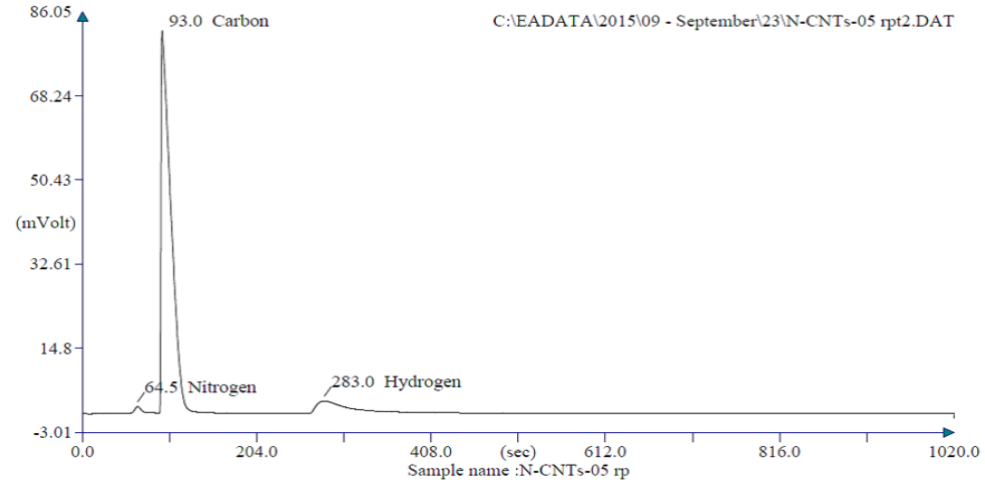

Retention Time (min)	Element Name	Element %
1.075	Nitrogen	1.590
1.550	Carbon	55.905
4.717	Hydrogen	2.418
		59.914

Figure B10: CHNS spectrum of N-MWCNTs synthesized from ferrocene at a growth temperature of 800 °C

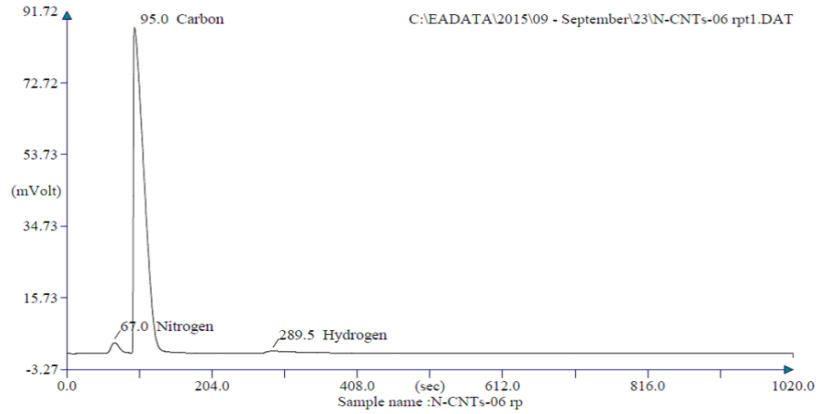

Retention Time (min)	Element Name	Element %
1.117	Nitrogen	5.122
1.583	Carbon	81.032
4.825	Hydrogen	0.698
		86.852

Figure B11: CHNS spectrum of N-MWCNTs synthesized from nickelocene at a growth temperature of 1000 °C

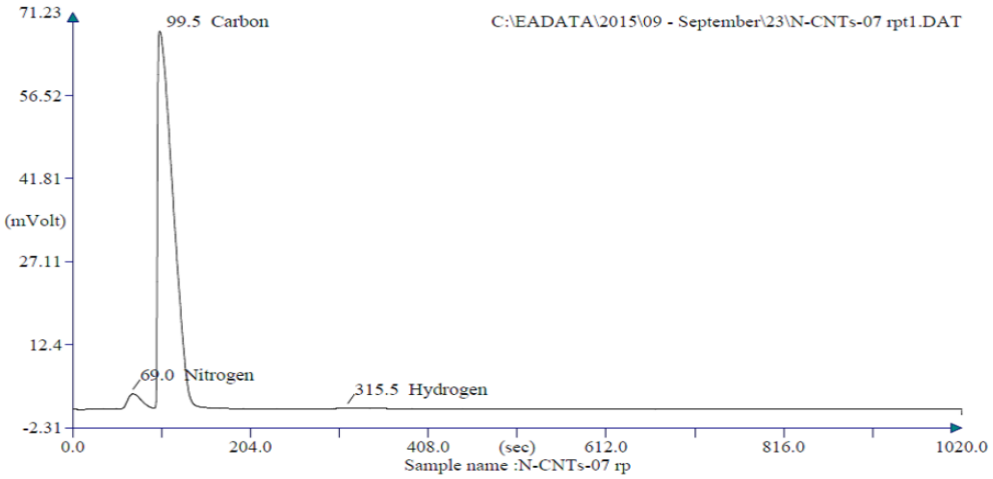

Retention Time (min)	Element Name	Element %
1.150	Nitrogen	7.394
1.658	Carbon	83.392
5.258	Hydrogen	0.298
		91.085

Figure B12: CHNS spectrum of N-MWCNTs synthesized from nickelocene at a growth temperature of 950 °C

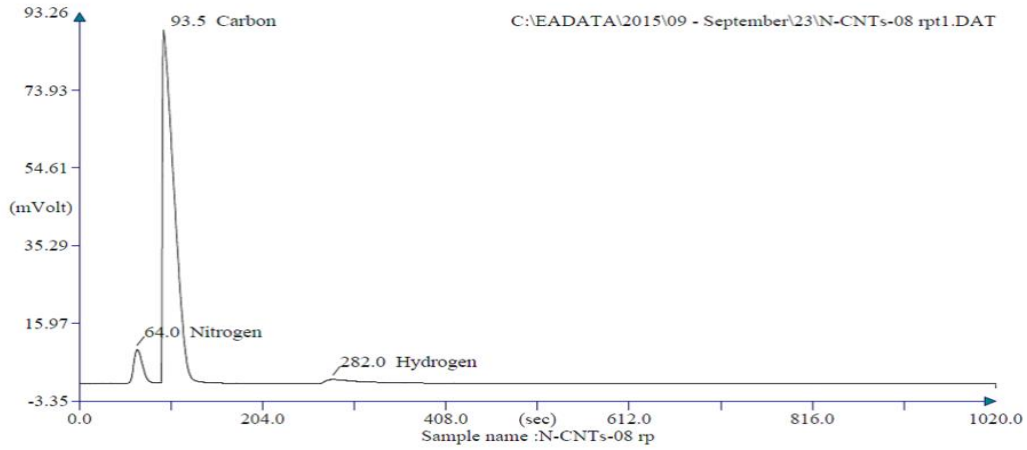

Retention Time (min)	Element Name	Element %
1.067	Nitrogen	13.630
1.558	Carbon	74.567
4.700	Hydrogen	1.103
		89.300

Figure B13: CHNS spectrum of N-MWCNTs synthesized from nickelocene at a growth temperature of 900 °C

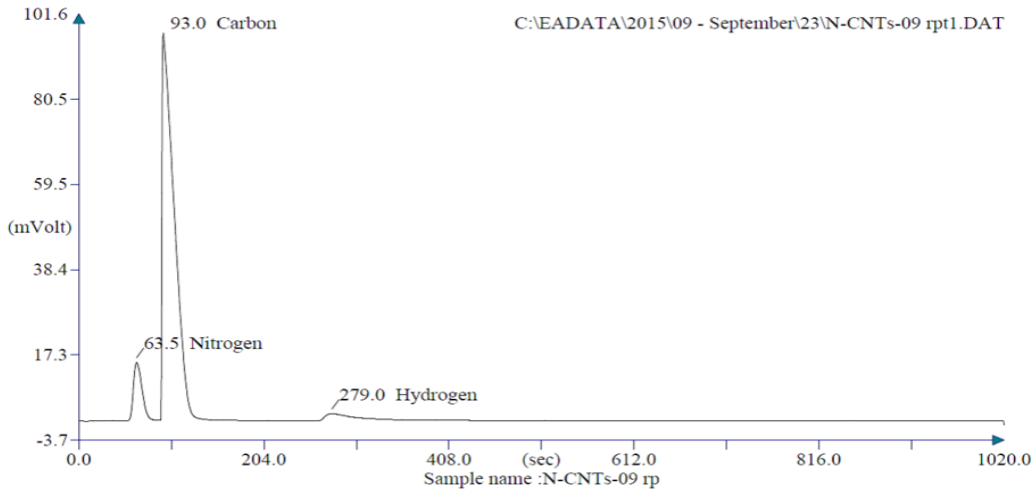

Retention Time (min)	Element Name	Element %
1.058	Nitrogen	18.207
1.550	Carbon	66.760
4.650	Hydrogen	1.320
		86.287

Figure B14: CHNS spectrum of N-MWCNTs synthesized from nickelocene at a growth temperature of 850 °C

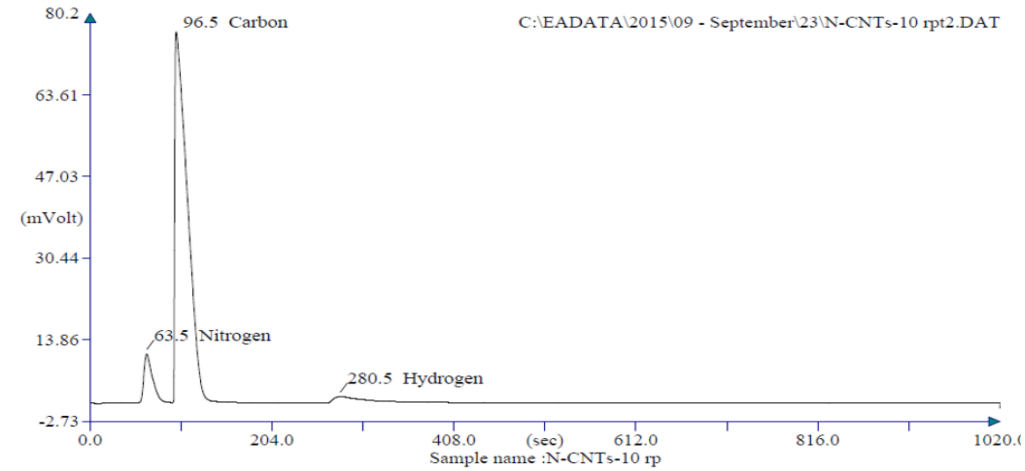

Retention Time (min)	Element Name	Element %
1.058	Nitrogen	14.945
1.608	Carbon	64.440
4.675	Hydrogen	1.235
		80.620

Figure B15: CHNS spectrum of N-MWCNTs synthesized from nickelocene at a growth temperature of 800 °C

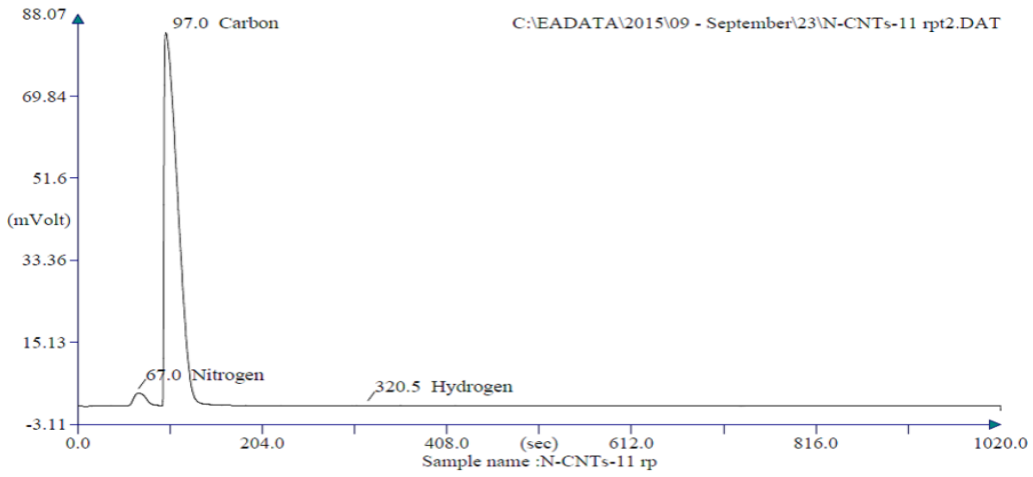

Retention Time (min)	Element Name	Element %
1.117	Nitrogen	5.906
1.617	Carbon	77.730
5.342	Hydrogen	0.176
		83.812

Figure B16: CHNS spectrum of N-MWCNTs synthesized from cobaltocene at a growth temperature of 1000 °C

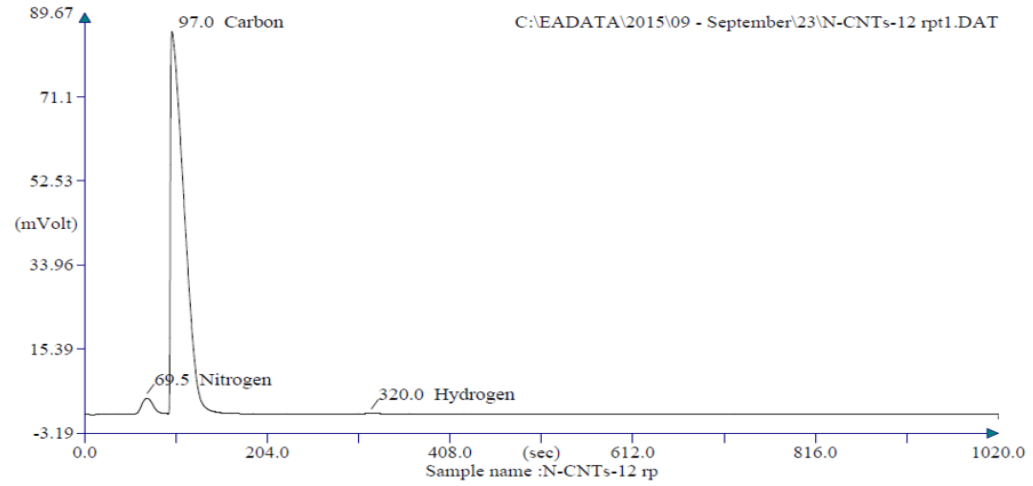

Retention Time (min)	Element Name	Element %
1.158	Nitrogen	7.710
1.617	Carbon	89.081
5.333	Hydrogen	0.224
		97.015

Figure B17: CHNS spectrum of N-MWCNTs synthesized from cobaltocene at a growth temperature of 950 °C

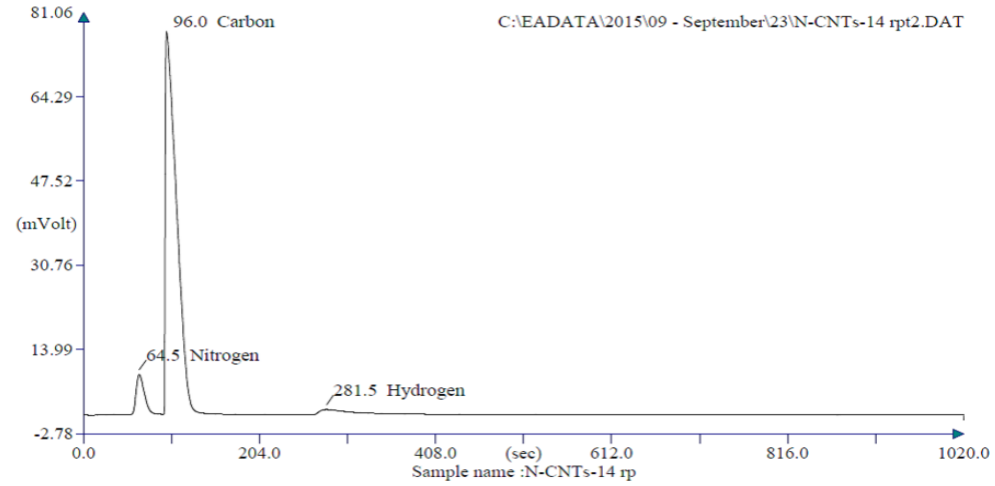

Retention Time (min)	Element Name	Element %
1.075	Nitrogen	11.881
1.600	Carbon	60.544
4.692	Hydrogen	1.078
		73.503

Figure B18: CHNS spectrum of N-MWCNTs synthesized from cobaltocene at a growth temperature of 900 °C

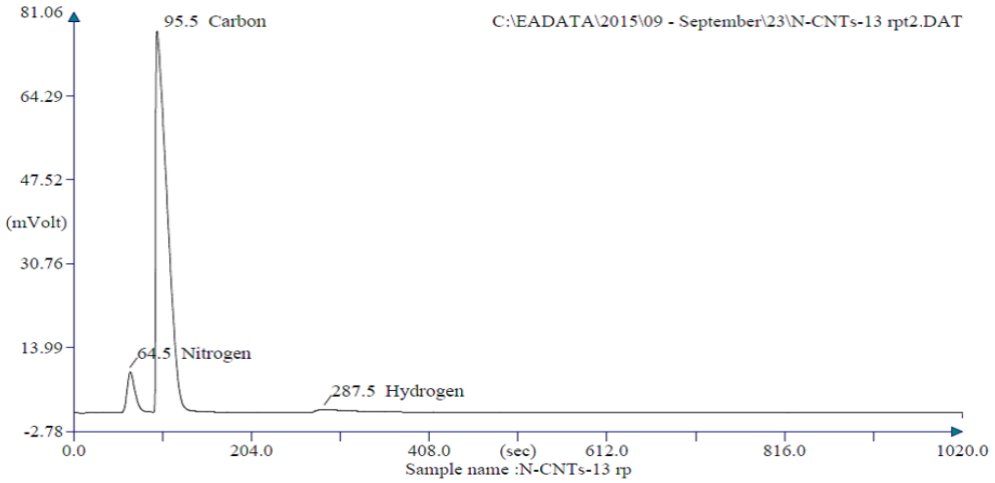

Retention Time (min)	Element Name	Element %
1.075	Nitrogen	12.742
1.592	Carbon	67.971
4.792	Hydrogen	0.777
		81.490

Figure B19: CHNS spectrum of N-MWCNTs synthesized from cobaltocene at a growth temperature of 850 °C

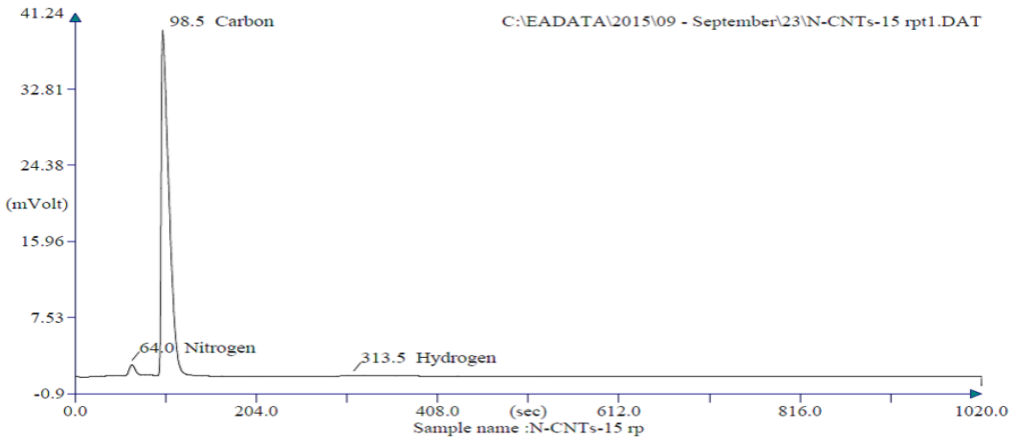

Retention Time (min)	Element Name	Element %
1.067	Nitrogen	1.160
1.642	Carbon	20.256
5.225	Hydrogen	0.230
		21.646

Figure B20: CHNS spectrum of N-MWCNTs synthesized from cobaltocene at a growth temperature of 800 °C

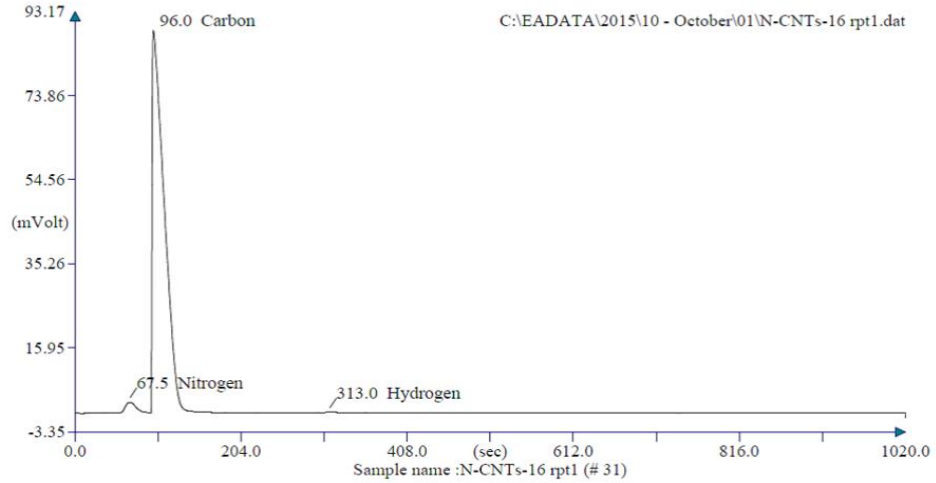

Retention Time (min)	Element Name	Element %
1.125	Nitrogen	5.215
1.600	Carbon	87.031
5.217	Hydrogen	0.154
		92.400

Figure B21: CHNS spectrum of N-MWCNTs synthesized from ruthenocene at a growth temperature of 1000 °C

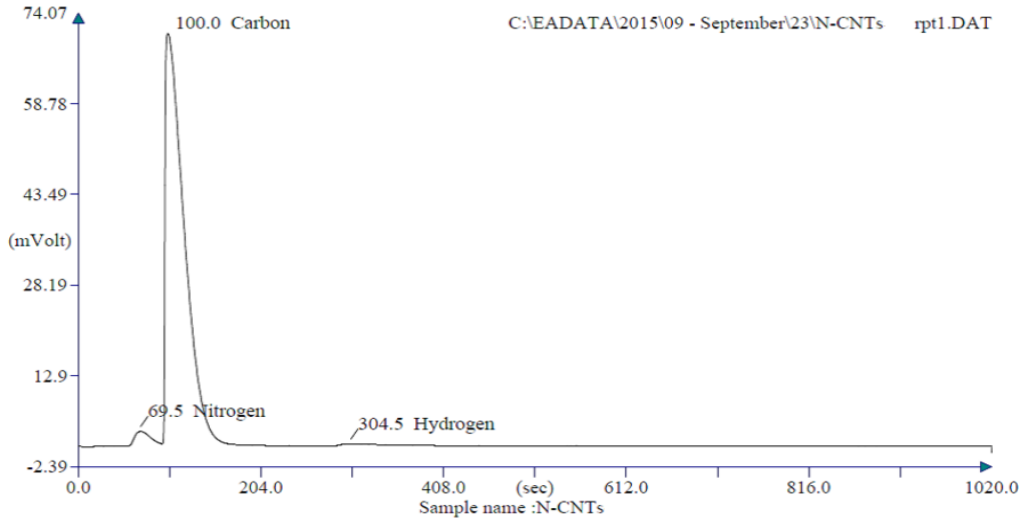

Retention Time (min)	Element Name	Element %
1.158	Nitrogen	5.894
1.667	Carbon	76.623
5.075	Hydrogen	0.379
		82.896

Figure B22: CHNS spectrum of N-MWCNTs synthesized from ruthenocene at a growth temperature of 950 °C

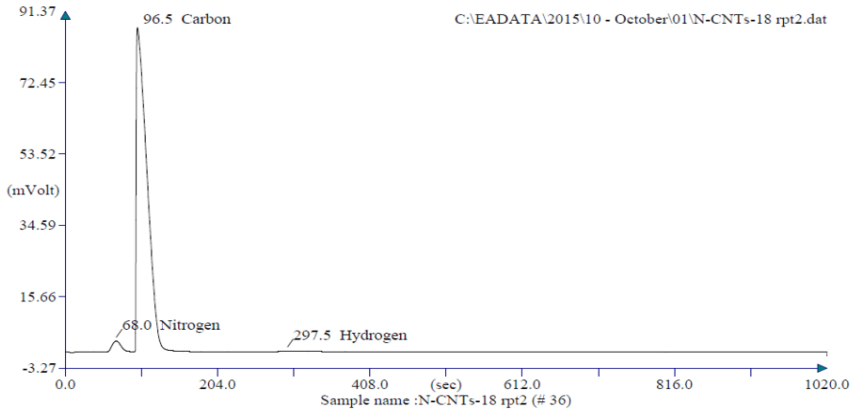

Retention Time (min)	Element Name	Element %
1.133	Nitrogen	5.792
1.608	Carbon	83.527
4.958	Hydrogen	0.319
		89.637

Figure B23: CHNS spectrum of N-MWCNTs synthesized from ruthenocene at a growth temperature of 900 °C

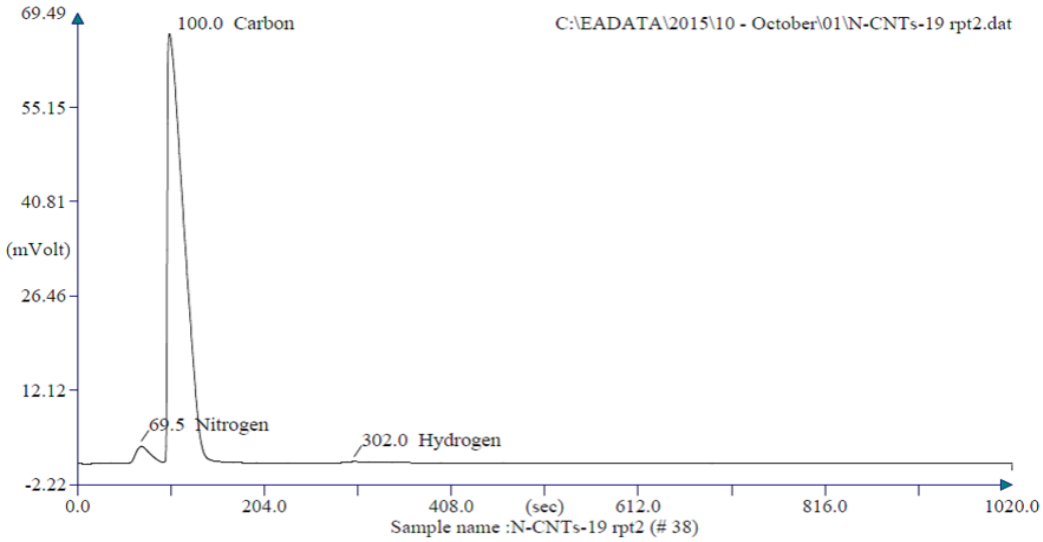

Retention Time (min)	Element Name	Element %
1.158	Nitrogen	6.521
1.667	Carbon	77.203
5.033	Hydrogen	0.292
		84.017

Figure B24: CHNS spectrum of N-MWCNTs synthesized from ruthenocene at a growth temperature of 850 °C

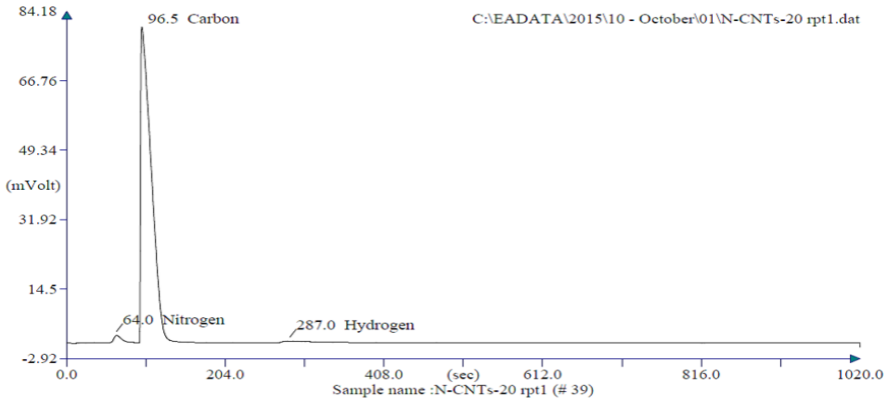

Retention Time (min)	Element Name	Element %
1.067	Nitrogen	3.367
1.608	Carbon	80.548
4.783	Hydrogen	0.611
		84.526

Figure B25: CHNS spectrum of N-MWCNTs synthesized from ruthenocene at a growth temperature of 800 °C

TGA Analysis

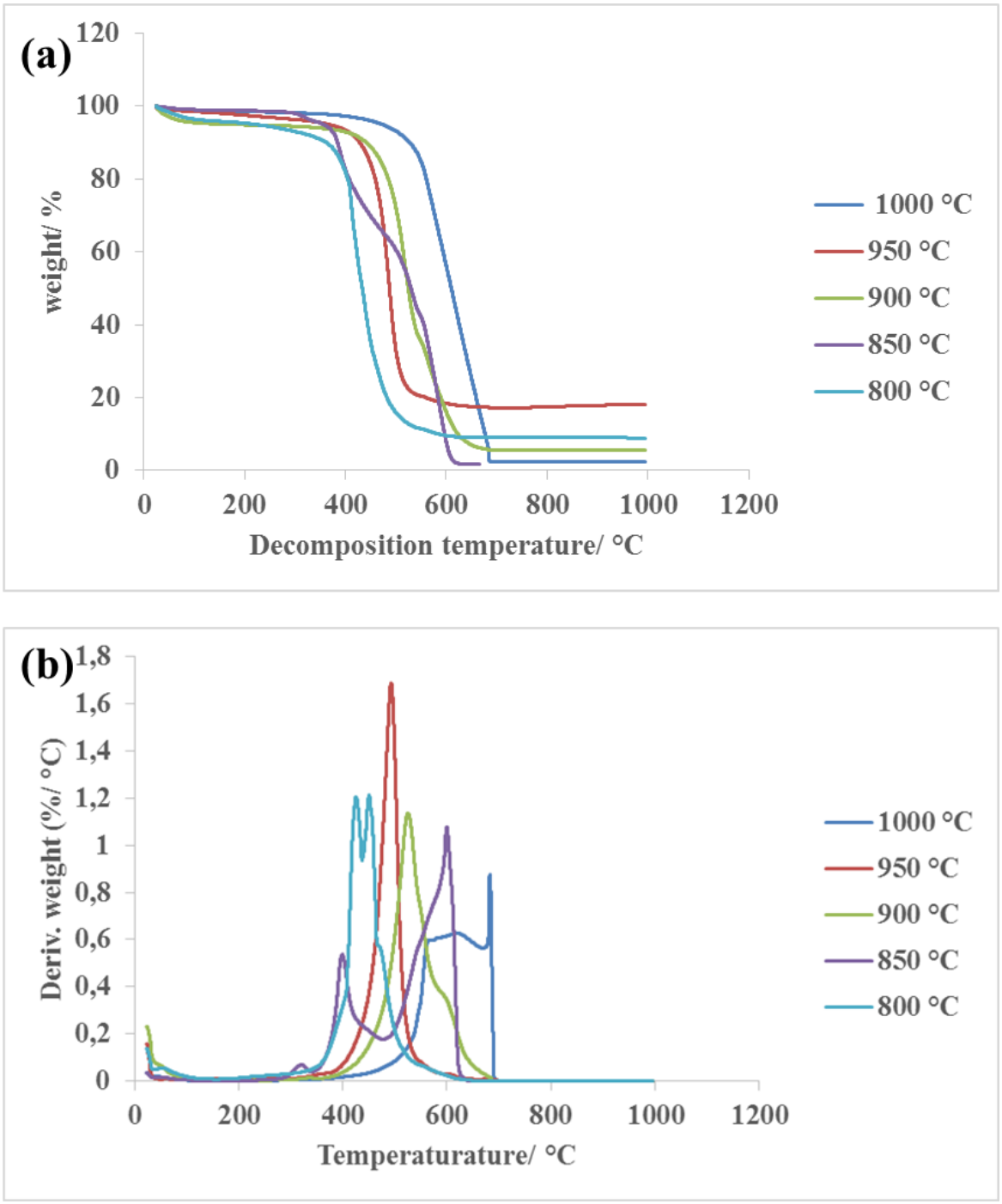

Figure B26: Thermogravimetric analysis of N-MWCNTs synthesized from ferrocene (a) showing amount of residue remaining on the purified samples and (b) their derivatives % weight loss

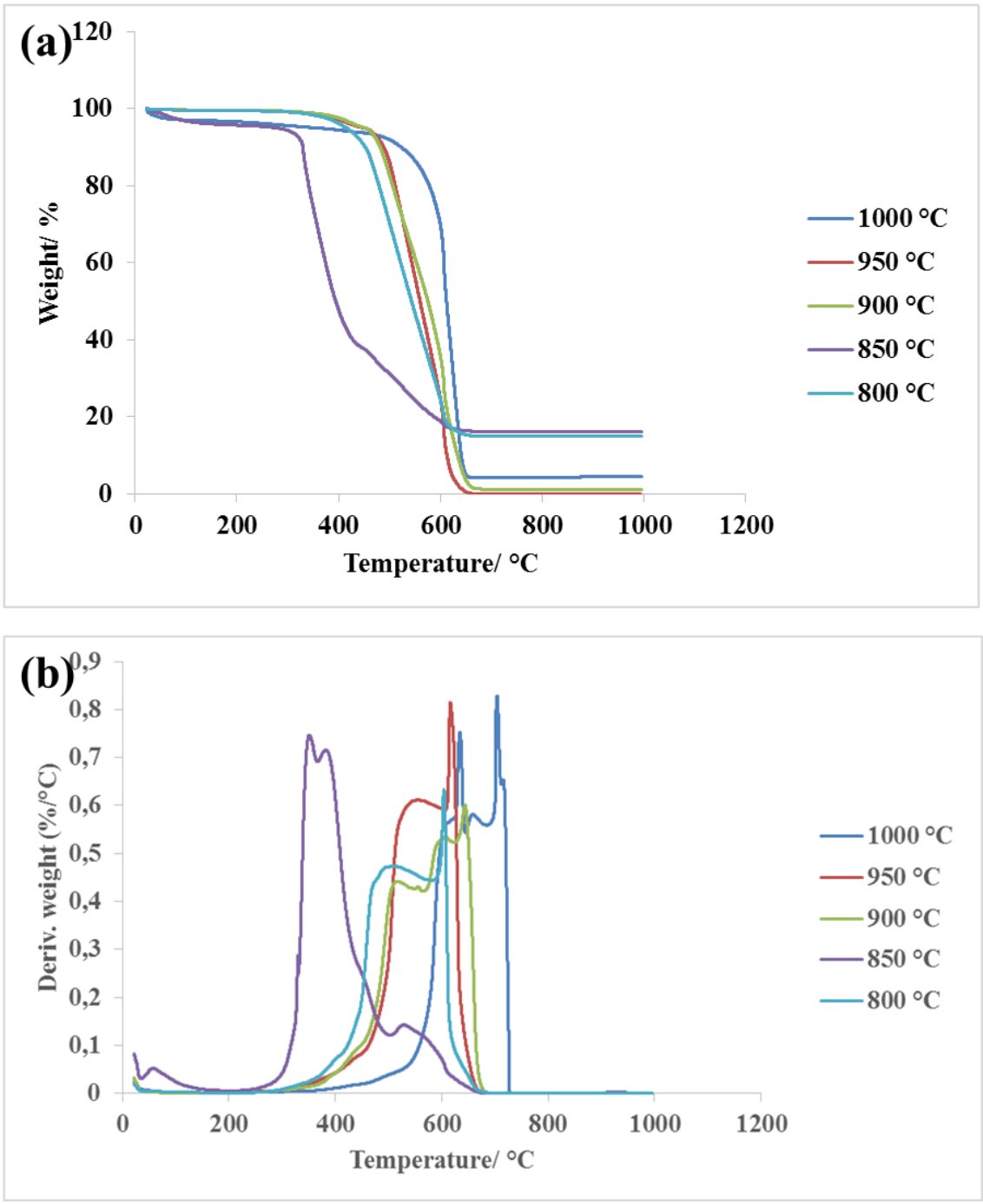

Figure B27: Thermogravimetric analysis of N-MWCNTs synthesized from nickelocene (a) showing amount of residue remaining on the purified samples and (b) their derivatives % weight loss

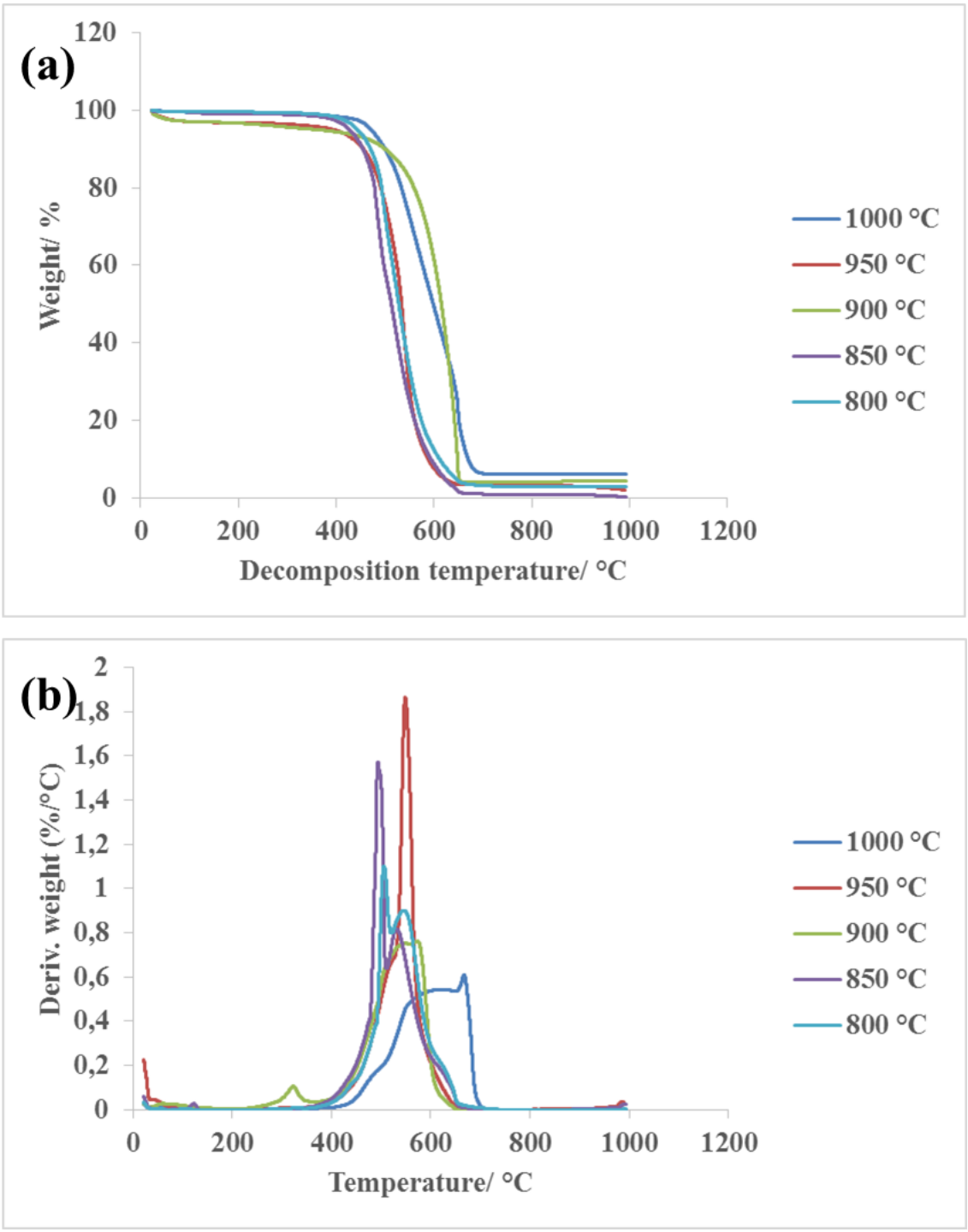

Figure B 28: Thermogravimetric analysis of N-CNTs synthesized from nickelocene (a) showing amount of residue remaining on the purified samples and (b) their derivatives % weight loss

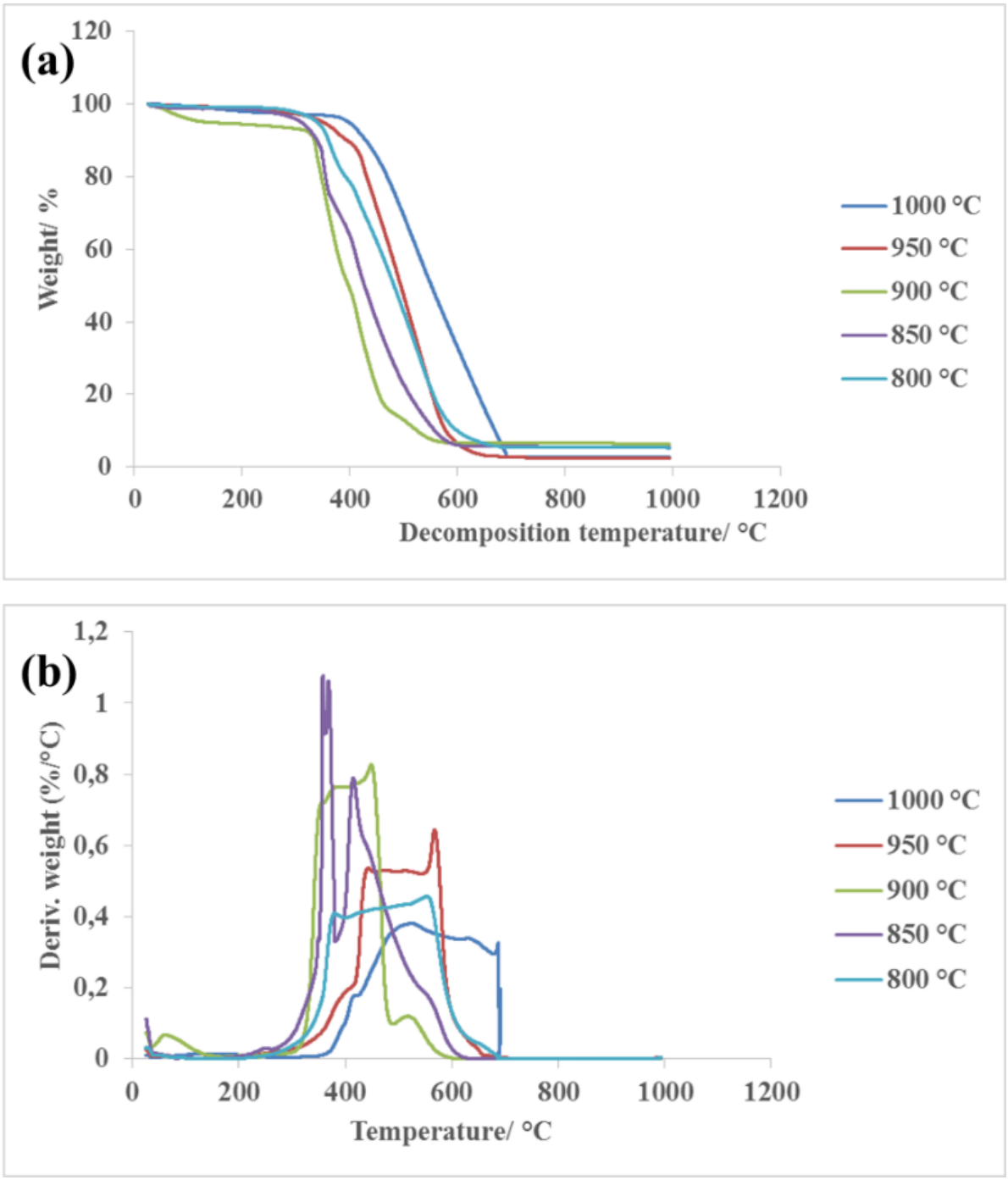

Figure B29: Thermogravimetric analysis of N-MWCNTs synthesized from ruthenocene (a) showing amount of residue remaining on the purified samples and (b) their derivatives % weight loss

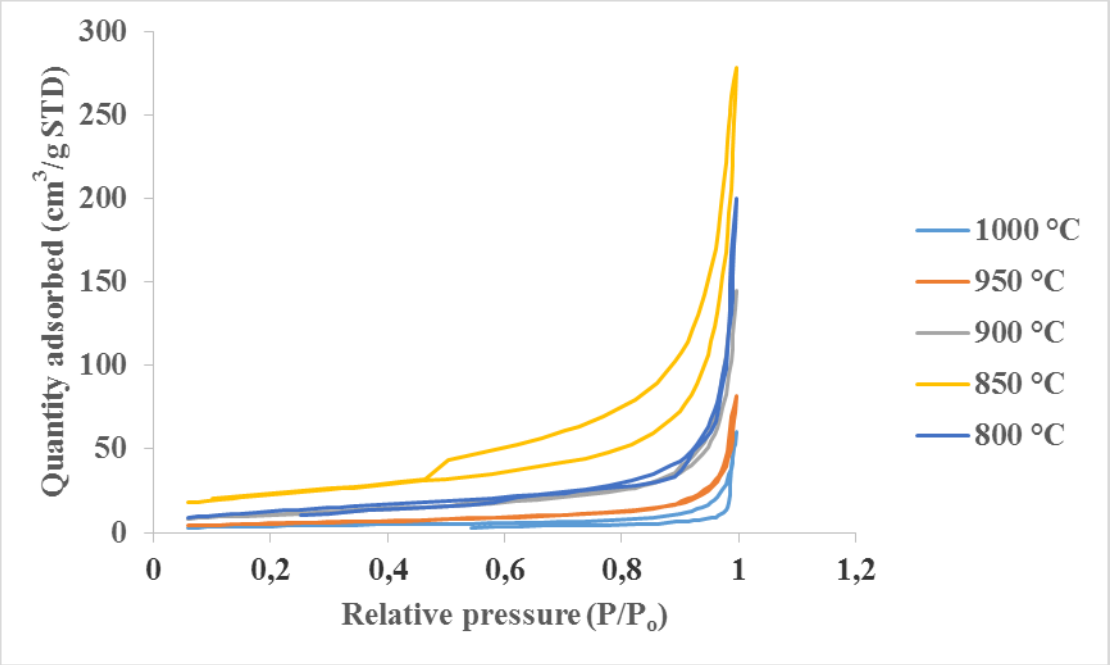

Figure B30: Representative N_2 adsorption isotherms of N-MWCNTs synthesized from ferrocene at different growth temperatures

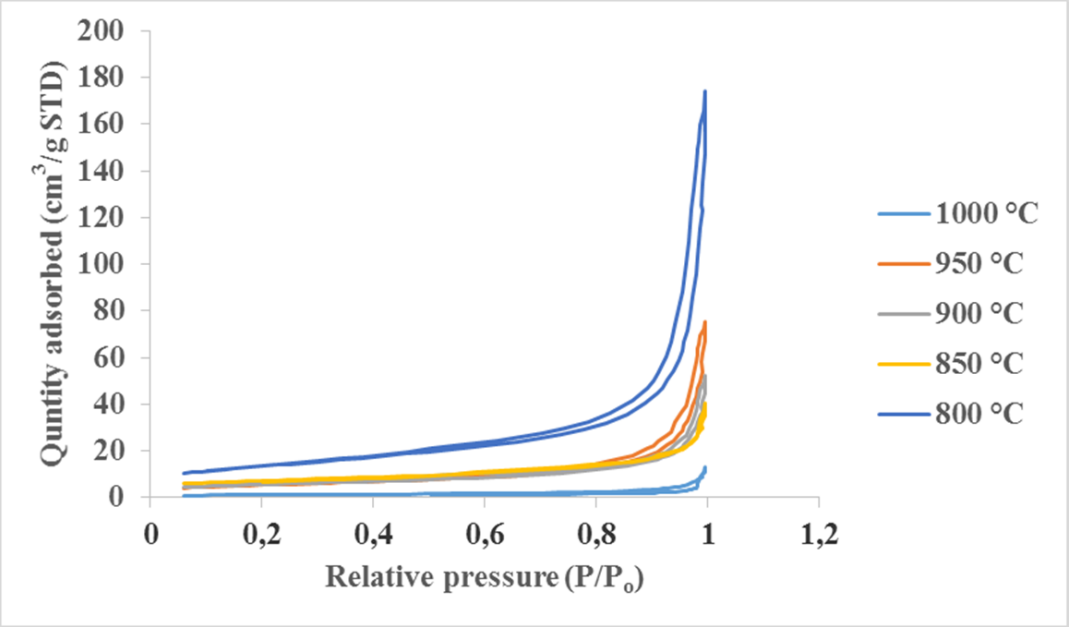

Figure B31: Representative N_2 adsorption isotherms of N-MWCNTs synthesized from nickelocene at different growth temperatures

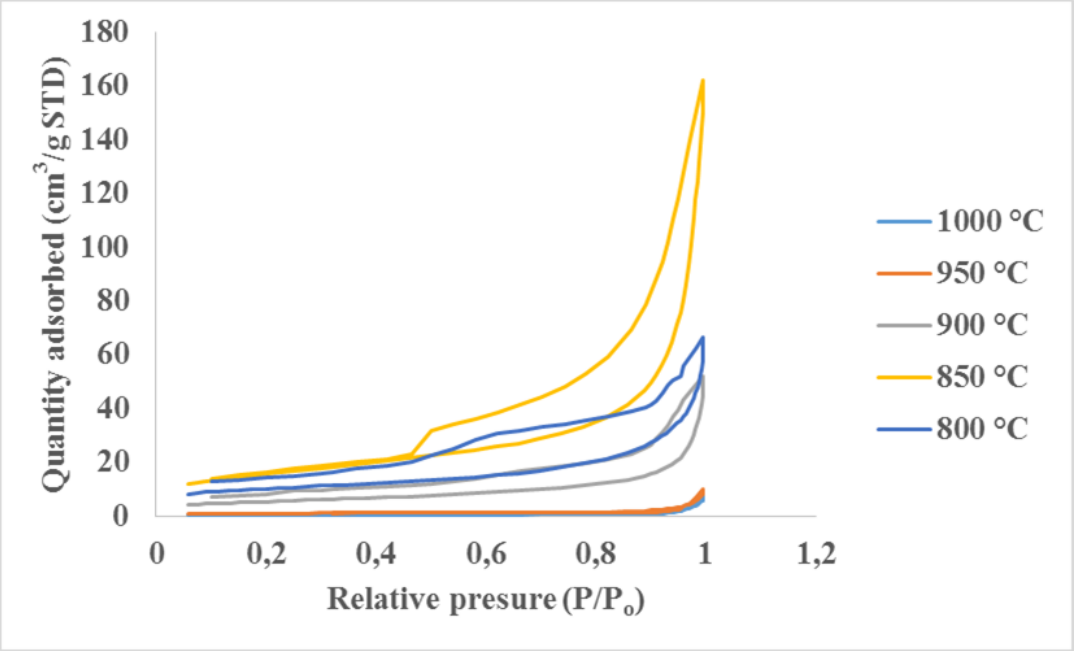

Figure B32: Representative N_2 adsorption isotherms of N-MWCNTs synthesized from cobaltocene at different growth temperatures

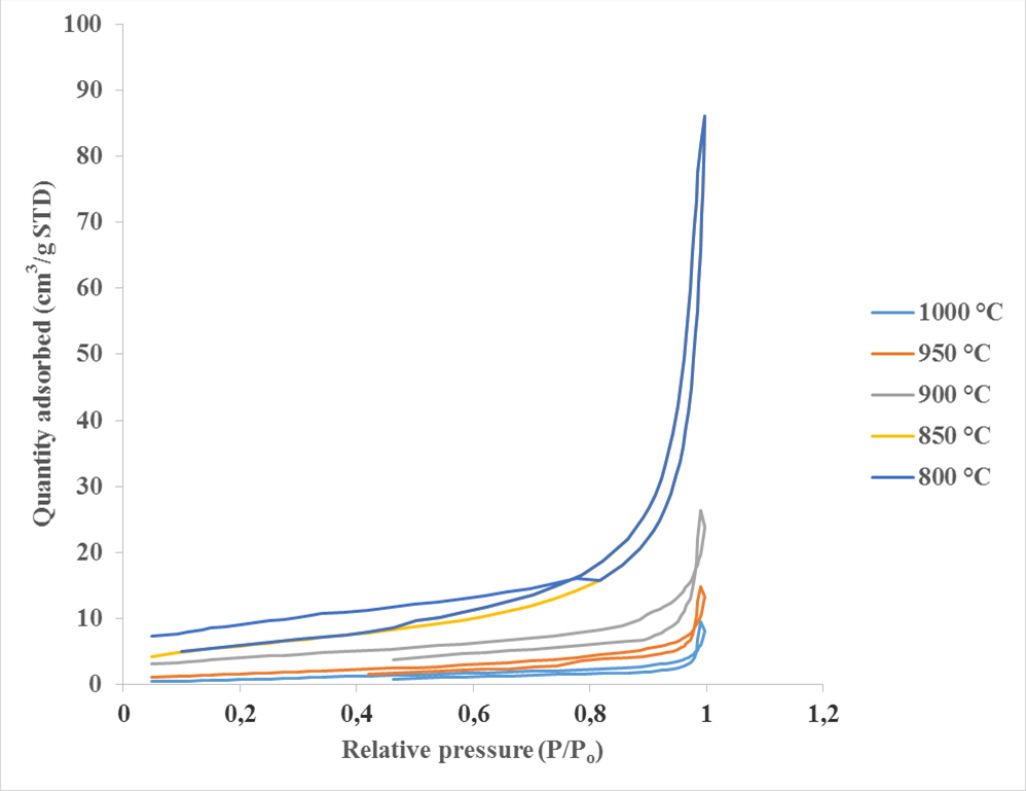

Figure B33: Representative N_2 adsorption isotherms of N-MWCNTs synthesized from ruthenocene at different growth temperatures